NASA-CR-189157
March 1992

CR 189157

7N-20
2853
p. 114

PROBABILISTIC STRUCTURAL ANALYSIS METHODS FOR SELECT SPACE PROPULSION SYSTEM COMPONENTS (PSAM) VOLUME I

by

Southwest Research Institute
Rocketdyne
University of Arizona
MARC Analysis Corporation
Columbia University

1st Annual Report
NASA Contract NAS3-24389
SwRI Project 06-8339

Prepared for

NATIONAL AERONAUTICS AND SPACE ADMINISTRATION
NASA-Lewis Research Center
Cleveland, OH 44135

March 1986

(NASA-CR-189157) PROBABILISTIC STRUCTURAL ANALYSIS METHODS FOR SELECT SPACE PROPULSION SYSTEM COMPONENTS (PSAM), VOLUME 1 Annual Report No. 1 (Southwest Research Inst.) 114 p

N94-71796

Unclas

Z9/20 0002853

List of Tables

Table		Page
2.1	Nozzle, Stator-Vane, and Rotor-Blade Data for Representative Turbines	20
2.2	Individual Load Summary on Turbine Blades	25-26
2.3	Design Geometry of Co-Axial Elements (GH_2/LO_2) for Various Rocket Engines	30
2.4	Individual Load Summary on LOX Posts	34-35
2.5	Individual Load Summary Transfer Ducts & Liners	40-41
2.6	Summary of Interconnects	42
2.7	Summary of Major Propellant Ducts	51-52
4.1	Example of FPI Performance	74
4.2	Design Factors for Example	78
4.3	Statistical Analysis of Yield Strength Data of MAR-M-246 to Obtain the Best Fit Distribution	84
5.1	Summary of the NESSUS Element Library	97

PRECEDING PAGE BLANK NOT FILMED

PAGE ii INTENTIONALLY BLANK

List of Figures

Figure		Page
1.1	The Probabilistic Structural Analysis Problem	2
1.2	Concept of Probabilistic Structural Analysis	4
2.1	Space Shuttle Main Engine Characteristics	15
2.2	SSME High Pressure Turbopump Blades	19
2.3	Impact of Geometrical Variations on Alternating stresses	21
2.4	Effect of Orientation on Elastic Properties of MAR-M-246 (HF)	23
2.5	Effect of Orientation on Elastic Properties of MAR-M-246 (HF)	24
2.6	SSME Preburner Injectors and Main Injector Arrangement	28
2.7	Atomization Concept in Co-axial Injectors	29
2.8	Typical Components of the Main Injector Element	31
2.9	SSME Powerhead Component Arrangement	36
2.10	Scrub Liner and Structural Liner Concept Used in Transfer Tube Design	38
2.11	SSME Flight Nozzle Configuration	44
2.12	Summary of J-2 Engine Maximum Side-Load Moments About Gimbal Point	45
2.13	History of Maximum Strains	46
2.14	SSME Main Combustion Chamber Materials and Configuration	48
2.15	Throat Section of SSME-MCC Showing Thinned Hot Gas Wall	49
2.16	High Pressure Oxidizer Duct	50
3.1	Exact Transformation of a Linear Limit State	59
4.1	Elementary Design Considerations of Simple Structural Component	65
4.2	Relationship of Safety Index to Risk and to μ_z and σ_z	71
4.3	Block Diagram for Computation of the Safety Index, β, when the Failure Function is not Available as a Closed Algebraic Form	76
4.4	Three Bar Truss	77

List of Figures (Continued)

Figure		Page
4.5	Comparison of Monte Carlo ("exact") to Fast Probability Integration (FPI)	79
4.6	Deviations for: (a) S-Statistic; (b) W-Statistic	83
4.7	Comparisons of Histogram with Best Fit Distribution (No Tail Bias) for Yield Strength of MAR-M-246; Room Temperature; n = 92	85
4.8	Lognormal Probability Plot of Yield Strength of MAR-M-246 (n = 92)	88
5.1	1-D Interpretation of the Algorithm in Box 5.1	103
5.2	Flow Diagrams for the Integration of the FE and FPI Modules of the NESSUS Code	104
6.1	Rocketdyne Finite Element Plate Model of the SSME High Pressure Fuel Turbopump Second Stage Blade (a)	107
6.2	Rocketdyne Finite Element Plate Model of the SSME High Pressure Fuel Turbopump Second Stage Blade (b)	108

1.0 INTRODUCTION

1.1 Overview of PSAM Program

Probabilistic Structural Analysis Methods for Select Space Propulsion System Components (PSAM) is a research and technology program sponsored by the National Aeronautics and Space Administration-Lewis Research Center (NASA-LeRC). The prime contractor is Southwest Research Institute (SwRI). Its efforts are supported by: MARC Analysis Research Corporation - code development for probabilistic finite element methods; Rocketdyne Division, Rockwell International Corp. - Space Shuttle Main Engine (SSME) design and hardware experience; and several university consultants and subcontractors. The objective of PSAM is to develop analysis techniques and computer programs for the probabilistic structural analysis of engine components for current and future space propulsion systems. It is envisioned that these probabilistic techniques will play a critical role in establishing increased system performance and durability.

The problem addressed by the PSAM program is depicted in Fig. 1.1. The structure, illustrated by a SSME turbine blade, is subjected to stochastic thermomechanical launch loads. Uncertainties or randomness may also occur in material properties, structural geometry, and boundary conditions. Material property stochasticity, such as in modulus of elasticity or yield strength, exists in every structure and is a consequence of variations in material composition and manufacturing processes. Mechanical properties vary significantly over the temperature ranges encountered in SSME operation, and uncertainty in the thermal environment introduces another element of stochasticity into the material description.

Component fabrication, through variations in normal manufacturing dimensions such as thickness, adds another degree of randomness. Critical engine components are manufactured with high precision, and thus, nominal geometrical variations are expected to be small. However, for the turbine blade shown in Fig. 1.1, variations in blade twist in the span-wise direction could have a significant effect on the structural response to aerodynamic loads.

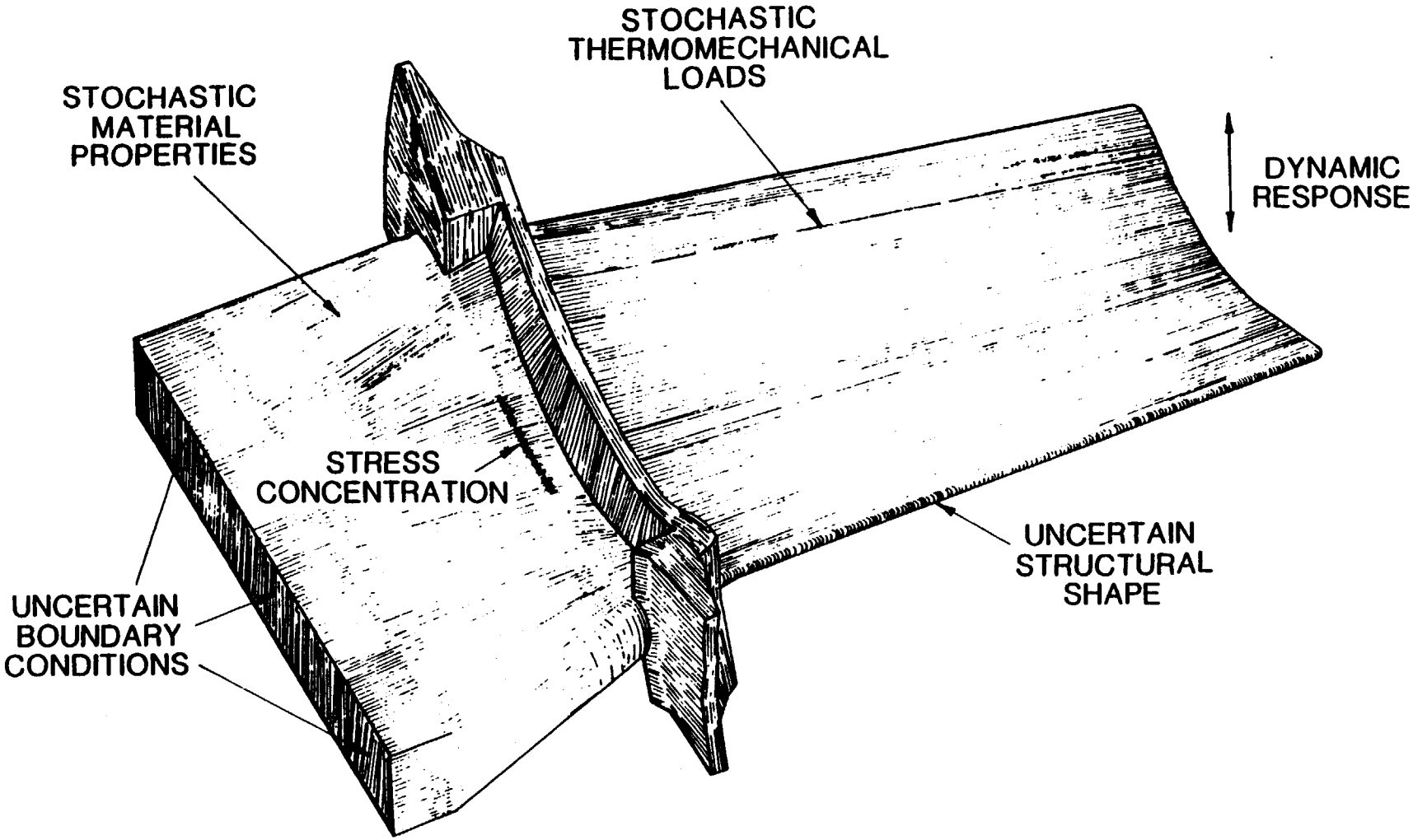

Figure 1.1 The Probabilistic Structural Analysis Problem

Assumptions in boundary conditions are frequently a major source of uncertainty in analysis. Cantilever type structures, such as this turbine blade, are often modeled as fully restrained for simplicity. On the other hand, because of assembly procedures, real structures may exhibit some degree of flexibility at the support. The assumption on boundary conditions may not be important in some types of analyses. However, computations involving the dynamic response of a turbine blade would be very sensitive to variations in boundary conditions.

Assuming that the loading, material properties, structural geometry and boundary conditions are described in a probabilistic sense, the objective of the PSAM is to develop analytical methods and computer programs for computing the probabilistic structural response. The response variable or variables could be static or dynamic deflections, strains, and stresses at one or several locations, or natural frequencies. One useful concept is to consider that the structure acts as a filter for the random input variables, as illustrated in Fig. 1.2. The response, for the variable of interest, will be random and will be described by its probability density (pdf) or cumulative distribution (cdf) function. In general, the form of these functions will not correspond to any standard analytical distribution and must be evaluated numerically, as described in this report.

1.2 Report Outline

The four-year PSAM program was initiated in October 1984. The first year has concentrated on probabilistic finite element formulation and code development, and the survey of the critical materials and SSME components. This report, which consists of three volumes, contains the work accomplished by the PSAM team in the first year of the program.

There are six sections in this volume. Section 1 provides the overview and objectives of the PSAM program; what has been accomplished and what will be done in the remaining years of the program.

Section 2 is a summary of a survey of critical SSME components, conducted by Rocketdyne. The purpose of the survey was to scope the structural analysis requirement for the selected

CONCEPT OF PROBABILISTIC STRUCTURAL ANALYSIS

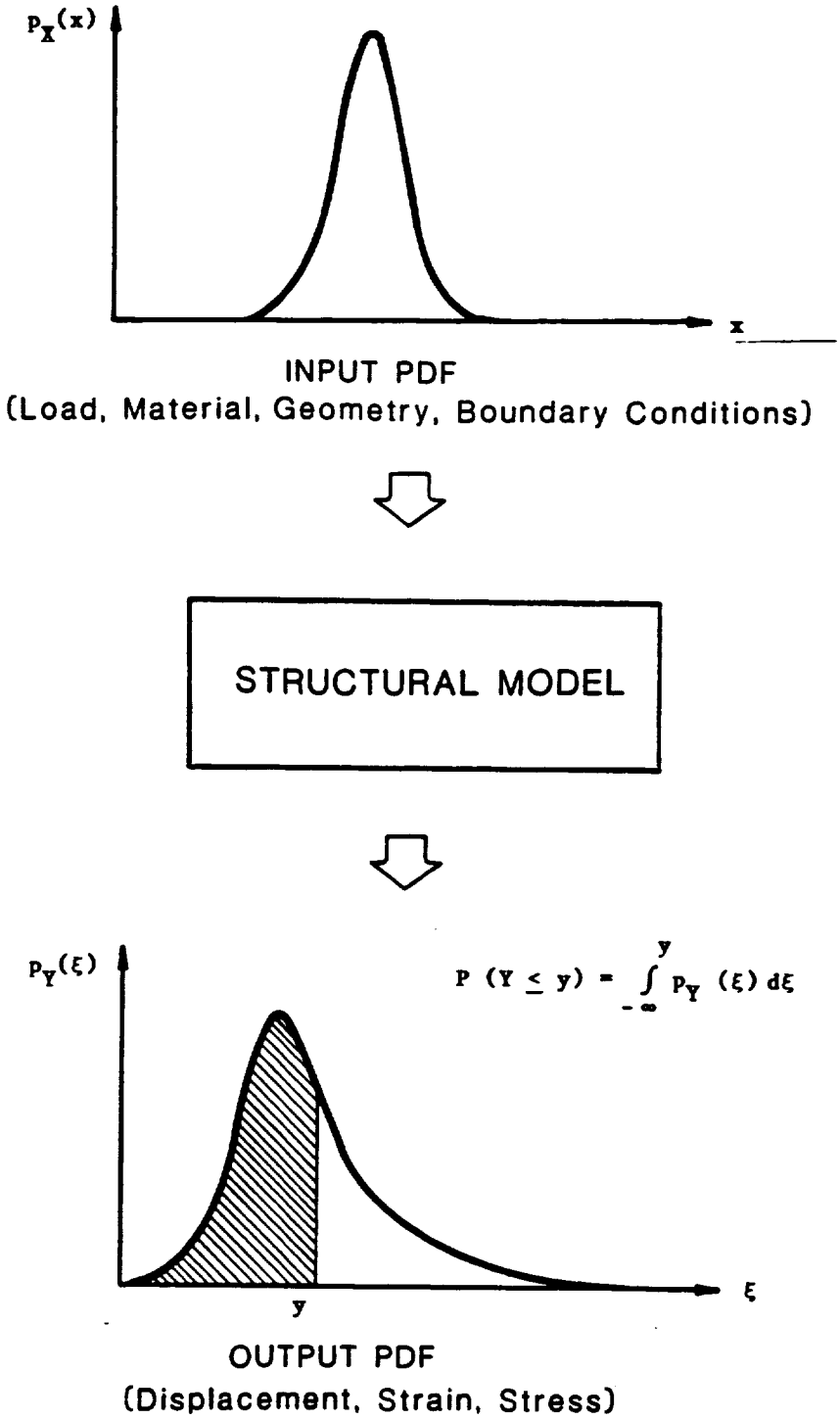

Figure 1.2 Concept of Probabilistic Structural Analysis

components with reference to probabilistic structural analysis methods. The complete surveys are contained in Volume II.

Section 3 provides an overview of the concept of probabilistic structural analysis. This section reviews the general probabilistic analysis methods that may be applied to the PSAM program, and critiques the methods currently being employed to develop the probabilistic structural analysis computer programs. Detailed literature reviews are contained in Volume III which also includes other technical reports written by the PSAM team.

More detailed computational strategies for the probabilistic analysis are contained in Section 4. It provides a tutorial summary of the strategies currently used in the PSAM program, such as the fast probability integration (FPI) methods, the choice of distribution functions and the maximum entropy model.

The Numerical Evaluation of Stochastic Structures Under Stress (NESSUS) code has been developing by MARC Analysis Research Corporation. The overview and general capabilities of the NESSUS code is given in Section 5. A major feature of the code is that it applies an efficient iteration algorithm for generating perturbation data. The data are subsequently used to establish the approximating response or performance functions suitable for probabilistic analysis.

Work in progress is contained in Section 6. The discussions focus on the implementation of the NESSUS code.

1.3 Program Objectives

The purpose of the Probabilistic Structural Analysis Methods (PSAM) project is to develop a new technology capability for the design analysis of advanced space propulsion system hardware. The focus of the PSAM effort is on the development of specific structural analysis capabilities which model stochastic mechanical and thermal loads, geometry, and material response. The PSAM effort consists of three major technical thrusts: probabilistic finite element methods (PFEM), probabilistic approximate analysis methods (PAAM), and probabilistic advanced analysis methods (PAdvAM).

The developed methods of analysis are to treat linear problems as well as those with nonlinear material and geometric response. Stochastic modelling of loads (e.g., centrifugal, thermal, pressure), geometry, and material behavior are being modeled with three levels of approximation, relative to accuracy and confidence. Level I analyses treat randomness as being spatially homogeneous (e.g., each part has a different modulus, yield stress, thermal load, etc.). Level II analyses treat random variables as random fields (e.g., modulus variability is different in the bore of a disk, versus the rim of the disk; pressure uncertainty is different at the root of an airfoil versus the tip of the blade). Level III stochastic modelling is to be able to reflect uncertainty between variables in the governing equations (e.g., strain agrees with displacement gradients only in stochastic, not deterministic, terms; stress is related to strain through stochastic relations).

Two methods of probabilistic modelling are to be included in the various analysis methods. The first of these is the Fast Probability Integration (FPI) method. The FPI method is adopted from the field of structural reliability as a way of predicting the probability that a response variable (e.g., stress, frequency) will exceed some allowable. The method is based on establishing the approximate sensitivity of a response variable to the stochastic variables, and then processing these sensitivities by the FPI algorithm to establish the cumulative response distributions for the variables. The second method is simulation using Monte Carlo methods. Confidence levels will be estimated for the response variable distributions that are calculated.

Task 1: Probabilistic Finite Element Method (PFEM)

The PFEM is a direct adaptation of standard finite element methodology to the needs of PSAM. The finite element code (NESSUS) is to include plate and shell elements based initially on the displacement method of formulation, and on linear equations of motion and material behavior. Hybrid plate and shell elements are to be included, as well as nonlinear geometric and material behavior. Material response is to include the range from elastic to thermoviscoplastic. All three levels of stochasticity are to be included, as well as two probability evaluation methods. The material

models will be expanded to include distributed models of discontinuities and damage. Special interpolation capability for severe thermal gradients is planned. A composite load spectrum analysis procedure will be included.

The user interface for PFEM will be based on an interactive, knowledge based system for the probabilistic input and response variables. Structural analysis variables such as nodal coordinates, material properties, etc., representing the deterministic solution will be defined in a batch mode, compatible with the needs of a variety of finite element pre-processors.

The PFEM code is modular for adaptation to the General Purpose Structural Analysis (GPSA) framework. The user interfaces for probabilistic data input and post-processing are separate modules from the finite element code (NESSUS). The database that is developed by NESSUS is another possible module. Interfaces between these modules will be clearly defined.

The PFEM code is to be validated through its application to well-defined problems with known probabilistic responses to demonstrate the full and reliable capability of the code. Further, the PFEM will be verified by its application to four selected space propulsion system hardware items. These will include the turbine blade, transfer duct, LOX post, and a fourth to be selected. Experimental verification will be sought when the data are possible to obtain.

Task 2: Probabilistic Approximate Analysis Methods (PAAM)

The PAAM code is to have the general range of capabilities defined for the PFEM. However, the principal focus will be to establish approximate models to replace the NESSUS module, in order to establish results for preliminary design or evaluation of probabilistic structural response.

The PAAM is to include simplified structural models for plate and shell structures representative of space propulsion system hardware. Candidates for PAAM include reduced modal models of the structural response, and the development of a library of simplified design analysis models based on the actual design procedures in place at the Rocketdyne Division of Rockwell.

Validation and verification of the PAAM code will follow the procedures outlined for PFEM. Validation will be based on the use of closed form solution problems. Verification will be based on the selected space propulsion system components.

Task 3: Probabilistic Advanced Analysis Methods

The focus of the PAdvAM is to develop technology advances which will lead to an advanced analysis code. The effort is focussed on algorithm advances to be included in the NESSUS code being developed in the Task 1 effort. Advances will be established for the structural elements as well as the probabilistic evaluation procedures.

The basis of advanced structural analysis developments includes new models for plate and shell elements, and a review of the variational method basis for structural analysis adapted to stochastic problems. Boundary element methods (BEM) and finite element methods (FEM) will be the general frameworks evaluated to establish the advanced element formulations for plate and shell elements.

The stochastic basis of a variational model of structural response will be established. The stochastic variational statement will be used to demonstrate the formulation basis of the Level I, II NESSUS PFEM models. Further, it will be used to establish the Level III formulation for adoption into NESSUS. Novel solution algorithms for the stochastic variational statement formulation will also be sought.

Validation and verification of the PAAM code will follow the procedures outlined for PFEM. Validation will be based on the use of closed form solution problems. Verification will be based on the selected space propulsion system components.

1.4 Accomplishments to Date

The objective of the first year program is to plan, formulate or identify the Probabilistic Finite Element Methods (PFEM) for plates and shells, and to develop PFEM Code (i.e., NESSUS) for delivery and installation.

In the beginning of the first year program, SwRI prepared a Work Plan after discussions with the SwRI subcontractors defining the participation in the technical tasks.

Rocketdyne has conducted a series of SSME component surveys to identify the critical components and also provide the information, related to the critical components, necessary for probabilistic structural analysis. The effort has resulted in the following documents:

1) Surveys of Critical Space Shuttle Main Engine Components (see Volume II).

2) Material data of turbine blade:
   Alloy 1480 (Measured material axes variations; ultimate and yield strengths; percent elongation and reduction in areas; elastic and shear modulus; coefficient of thermal expansion).
   MAR-M-246 (Ultimate and yield strengths; percent elongation and reduction in areas; static strength with temperature effect).

3) Geometry data of SSME high pressure oxidizer turbopump first stage and second stage blades (Nominal values, tolerances and measured data).

The University of Arizona and SwRI have produced methods for analyzing data and resulted in distribution models using the MAR-M-246 and alloy 1480 data provided by Rocketdyne. The distribution models will be used for NESSUS code verification.

The first year code, which is nearly complete (validation work is in progress, see Section 6) has linear, elastic analysis capabilities. This includes the ability to address static problems in which the loading vector and the structural matrices are considered probabilistic. The randomness in these matrices can arise from both material property variations and uncertainties in the structural geometry and boundary conditions. This first-year code is capable of solving the probabilistic eigenvalue and eigenvector problems arising from stochastic stiffness and mass matrices.

The theoretical aspects of the first-year NESSUS code are documented in the PSAM Monthly Reports. A summary of both the finite element and probabilistic methods used in the code can be found in the following four papers presented at the Symposium on Probabilistic Structural Design and Analysis of the ASME 1985 Winter Annual Meeting:

Dias, J. B., and Nategaal, J.C., (MARC Analysis Research Corp.), "Efficient Algorithms for Use in Probabilistic Finite Element Analysis"

Wirsching, P.H., and Wu, Y.-T., (University of Arizona), "Advanced Reliability Methods for Structural Evaluation"

Wu, Y.-T., (Southwest Research Institute), "Demonstration of a New, Fast probability Integration Method for Probability Analysis"

Burnside, O. H., (Southwest Research Institute), "Probabilistic Structural Analysis for Space Propulsion System Components"

The first-year effort has identified three levels of sophistication for PFEM. The first level is based on the use of homogeneous models of the stochastic variables. These variables are the stiffness, mass, and damping properties as well as the probabilistic loading. At this level, each term in the formulation is assumed to be represented by a function of the random variables multiplied by the usual deterministic matrix for the mass, stiffness, damping, and the loading vector.

The second level of sophistication considers inhomogeneous models. At this level, each element in the structural assemblage has its own state of material and geometric properties such that spatial inhomogeneities in the stochastic models of the basic variables and loading variables can be incorporated. The individual finite element stiffness formulation is based upon the standard finite element formulation procedures. For example, the element strain definition is derived deterministically from the element displacement interpolation functions. The stress within the element is related through the usual deterministic relations to the strains by means of the element modulus. Terms in the element's elasticity matrix are represented by appropriate distributional models. This is basically the formulation in the NESSUS Code. However, MARC found it to be more efficient to treat the random variables on a nodal rather than an element basis.

One approach for the Level 2 formulation for static, linear elastic system is discussed in detail in Section 3 of Volume III. This formulation is based upon a Taylor series expansion of the stochastic structural matrices about a deterministic solution. This method results in the response variables of interest being expressed as the functions of the random variables. Probabilistic analysis requires evaluating the partial derivatives of the structural matrices with respect to the random variables. As this formulation was reviewed, SwRI and MARC concluded that this was not a feasible approach. Partial derivatives could not be efficiently computed for the size of the structural matrices and the number of random variables expected in SSME analysis. This led to MARC's development of the

algorithm discussed in Dias and Nagtegaal's paper referenced above. The method is able to compute structural response efficiently in the neighborhood of a deterministic state without reformulating the system of structural matrices. Using the perturbation data, the probabilistic analysis can be performed using the methods given in Wirsching and Wu's papers.

NESSUS as it is currently structured can be considered both a Level 1 and Level 2 Code. It is Level 2 in that structural stochasticity can be described on a nodal basis. Spatial correlation can exist between the random variables and can range between independent to fully correlated. NESSUS uses a method to uncorrelate the random variables through a matrix transformation using the covariance matrix. Currently, the code assumes that the correlated random vector has a joint normal distribution. For a non-normal correlated vector, a procedure is available to transform the vector to a correlated normal vector, which can be incorporated into NESSUS. Section 5 of Volume III describes a computational procedure proposed by SwRI. The Level 2 formulation reduces to Level 1 if the random field is spatially homogeneous and becomes a random variable. The NESSUS can be employed as a Level 1 code by considering a fully correlated field. The Level 3 analysis will consider intra-element stochasticity. The formulation to this level of sophistication is discussed in Section 1.5.

The first-year's PSAM effort has identified the fast probability integration methods as the primary tool for constructing response distributions and other critical information (such as the design point discussed in Section 3) using the perturbation data generated by MARC's perturbation algorithm. The methods are discussed in Section 3 to Section 5 as well as in the above referenced papers. Burnside presented an application of the combined NESSUS and FPI algorithms to the analysis of a curved shell structure representing an SSME turbine blade. Although the validation process of the NESSUS code is still in progress (see Section 6), it is strongly believed that the first-year's PSAM effort has generated valuable knowledge, data, and a state-of-the-art computer code necessary for a successful PSAM program.

1.5 Next Year Goals

The major objectives for the next year of the PSAM program are described in the following in somewhat broad terms.

Formulation Strategy

The formulation of probabilistic structural analysis will be extended to Level 3 analysis which will be based on the variational principle for the finite element formulation so as to incorporate intra-element stochasticity. Thus, for example, the element strains will be statistically independent of the derived strains based on the nodal displacements. One of the key questions, which will be answered by the PSAM team, is the nature of the implied incompatibility of intra-element strains as a result of this approach. For example, should the element strain field distribution be constrained in a manner so as to assure compatibility or is it desirable to allow incompatibility on a stochastic basis for the intra-element strains. Further, by allowing the material properties to vary within the element, the derived quantity of stress will be permitted to have a stochastic nature within the element. As part of the Advanced Methods effort, Professor S. N. Atluri will direct the Georgia Institute of Technology team to establish a variational statement for the stochastic structural response in both Level 2 and Level 3.

New solution approaches to the defined stochastic variational statement of the problem for both the Level 2 and Level 3 approximations will be explored. Professor P. K. Banerjee will lead the University of New York at Buffalo team to investigate the feasibility of applying boundary element method to stochastic analysis.

The effort at the University of Arizona under Professor Paul Wirsching will focus on establishing the base of technology for confidence level estimation, further evaluation and refinements of the FPI algorithm, and the issue of modal decompositions for non-normal distributions.

A preliminary knowledge based user interface for PFEM is planned. The effort will be focussed at SwRI under Dr. P. Fink as Task Manager.

Verification

Rocketdyne will be the center for the code verification work. Effort will be continued to generate the necessary SSME components data for establishing the distribution models for the stochastic variables, including the loadings, the material properties, the geometries and the boundary conditions, etc. Also, Rocketdyne will continue to select and establish the finite element models of the critical components for probabilistic structural analysis using NESSUS Code.

From the SSME literature search conducted by Rocketdyne, SwRI will select the four components in the SSME engine to be analyzed by the NESSUS Code. Three of these components have already been generically identified by NASA-LeRC as a turbine blade, transfer duct, and LOX post. Rocketdyne recommended that the SSME High Pressure Duct be chosen as the fourth generic component.

The SSME turbine blade has been selected to be the first component to be analyzed with NESSUS. The remaining three components will be analyzed in series by MARC, with the second component selected in early 1986.

2.0 SPACE SHUTTLE MAIN ENGINE

2.1 Overview

The orbiter vehicle main propulsion system includes three Space Shuttle Main Engines (SSMEs). An SSME (Fig. 2.1) is a reusable, high-performance, liquid-propellant rocket engine with variable thrust. All three are ignited on the ground at launch, operating in parallel with the solid rocket boosters during the initial ascent phase, and continuing to operate for approximately 480 seconds during total firing duration. Each engine operates at a mixture ratio (liquid oxygen/liquid hydrogen) of 6:1 and a chamber pressure of approximately 3,000 psi to produce a sea level thrust of 375,000 pounds and a vacuum thrust of 470,000 pounds. The engines can be varied over a thrust range of 65 to 109 percent of the rated power level. This provides a higher thrust level during lift-off and the initial ascent phase, and allows orbiter acceleration to be limited to 3 g's during the final ascent phase. The engines are gimbaled to provide pitch, yaw and roll control during orbiter boost phase.

Significant to meeting performance requirements is the use of a staged combustion power cycle coupled with high combustion chamber pressures. In the SSME staged combustion cycle, the propellants are partially burned at low mixture ratio, very high pressure and relatively low temperature in the preburners to produce hydrogen-rich gas to power the high-pressure turbopumps. This hydrogen-rich steam is then routed to the main injector where it is injected, along with additional oxidizer and fuel, into the main combustion chamber at high mixture ratio and high pressure. Hydrogen fuel is used to cool all combustion devices directly exposed to contact with high-temperature combustion products. An electronic engine controller automatically performs checkout, start, mainstage and engine shutdown functions.

2.2 Summary of Critical Component Surveys

As part of the Probabilistic Structural Analysis Methods effort, detailed surveys were conducted on turbine blades, LOX posts and transfer ducts of the SSME (see Sections 1, 2, and 3

■ HIGH ALTITUDE THRUST 109%	512,300 LBS
■ CHAMBER PRESSURE	3200 PSIA
■ SPECIFIC IMPULSE AT ALTITUDE	453.5 SECONDS
■ THROTTLE RANGE	65 TO 109%
■ PROPELLANTS	OXYGEN/ HYDROGEN
■ WEIGHT	7000 LBS
■ DESIGN LIFE	27,000 SECONDS 55 STARTS
■ FULL POWER LEVEL	14,000 SECONDS

SC308-551S

Rockwell International
Rocketdyne Division

Figure 2.1 Space Shuttle Main Engine Characteristics

in Volume II). These components were explicitly identified by NASA. As possible candidate for the fourth component, High Pressure Oxidizer Duct, Nozzle Feed Line and Main Combustion Chamber Channel Wall were also studied (see Sections 4, 5 and 6 in Volume II). The purpose of the survey effort was to scope the structural analysis requirements for the selected components with reference to probabilistic structural analysis methods. The survey effort identified the linear and nonlinear analysis requirements, participating parameters and boundary conditions. The survey effort identified the various sources of uncertainty in the static and dynamic analysis of each component. Limited representative data were also collected wherever available so that a statistical analysis can be conducted on the observed data to obtain characteristic values.

The type of static and dynamic analysis conducted is component specific. The following features in a finite element code are needed in the analysis of one or more components surveyed.

Element Library

1) 2-D plane stress, plane strain and axisymmetric element
2) Plate shell element
3) 3-D solid element
4) 2-D or 3-D gap elements with friction
5) 3-D beam elements
6) Pipe elbow elements

Material Library

1) Elastic (isotropic, orthotropic and anisotropic)
2) Elastic-plastic (isotropic, orthotropic and anisotropic)
3) Temperature dependent material properties
4) Cyclic strain hardening
5) Creep/relaxation

Analysis/Solution Library

1) Eigenvalue buckling analysis

2) Material and geometric nonlinear analysis

3) Incremental and iterative analysis using full newton, modified newton and quasi-newton procedures

4) Modal frequency extraction

5) Sinusoidal pressure and base excitation analysis

6) Random response analysis due to pressure with specified correlation distances

7) Random response analysis due to multibase random vibration that can be correlated or uncorrelated

8) Dynamic response using direct time integration and using modal superposition techniques

9) Excitation input in the form of a power spectral density

The finite element models used generally fall into two categories, local and global. The local models are used to study the local stress-concentration effects, while the global models are used to study the overall response.

2.2.1 Turbine Blades

In the advanced rocket engines such as those of the SSME, demands have been placed on turbine blades to perform under extreme conditions with many restarts.

Distinguishing features of rocket engine turbines, which form the drive mechanism for high-pressure turbopumps, include:

a) Comparatively short but severe life

b) Strict limitations on size and weight

c) High energy content of fluids

d) High specific work output

e) Rapid start and short run duration

f) Severe thermal shock considerations

g) High stage loading and stress

The currently used turbine blades are subject to fatigue cracks. The fatigue problem in turbine blades may become even more critical with advanced versions of SSME and other liquid rocket engines when they impose even more severe thermal and stress conditions. Probabilistic structural analysis methods, which can account for variations in geometry, material properties, boundary conditions and loadings, may eventually lead to calculation of probabilistic life estimates by combining probabilistic response with probabilistic strength data. Some of the major uncertainties that contribute to the variations in turbine blade response are:

a) Geometric variations

b) Material property and material orientation variations

c) Boundary condition (firtree tolerance) variations

d) Loading variations

e) Friction damper effectiveness variations

Typical SSME oxidizer turbine blade and SSME fuel turbine blade are shown in Fig. 2.2.

Geometrical variations result from specified geometrical tolerances and manufacturing methods. This results in variations in mass and mass center and contribute to the variations in turbine blade response from blade to blade. High-performance turbine blades are tilted such that centrifugal force induced stresses counteract power bending stresses. Any shift in the center of mass of the turbine blade affects the alternating and the mean stress in the turbine blade. An analysis of variations in alternating stress with variations in profile is shown in Fig. 2.3 for a typical blade. The geometrical variations are more critical for small blades as opposed to larger blades. Turbine blade dimensions can vary over a wide range between pump to pump (Table 2.1). Development of advanced turbine blade materials has been an area of intensive research in recent years. Nickel-based super alloys like MAR-M-246 (Hf, DS) and single-crystal alloy 1480 have been used or are seriously being considered for use in reusable rocket engines. These materials are anisotropic in nature and exhibit strong directionally oriented properties. In addition to the normal scatter that is encountered in material properties, elastic as well as plastic (though to a lesser degree than

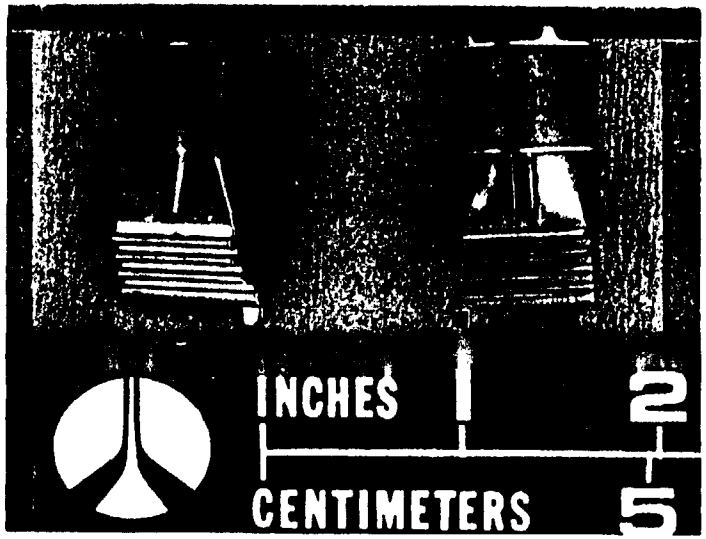

LOX PUMP TURBINE
BLADE

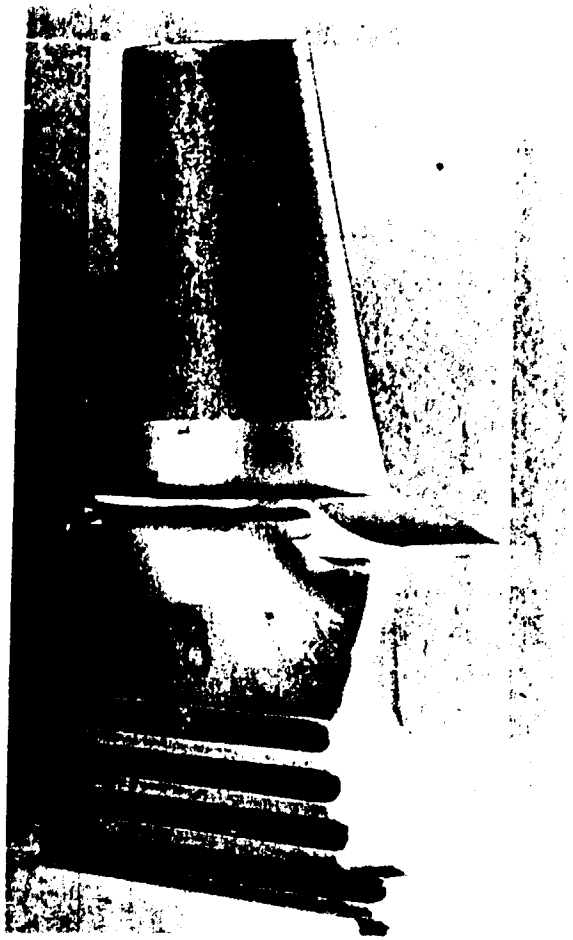

FUEL PUMP TURBINE
BLADE

Figure 2.2 SSME High Pressure Turbopump Blades

TABLE 2.1

Nozzle, Stator-Vane, and Rotor-Blade Data for Representative Turbines

Turbine	Type	D_m	Nozzle N			1st Rotor 1 - r			Stator S			2nd Rotor 2 -R		
			Z	H	b	Z	H entrance/exit	b	Z	H entrance/exit	b	Z	H entrance/exit	b
Mark 10	Reaction	34.90	61	1.55	3.00	119	1.862/2.484	1.50	130	2.604/3.372	1.50	109	3.683/4.223	1.50
Mark 15-F	Reaction	12.50	43	0.42	0.700	97	0.53	0.596	115	0.640/0.770	0.596	93	0.88	0.58
M-1-F	Reaction	23.00	37	1.492	2.175	80	1.741	1.350	67	1.931/2.309	1.360	78	2.683	1.50
Mark 38-F (HPFTP)	Reaction	10.19	41	0.884	1.0475	63	0.884	0.7375	39	0.984	1.0465	59	0.984	0.76
Mark 38-0 (HPOTP)	Reaction	10.09	47	0.490	0.850	78	0.497	0.600	41	0.670	1.030	73	0.672	0.65
Mark 48-F	Reaction	3.50	41	0.280	0.363	52	0.290	0.320	41	0.300	0.363	52	0.330	0.32

Notes:
D_m = pitch diameter, in.
Z = number of blades or vanes
H = height, in.
b = axial width, in.

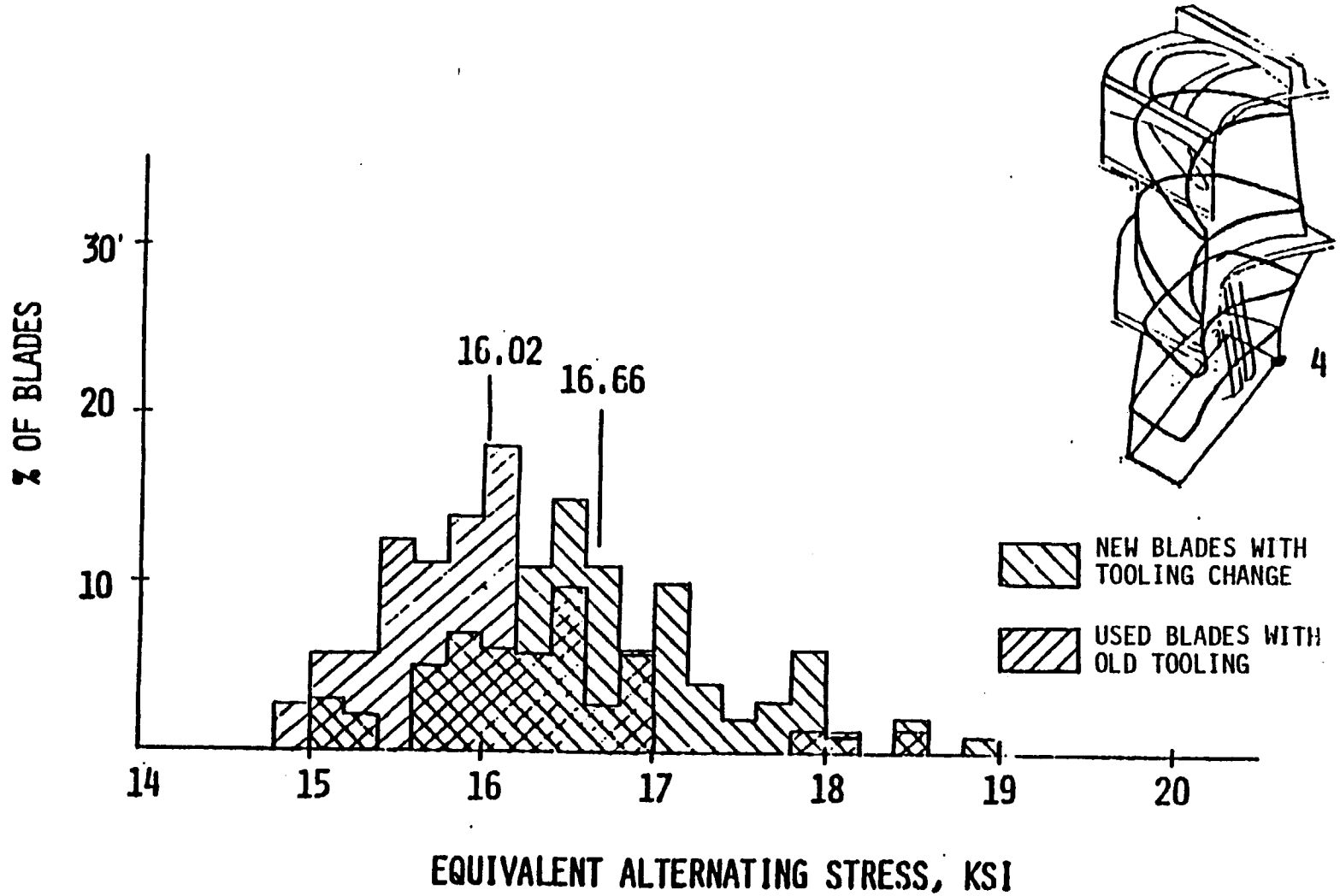

Figure 2.3 Impact of Geometrical Variations on Alternating Stresses

conventional alloys), variations in directionality of the material axes from blade to blade also need to be considered. The variations in apparent elastic properties with orientation is illustrated in Fig. 2.4 and Fig. 2.5. In general, blade acceptance criteria specify the maximum deviation of the primary axis with reference to stacking axis, usually 10. In some instances, the orientation of the secondary axes is also specified and controlled. The indirect variation in material properties due to the scatter in blade temperatures must also be considered.

It can be expected that any variations in boundary conditions can significantly affect the blade response. The variations in firtree tolerances can result in varying amount of fixity at the root of the blade. An effective calculation of the degree of fixity would require 3-D contact solutions with contactor surface algorithms. This is because the normal node-to-node contact elements presupposes contact points and do not handle satisfactorily the large tangential motion relative to normal motion at the contact surfaces. In addition, the variations in degree of fixity is related to the scatter in temperature distributions in the disk which vary with time.

Loadings on turbine blades are a major source of uncertainty in turbine blade analysis. There are variations between pump to pump, engine to engine and firing to firing. A summary of loads on the turbine blades is tabulated in Table 2.2. The blade is exposed to various types of loading during mission history profile as follows:

<u>Start Transient</u>

1) Rapid temperature excursions. A high enough rapid rate can result in surface yielding.

2) Transition through blade resonances -- upstream and downstream disturbances

3) Potential for rubbing

4) Centrifugal and gas forces

5) Gas generator disturbances

<u>Steady State</u>

1) Centrifugal and gas forces

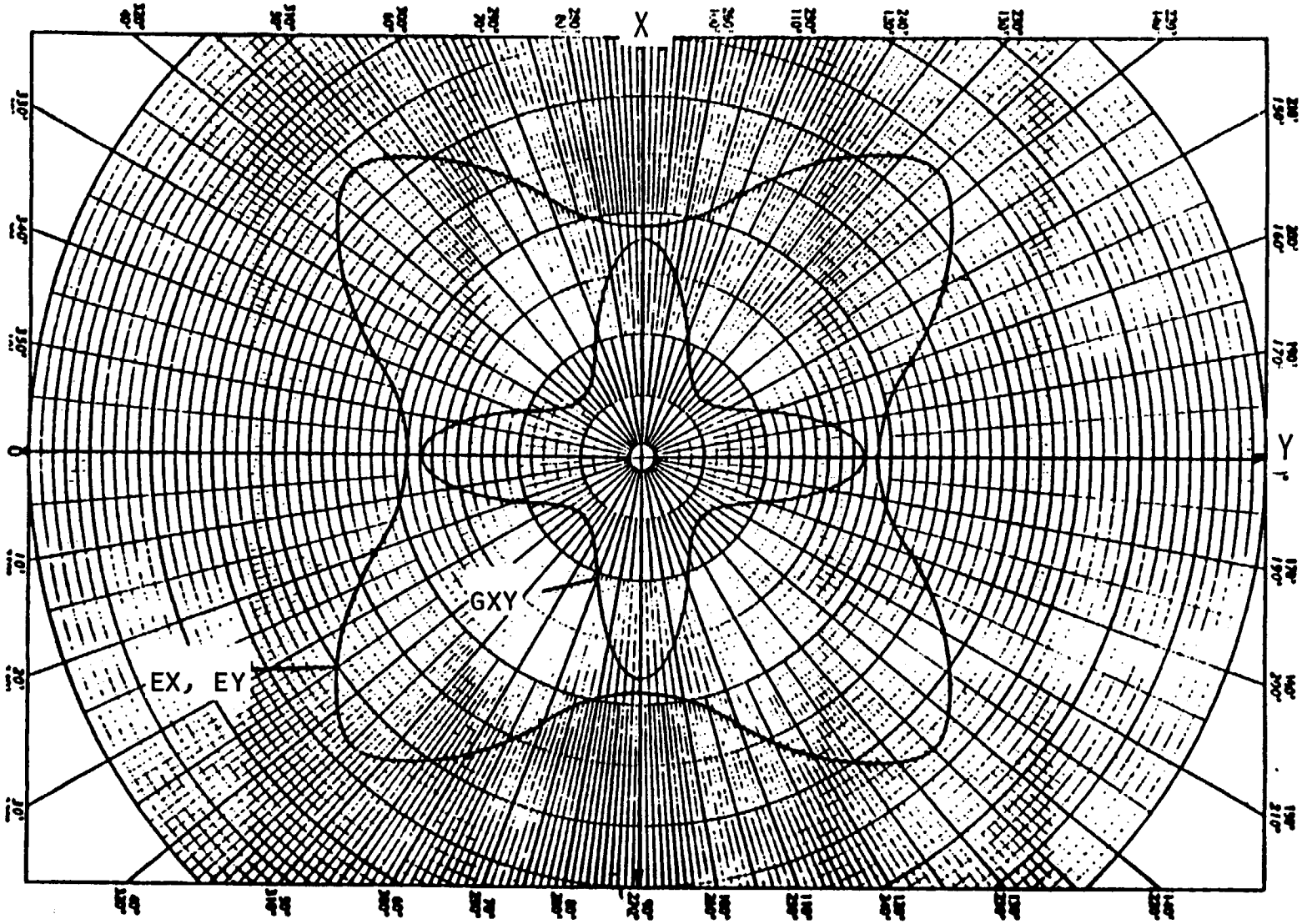

Figure 2.4 Effect of Orientation on Elastic Properties of MAR-M-246 (HF)

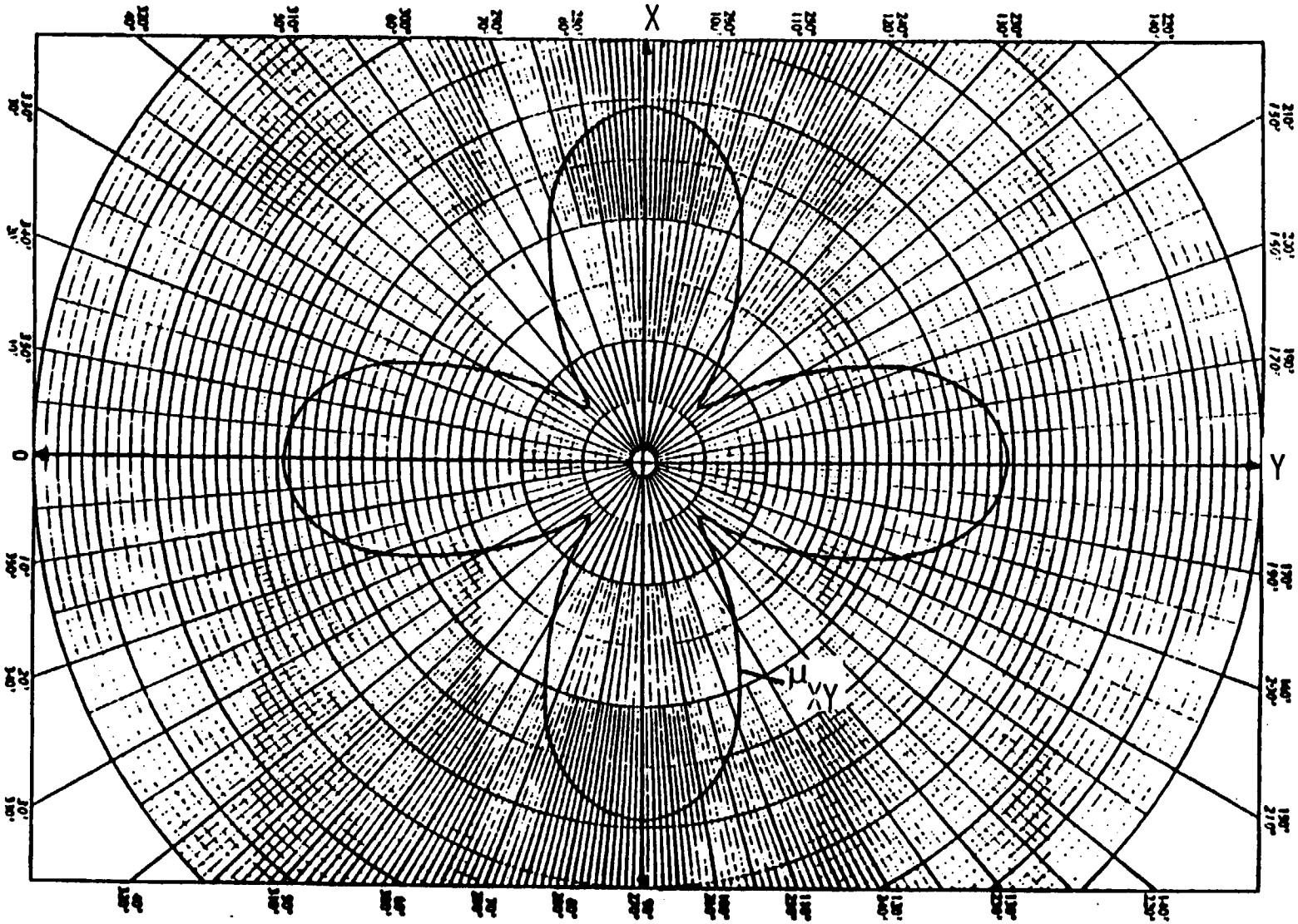

Figure 2.5 Effect of Orientation on Elastic Properties of MAR-M-246 (HF)

Table 2.2

Individual Load Summary on Turbine Blades

Individual Loads	How Determined	Form Available	Degree of Certainty	How Used
Centrifugal	Measured	Duty Cycle & Limits	High	Input to structural analysis
Static pressure and Δp	Predicted from turbine analysis	Pressure profiles at streamlines on air foil	Total magnitude high (torque) distribution moderate	Input to structural analysis
Dynamic pressure	Predicted from turbine analysis & cascade est. or tests	Pressure profile scaled to forcing function shape (*)	Moderate to low	Input to forced vibration analysis, Campbell diagram limits
Temperature	Predicted from turbine plus thermal analysis	Temperatures at locations throughout the blade	Steady state—high transient-low	Input to structural analysis
Debris	Predicted, based on history of incidents	Particle size and velocity	Low	Sensitive analysis or incident investigation

Table 2.2

Individual Load Summary on Turbine Blades (Continued)

Individual Loads	How Determined	Form Available	Degree of Certainty	How Used
Rubbing at seals	Predicted, based on observed marks on blades & seals	Load range	Low	Sensitivity analysis
Fabrication	Predicted/measured		Low	
Damper	Measured	Sample lot weight distribution	High	Inputs to structural anal., fatigue analysis
Friction	Measured/predicted based on whirligig tests & dynamic analysis	Range of values	Moderate based on measurements	Dynamics analysis forced vibration
Tolerance of blade & cross section	Measured/predicted based on lot blade measurements	Range of values	Moderate to high	Static analysis forced Vibration

2) Steady state thermal stresses

3) Flow disturbances

4) Power level excursions

Cutoff

1) Rapid temperature excursion

2) Transition through blade resonance

3) Potential for rubbing

4) Gas generator disturbances

The development of probabilistic load models for turbine blades is complicated due to the lack of detailed measurements from actual engine firings. For example, detailed surface temperature and surface dynamic pressure measurements are not available at transient or steady state conditions. A limited amount of data is available from instrumented turbopumps. There are plans underway for detailed measurements from heavily instrumented test bed engines. The development of probabilistic load models is the subject of a separate contract study.

2.2.2 LOX Posts

The LOX posts are injectors that introduce and meter the propellant flow to the combustion chamber (Fig. 2.6). Of the various types of injectors, the coaxial element type (Fig. 2.7) is particularly adapted to mixing of gaseous propellants such as hydrogen with liquid propellants such as oxygen. Typical injectors have many hundreds of LOX posts to obtain uniform combustion. In SSME there are three sets of injectors, two on the preburners and one on the main injector. There are 264 LOX posts in the fuel preburner, 120 LOX posts in the oxidizer preburner and 600 LOX posts in the main injector, all of different sizes and geometric characteristics. Distinguishing features of LOX posts used in several engines are illustrated in Table 2.3. The final LOX post assembly can have many components such as (Fig. 2.8) retainer, fuel sleeve, flow shields and heat shields. The distinguishing

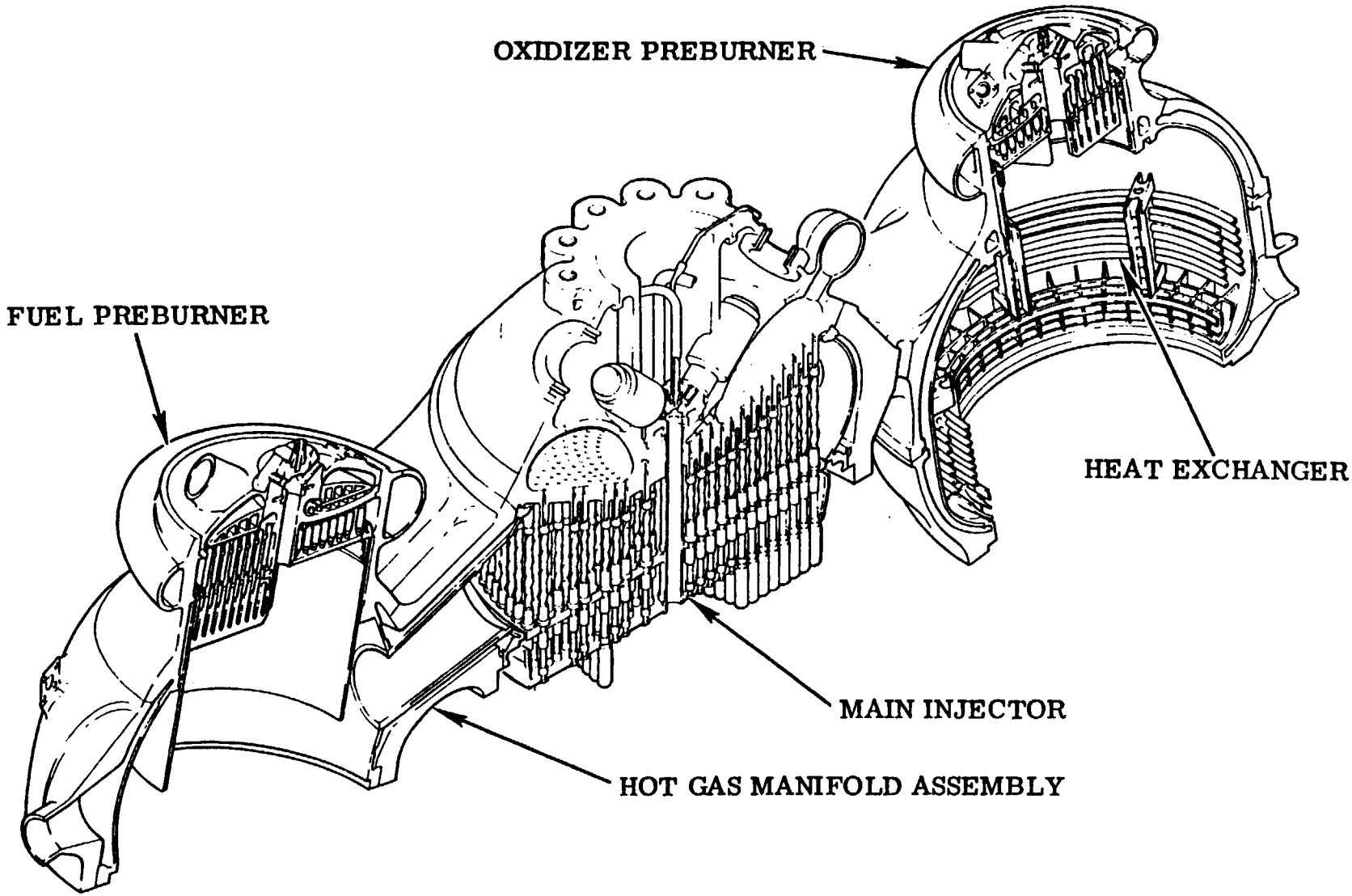

Figure 2.6 SSME Preburner Injectors and Main Injector Arrangement

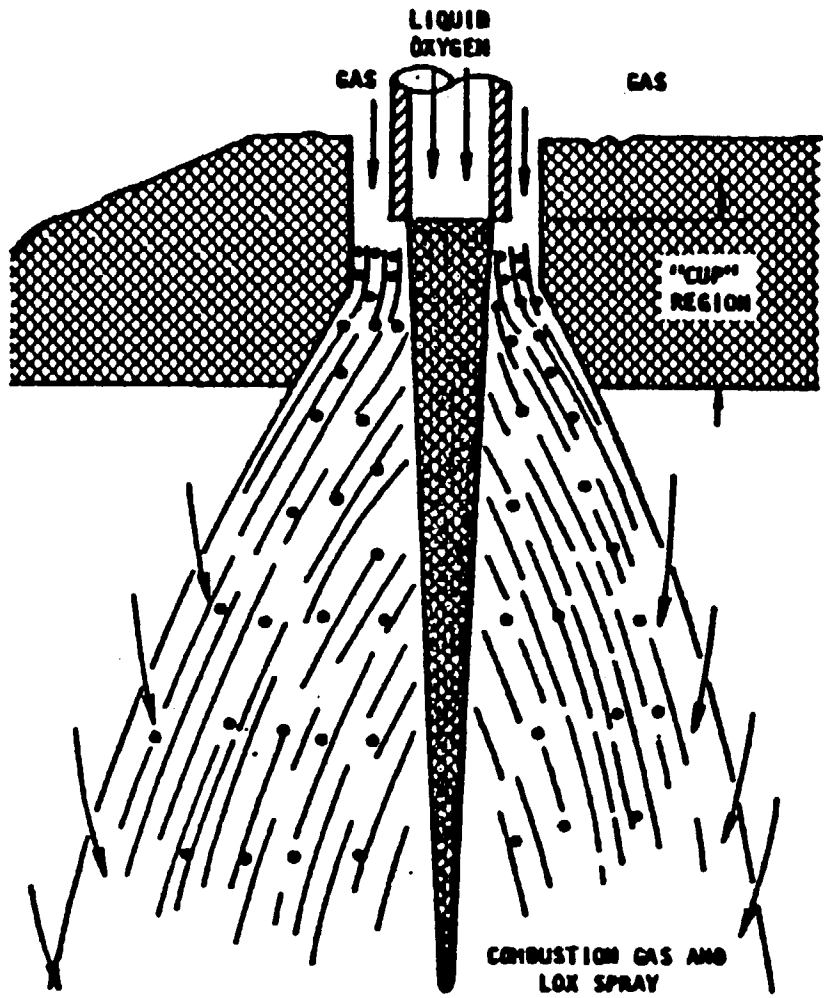

Figure 2.7 Atomization Concept in Co-axial Injectors

Table 2.3

Design Geometry of Co-Axial Elements (GH_2/LO_2) for Various Rocket Engines

Engine	#Coax Elements	(in) Fuel Sleeve Dia. (O.D.)	(In) OX. Post Dia. (I.D.)/O.D.	(IN^2) Area OX/Fuel	LB/S Flowrate per Element OX/Fuel	LBS Thrust/EL	Cup Recess	ΔP_{ox}	ΔP_{Fuel}	P_C	Injector Dia. (IN)	Injector Face to Throat Length	Contr. Ratio	ΔT Thermal LOX Temp	ΔT Thermal Fuel Temp
J2	614	.332	.182/.244	15.97/25.26	.741/.118	325.0	.200	207	102	787	18.50	17.926	2.30	180°R	195°R
M1	3248	.334	.210/.290	159.5/70.15	.831/.153	300.0	.231	335	175.0	1000.0	42.17	30.0	1.74	180°R	140°R
SSME M.C.C. (FPL)	600	.389	.188/.220	16.66/46.38	1.42/.4298	783.0	.255	641.7	251.2	3000.0	17.74	14.0	2.96	191	1444
J2S	614	.323	.119/.254	19.10/19.20	.849/.132	431.0	.200	210	130.0	1245	18.50	17.926	1.57	180	257
RL-10	216	.186	.014/.120	.9289/3.426	.130/.024	70.3		52.4	77.6	395.0	10.30	15.0	4.0	167	451
Adv. Exp. Cycle	108	.190	.094/.126	—	.247/.0357	—	.093	—	—	1540	5.0	20.0	3.85	183	660

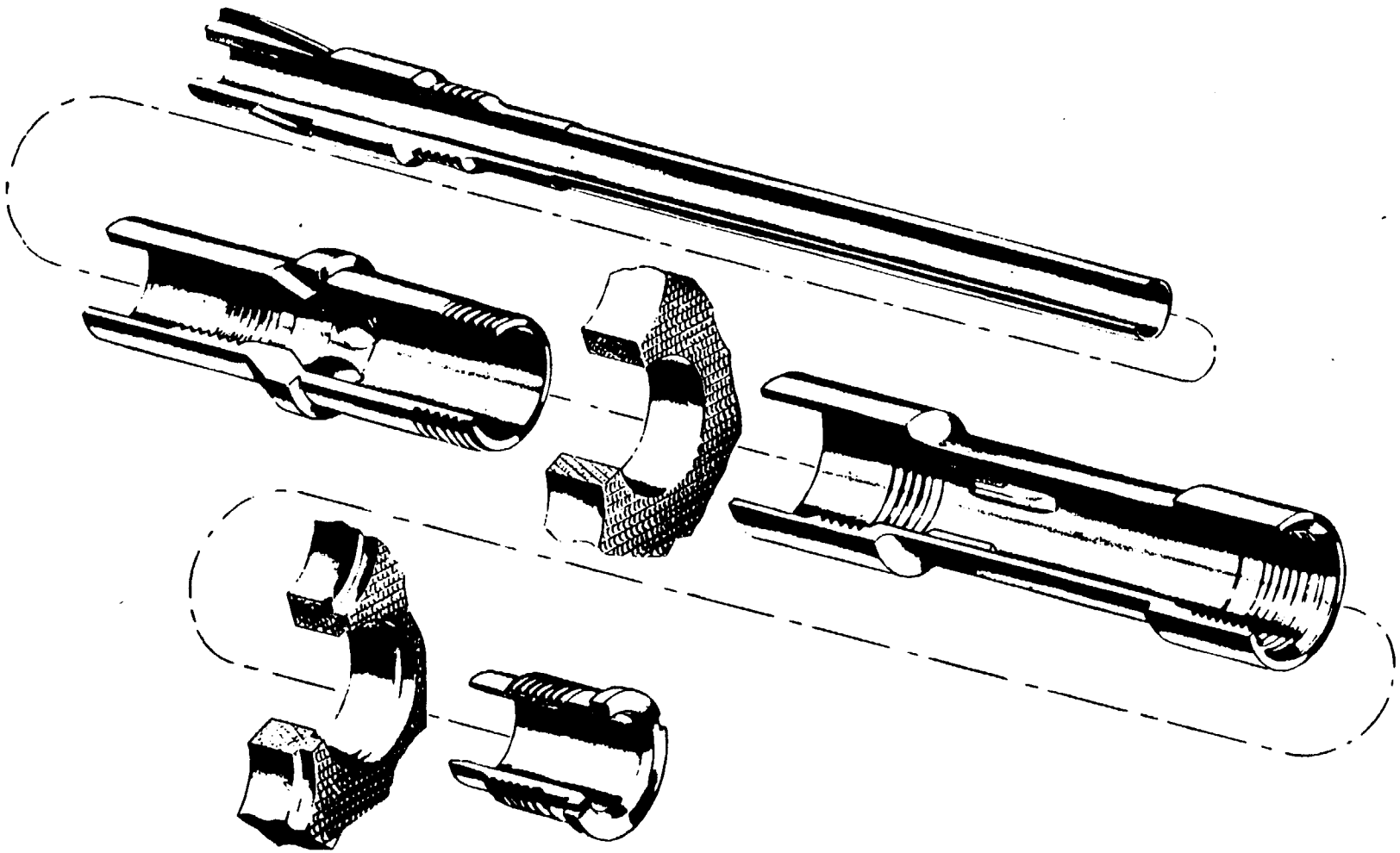

Figure 2.8 Typical Components of the Main Injector Element

feature of LOX posts used in staged combustion cycle engines is the high temperature differential present between the inner LOX (200R) and the outer hot gas (1400R). The parameters that might be considered in a probabilistic structural analysis methodology are:

1) Loading
2) Boundary conditions
3) Material property variations
4) Geometrical variations

The major loads on the LOX posts are:

1) Thermal loads
2) Pressure loads, static and dynamic
3) Mechanical vibration
4) Fluid-structure interaction loads

Thermal loads play a critical role in the design of LOX posts in engines having a staged combustion cycle. While there can be small fluctuations in LOX temperature, the metal temperature exposed to hot gas can vary. Fluctuations in local temperatures can occur with dislocations of heat shield and variable part-to-part contact effectiveness such as in threads. Variations in metal temperature can also occur due to variable heat transfer coefficients.

The pressure loads on injectors are a consequence of hot gas entering the injector and impinging on the posts. These streams are of high velocity and highly turbulent nature. The characteristics of the flow field that enter the injector are strongly dependent upon the geometry of duct upstream, as well as interface between injector bowl and transfer ducts. For example, the presence of separated flow regions upstream has a significant effect on the dynamic pressure environment seen by the posts. Analytical determination of high-frequency dynamic pressure fluctuations in complicated geometrical regions with tube banks is beyond the current computational fluid dynamics analytical capability. Dynamic high-frequency pressure measurements in the injector bowl from many engine tests are available. However, these measurements are mainly in

one location, and the loads seen by LOX posts can be different because of geometrical location variation. In addition, the correlation distance for pressure along the length of the post is unknown. Additional, more detailed measurements are planned for the test bed engine.

The mechanical vibrations that the LOX post see are combustion-related random vibration, pump-induced periodic vibration, transient vibration due to engine side loads and combustion pops. Extensive engine test measurements that have been taken with accelerometers can be used to construct load models that can then be used for multibase random vibration analysis of LOX posts.

Potential for fluid elastic excitation in LOX post arrays exist similar to the vibration observed in heat exchangers. This mechanism is characterized by a critical flow velocity below which vibration amplitudes are small and above which the amplitudes increase rapidly. A brief summary of loads on LOX posts is presented in Table 2.4.

The boundary conditions variation in LOX post can affect its response. The threaded connections in the assembly are used as positioning devices and are not preloaded. The conditions can vary from fixed to hinged conditions, and it can be nonlinear due to gaps.

Geometrical variations that affect the local stress concentrations assume importance in highly stressed fatigue critical components such as LOX posts. The parameters that fall into this category include surface scratches, their location and depth, variations in fillet radii and weld offsets.

LOX posts are generally constructed from materials with superior properties at elevated temperatures such as Haynes 188. The scatter in material properties also contribute to the probabilistic structural response.

2.2.3 Transfer Ducts

Efficient integration of an engine's major components such as preburners, turbopumps, main injector and thrust chamber is achieved in SSME through the use of a Hot Gas Manifold (HGM) (Fig. 2.9). Hot gases from preburners are ducted directly to the high-pressure turbines that then

Table 2.4

Individual Load Summary on LOX Posts

Individual Loads	How Determined	Form Available	Degree of Certainty	How Used
•Structural Dynamics •Transient: •Pops, Sideloads •Random Vibration •Steady State •Random Vibration •Random Periodic (Combustion Instability) •Steady State Sinusoidal	Accelerometers (Measured)	Time Traces, PSD's Isoplots, AMS, Trace Summaries or Plots	High	Input to Dynamic Analysis
•Flow Loads •Fluid Excitation (Sinusoidal) •Turbulence (Random) •Vortex Shedding (Random) •Jet Impingement (Sinusoidal)	•Instrumented Flow Tests •Engine Pressure Measurements •Limited Strain Gage Responses	PSD, Spectrum of Levels (GGIP) Analytical Model's Water Table Test Pictures	Low to Moderate	Input to Dynamic Analysis

Table 2.4

Individual Load Summary on LOX Post (Continued)

Individual Loads	How Determined	Form Available	Degree of Certainty	How Used
Temperature Loads	Predicted Flow Test Measurements	Temperature Field on Geometry Cross-Section(s)	Moderate	Input to Structural Analysis
Static Pressure	Measured and Calculated	Distributed Values on Post Surface	Moderate to High	Structural Analysis
Debris	Predicted, Based on History of Engine	Debris Size and Velocity	Low	Sensitivity Analysis or Incident Investigation
Static	Engine Loads Analysis	Table	Moderate	Structural Analysis
Fabrication	Predicted	Analysis Results	Low	Structural Analysis
Damping	Correlate from Strain Gages Predicted-Row 13, Life Comparison Other Rows	Table	Moderate	Dynamic Analysis

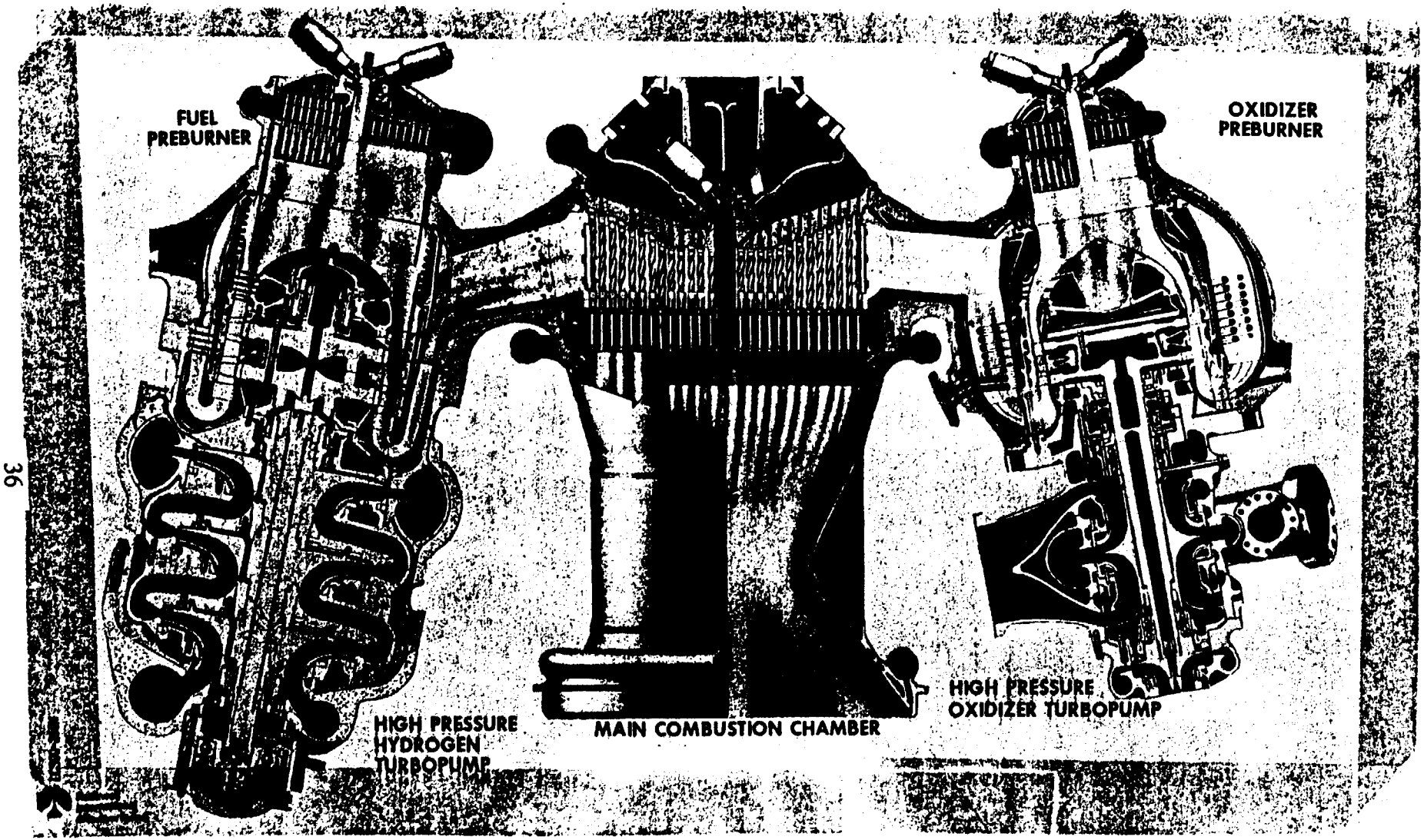

Figure 2.9 SSME Powerhead Component Arrangement

discharge the gas to a toroidel manifold. The hydrogen-rich gas is then routed to main injector torous through the transfer ducts, two on the oxidizer side and three on the fuel side. The transfer ducts, commonly of circular cross section, contain an outer structural shell, a structural liner and a scrub liner (Fig. 2.10). The structural shell is kept cool through hydrogen coolant circulating between the structural liner and the outer. The scrub liners protect the structural liner from the direct impingement of hot gas and keep their bulk temperature low. The scrub liners are usually cantilevered to have unrestrained thermal expansion and also contain motion limiters to reduce lateral deflections. Extensive engine experience has indicated few problems with the outer case structural shell of the hot gas manifold. However, inner liners are subjected to environments and forces not well understood, and it is considered more appropriate to a treatment based on a probabilistic approach. The parameters that can be considered as variables in transfer tube liner analysis are: 1) loading, 2) geometry boundary conditions, and 3) material property variations. The loadings on the transfer tube liner analysis that should be considered are:

1) Thermal loads
2) Pressure loads
3) Vibration loads

The thermal loads on the transfer tube liners are dependent upon design philosophy and geometrical considerations. While measured turbine discharge temperatures are available, the gas temperatures in the transfer tubes themselves have not been measured. Currently, temperature calculations are based on engine system models. Variations in flow conditions of gas and coolant temperatures affect the thermal load on liners.

The static pressure load on the structural liner is due to the differential pressure between the hot gas and coolant. The dynamic pressure oscillation on the transfer tube liners is closely related to the hot gas flow circuit. The sources of pressure oscillation on the transfer tube liners have been identified to be boundary layer noise and the flow separation effects.

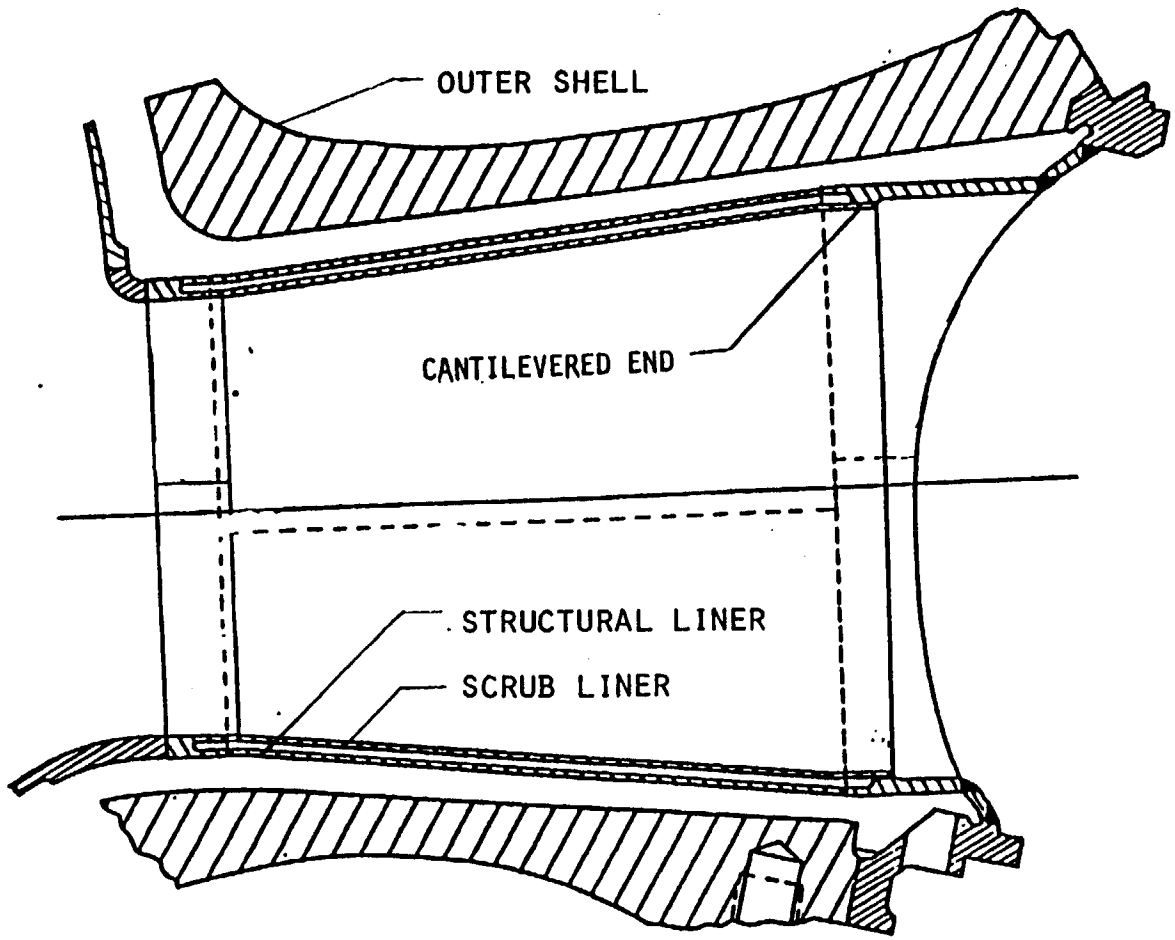

Figure 2.10 Scrub Liner and Structural Liner Concept Used in Transfer Tube Design

High-frequency dynamic pressure measurements in the transfer tubes from hot fire measurements are unavailable due to the difficulty of instrumentation that can survive the hostile environment. However, air flow test measurements at transfer tube inlets are available, which can be scaled to obtain engine pressures at FPL. No measurements are available to establish the correlation distances of pressures circumferentially, as well as longitudinally along the transfer tubes.

Extensive measured data from accelerometers mounted on the hot gas manifold are available to construct load models. Multibase sinusoidal and random vibration techniques can be used to analyze transfer tube liners subjected to mechanical vibration. A brief summary of loads on transfer tube liners is presented in Table 2.5.

The geometrical variations in transfer tube liners include variation in thickness, weld mismatches and motion limiter gap variations. Because of the difficulties of inspection in double-walled structures, variations in gap distances in motion limiters can be expected.

2.2.4 Other Candidate Components

The other candidate components that were studied included high pressure oxidizer duct, nozzle feed line and main combustion chamber wall. The fourth component can be selected based on:

1) its being a commonly used component in every type of rocket engine, or
2) the component is subjected to loads that are peculiar to rocket engines and is amenable to a probabilistic analysis treatment, or
3) the analysis of the component will exercise a structural analysis methodology that is being implemented in the computer codes that will not be exercised by the previously selected three components.

Falling into the first category are the ducting systems, which are used in all rocket engines. Ducting systems are used as component interconnects in the engine or used as vehicle-to-engine interconnects. They are used to transport fluids or gases under pressure. A brief summary of lines used in SSME is given in Table 2.6.

Table 2.5

Individual Load Summary Transfer Ducts & Liners

Individual Loads	How Determined	Form Available	Degree of Certainty	How Used
•Structural Dynamics •Transient •Sideloads •Random •Steady State •Random •Sinusoidal	Accelerometers (Measured)	Time Traces, PSD's, Isoplots & Summaries of Plots	High, although measurement on HGM Shell not directly on component	Input to dynamics analysis
•Static Pressure Structural Analysis •Average Cross Section •Transient with Chugging •Steady State •Coolant Flow and Liner ΔP •Circumferential Variation	Calculated from engine models and airflow tests		Moderate	

Table 2.5

Individual Load Summary Transfer Ducts & Liners (Continued)

Individual Loads	How Determined	Form Available	Degree of Certainty	How Used
•Dynamic Pressure •Turbulence •Flow Operation	Calculated From Airflow Tests and Scaled to Engine Operation	PSD'S	Moderate to Low	Input to Dynamic Analysis
•Temperature Loads	Predicted	Temperature Field on Geometry Cross-Section	Moderate	Input to Structural Analysis
•Debris	Predicted, Based on History of Engine	Debris Size and Velocity	Low	Sensitivity Analysis or Incident Investigation
•Fabrication	Predicted	—	Low	Structural Analysis

Table 2.6

Summary of Interconnects

Articulating Main Propellants	Fluid Interface Lines	Component Interconnects
LPFTP Pump Discharge LPFTP Turbine Drive LPFTP Turbine Discharge LPOTP Pump Discharge LPOTP Turbine Drive	ARTICULATING Fuel Bleed Oxidizer Bleed Oxidizer Tank Pressurant FLEX HOSES Hydraulic Supply Hydraulic Return Engine Gaseous Nitrogen Supply Engine Helium Supply Oxidizer Bleed HARD LINES Fuel Tank Pressurant	HARD LINES HPFTP Discharge Preburner Fuel Supply HPOTP Discharge Preburner Oxidizer Supply Heat Exchanger Supply HGM Coolant Duct Preburner Pump Supply FLEX HOSES Pneumatic Shutdown Control Fuel Pump Liftoff Seal Control

Falling into the second category are nozzle feed lines, which are used in regeneratively cooled nozzles as is the case in SSME (Fig. 2.11). The nozzle feed lines carry the liquid hydrogen propellant to the lower inlet manifold. The coolant flows from lower inlet manifold up the tubes that form the nozzle wall and into the upper collection manifold. The nozzle feed lines are attached to the nozzle at selected hat bands of the nozzle. One of the primary loads that need to be considered in flexible lightweight nozzles and their attachments design is the fluid dynamic load. In large expansion ratio nozzles, at sea level firing, flow separation occurs at start and cutoff transient. This has been observed in SSME as well as in J-2 engine (an upper stage Saturn engine) firings at sea level. This results in side loads and shock transients. Typically, the side loads result in a bell mode distortion of the nozzle. A statistical summary from 186 engine tests of the J-2 engine side load study is presented in Fig. 2.12. The plot presents the variation in moment developed at gimbal point due to side loads. The response of the nozzle due to side loads is primarily in the low-frequency range. Another aerodynamic load that needs to be considered is the formation of shock at nozzle exit during start and cutoff transients. Tests have shown that large pressure oscillations in the lower half of the nozzle occur because of the attachment and detachment of flow from the nozzle wall at a higher frequency range of 200 to 400 Hz. The resulting peak strains due to this shock transient (Fig. 2.13) is a statistical quantity. Typically, the peak strains occur for only one cycle and the magnitude of peak strain varies from test to test. Thus, the low cycle fatigue life calculations for nozzle feed line is based on probabilistic considerations.

Falling into the third category is the analysis and design of the main combustion chamber wall. To analyze this structure adequately, the standard structural considerations of strength, creep, and low cycle fatigue must be supplemented by a cyclic thermal ratchet analysis termed cyclic creep. The SSME main combustion chamber operates in an environment in excess of 3000 psi chamber pressure at approximately 6500R combustion gas temperature. These conditions produce a heat flux of approximately 100 Btu/inch^2-sec in the life limited throat region. The chamber

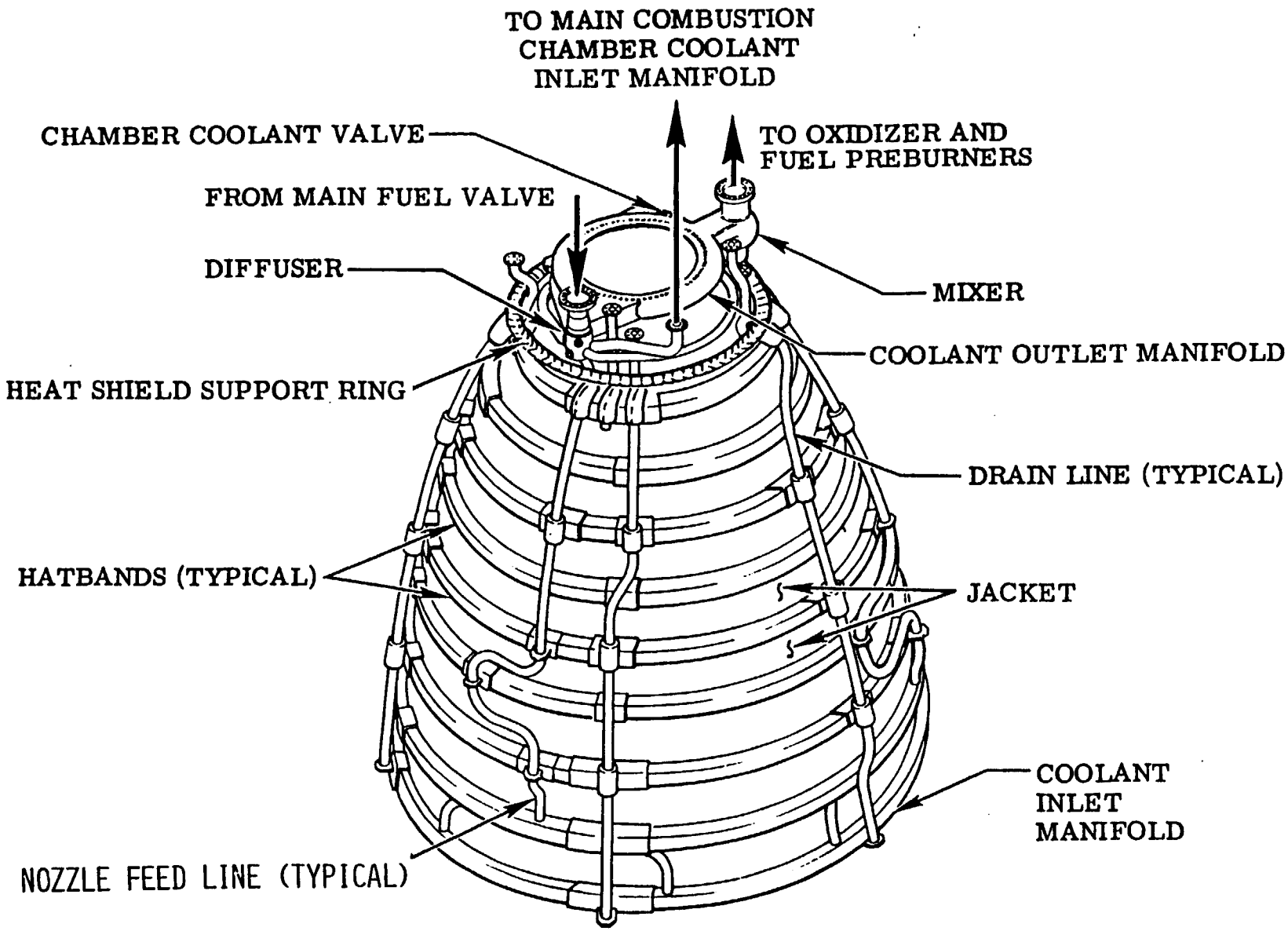

Figure 2.11 SSME Flight Nozzle Configuration

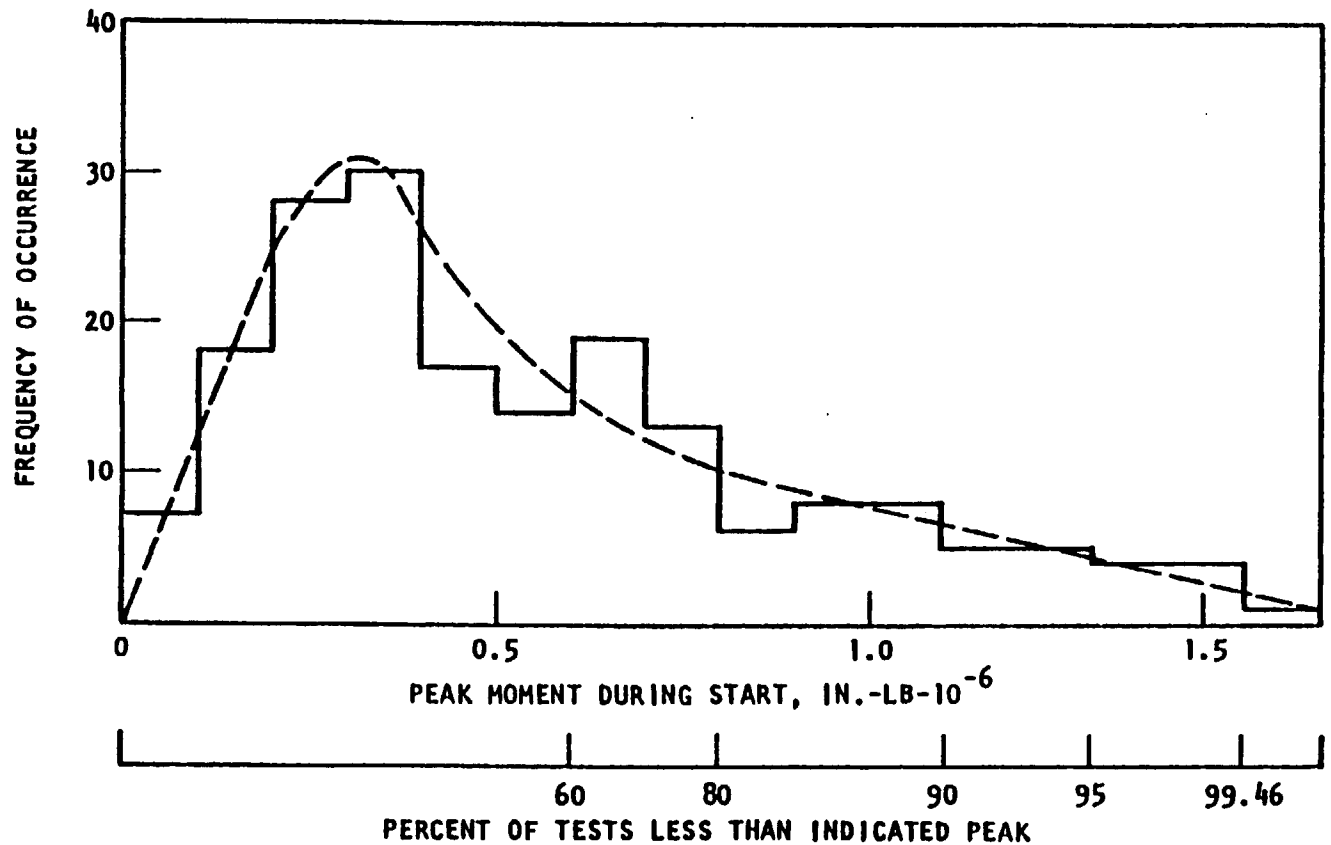

Figure 2.12 Summary of J-2 Engine Maximum Side-Load Moments About Gimbal Point (Reconstructed from 0.5 to 5.0 Hz Data from 186 Engine Tests)

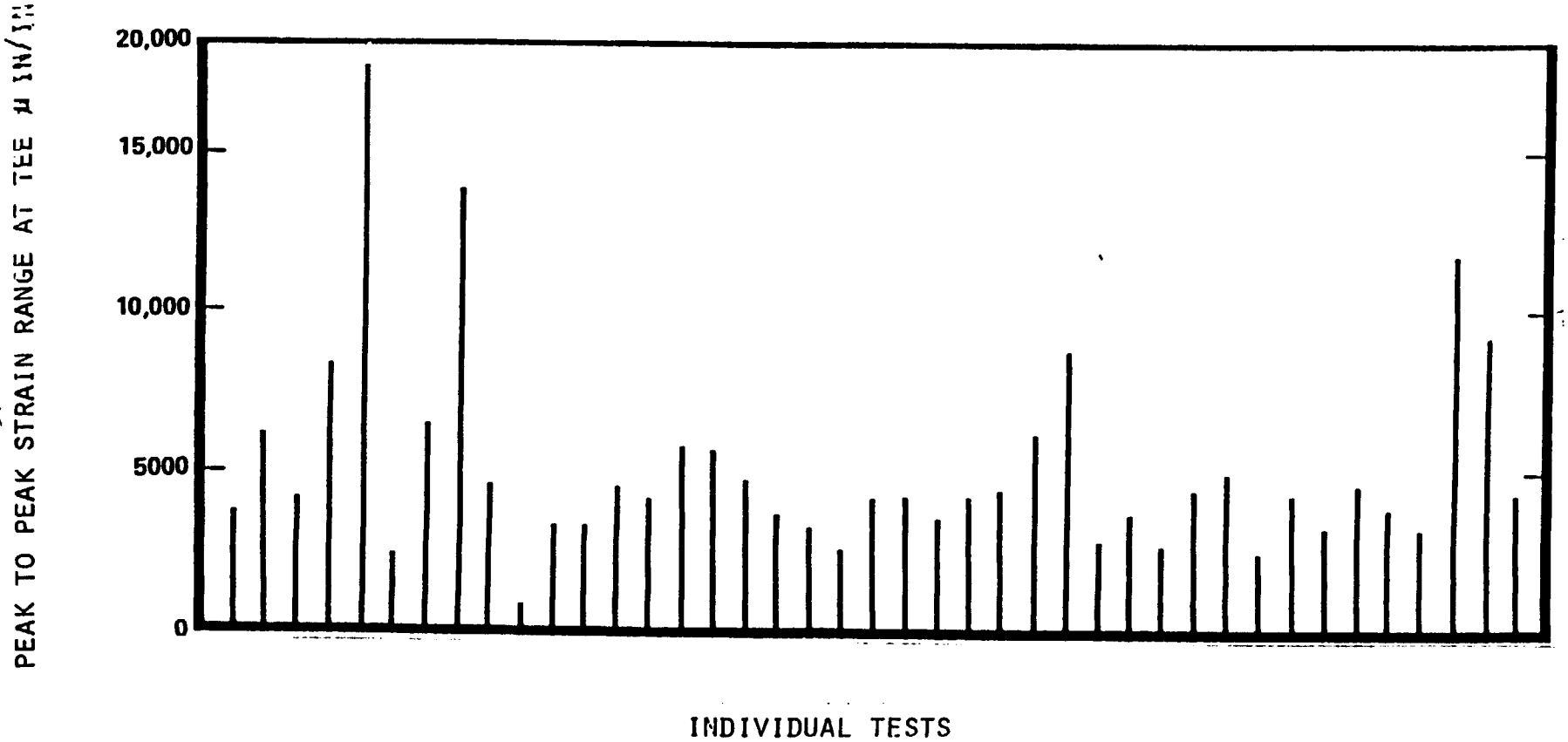

Figure 2.13 History of Maximum Strains

walls are regeneratively cooled using rectangular cooling channels (Fig. 2.14). After a series of duty cycles, the geometry of the channel cross-sectional wall distorts, thins along the channel hot wall and cracks (Fig. 2.15). For SSME MCC, cyclic creep occurs locally at hot spots with other biased conditions accentuating the cyclic creep phenomenon. The other biased conditions are pressure, creep-relaxation effects, material strength effects and the liner support. Probabilistic considerations in MCC chamber wall design should include local hot spot temperatures, which is the result of injector anomalies rather than a general deficiency in cooling capacity. The other parameters that might be considered include material property variations (cyclic stress-strain curves) and local surface roughness, which contribute to increased heat load.

2.2.5 Recommended Fourth Component — High Pressure Oxidizer Duct

The fourth component that is recommended is the SSME high pressure oxidizer duct (Fig. 2.16). The analysis of the duct using PSAM offers the following benefits:

1) A duct is a component that is common to all rocket engines. A new dimension in the analysis and design of the ducts is the high energy content of the fluids present in staged combustion cycle engines operating under high pressure. With the reduced system weight, fluid-induced vibrations can play a critical role in their design.

2) The duct provides an opportunity to exercise PSAM codes without being burdened with complex models involving many thousands of degrees of freedom. By modeling the ducts using simple beam elements, it offers an opportunity to conduct a Monte Carlo simulation of realistic models and compare the results with fast probability methods implemented in PSAM codes.

3) The ducts are typically subjected to many types of loads and the current methods of load combinations is very conservative. It provides an opportunity to study the load combination problems.

4) Further, experimentally measured data is available from actual engine firings for the high pressure oxidizer duct.

The high pressure oxidizer duct is one of the many propellant ducts present in the SSME fluid component system. A brief summary of the major propellant ducts used in SSME is presented in Table 2.7. The duct is subjected to thermal loads, static and dynamic pressure loads, gimbaling and acceleration loads, misalignment, and shock transient loads. Loads are combined in a

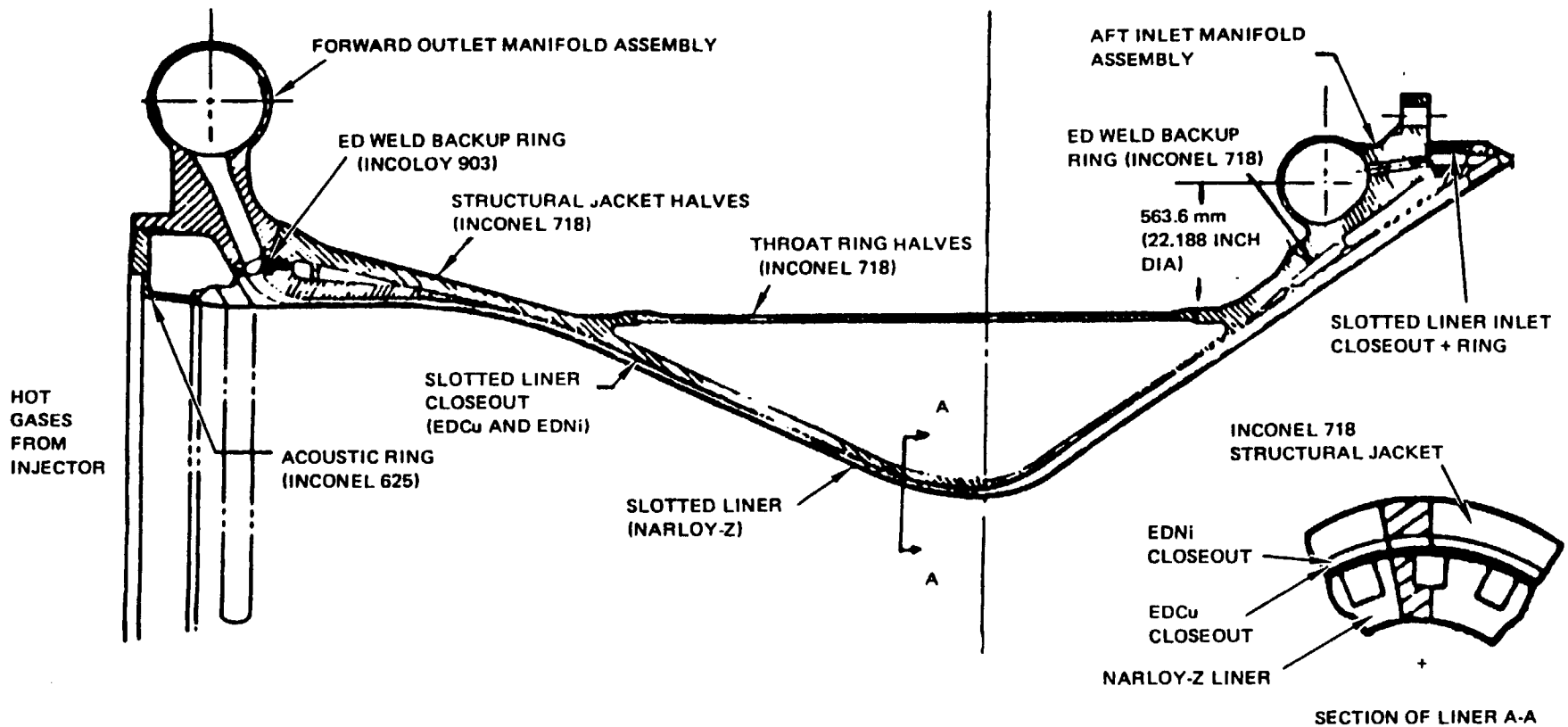

Figure 2.14 SSME Main Combustion Chamber Materials and Configuration

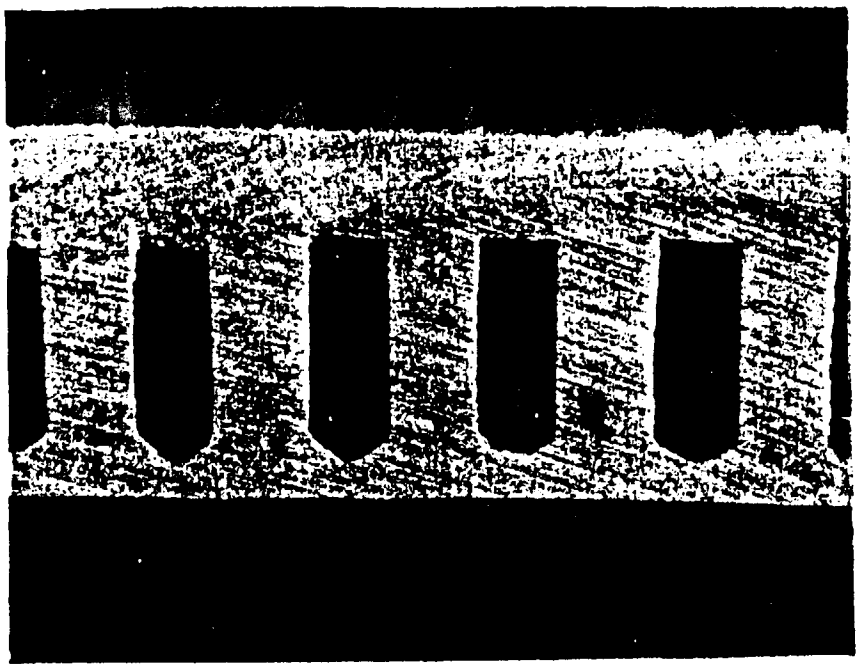

Figure 2.15 Throat Section of SSME-MCC Showing Thinned Hot Gas Wall

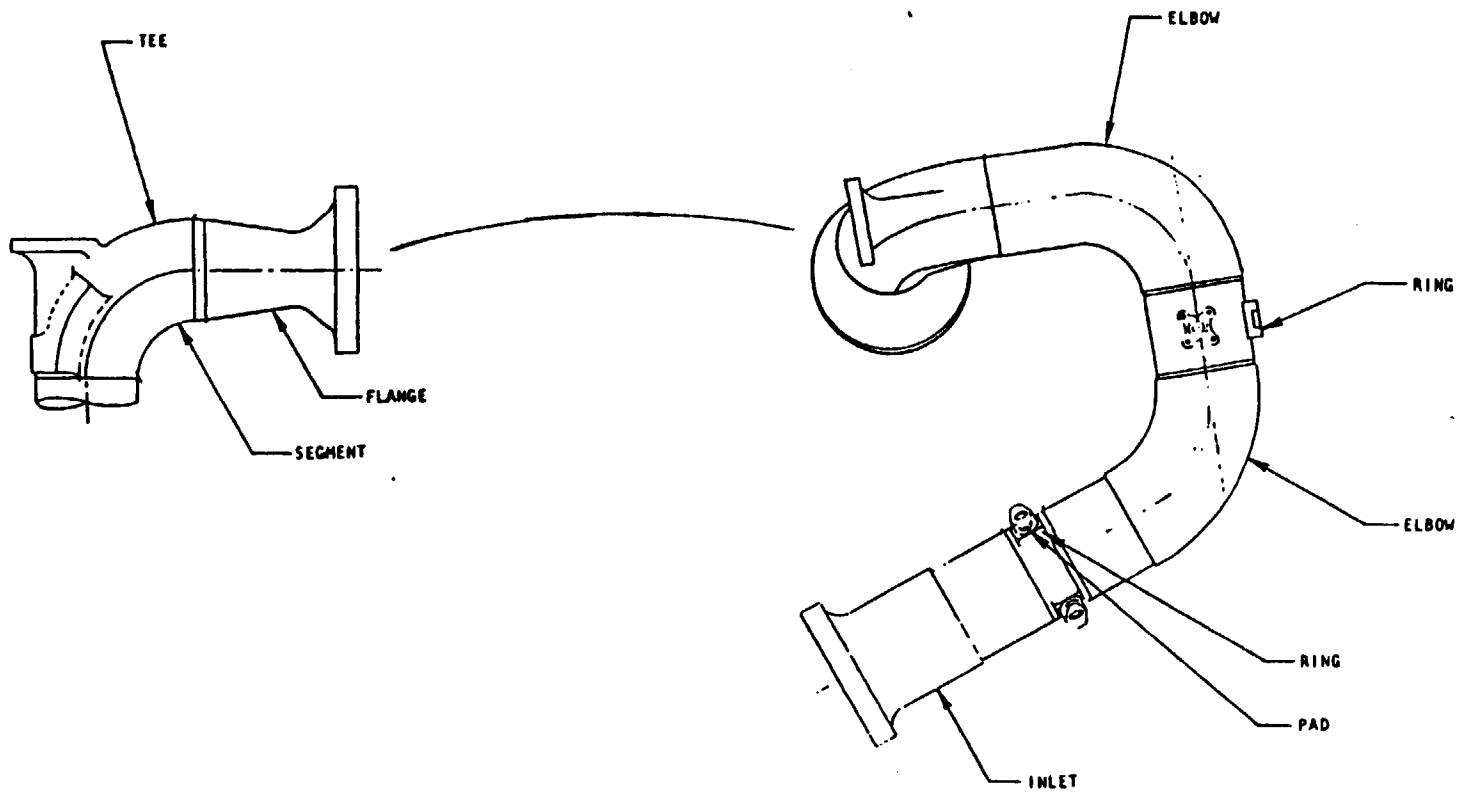

Figure 2.16 High Pressure Oxidizer Duct

Table 2.7

Summary of Major Propellant Ducts

	Description	Hard or Flexor Base	FPL (Max) Does Not Incl. Surge PSI Pressure	°R Temp.	I.D.	Thickness Range	Material	Typical Radius	Elbow Max. Angle	Thickness
A	Hydrogen									
1)	Low Pressure Fuel Pump Discharge	FLEX	311 (343)	45	5.20	28/.150	INCO 718 ALLOY 21-6-9	6→13	90°	.026/.063
2)	Low Pressure Fuel Pump Turbine Drive	FLEX	5307	472	2.00	.118/.270	INCO 903 TI 6-6-2	2.80/6.00	90°	.118.166
3)	Low Pressure Fuel Pump Turbine Discharge	FLEX	3871	457	2.70	.096/.274	INCO 903 TI 6-6-2	6.80	90°	.095/.170
4)	High Pressure Fuel Pump Discharge	RIGID	7221	110	3.40	.131/.203	TI 5.25	4.00	90°	.131/203
5)	Preburner Fuel Supply	RIGID	6437	289	2.00 ↓ 3.60	.089 ↓ .192	INCO 903	2.50 ↓ 6.00	50°	.089 .193
6)	Hot Gas Manifold Coolant Duct	RIGID	3784	457	2.30 ↓ 2.70	.069 ↓ .155	INCO 903	4→6	95°	.071 .110
7)	Fuel Bleed	FLEX & RIGID	300	110	1.245	.060	ALLOY 21-6-9	1.50/2.50	90°	.040/.060
8)	Fuel Tank Pressurant	RIGID	3871	457	.560	.0855	ALLOY 21-6-9	2.50	90°	.077/.096

Table 2.7

Summary of Major Propellant Ducts (Continued)

	Description	Hard or Flexor Base	FPL (Max) Does Not Incl. Surge PSI Pressure	°R Temp.	I.D.	Thickness Range	Material	Radius	Elbow Max. Angle	Thickness
B	Oxidizer									
1)	Low Pressure Oxidizer Pump Discharge	FLEX	554 (695)	178	6.30	.032→.160	INCO 718	12.00	90°	.032→.160
2)	Low Pressure Oxidizer Pump Turbine Drive	FLEX	4902	205	2.30	.090→.287	INCO 718 TI 6-6-2	3.50	90°	.086→.180
3)	High Pressure Oxidizer Pump Discharge	RIGID	4902	205	-4.000	.104→.270	INCO 718	4.50	90°	.104→.127
4)	Preburner Pump Oxidizer	RIGID	4801	205	2.3	.084→.120	INCO 718	2.75	90°	.084→.134
5)	Heat Exchange Oxidizer Supply	RIGID	4770	205	.555	.026→.075	INCO 718 INCO 628	2.00	90°	.026→.035
6)	Oxidizer Bleed	RIGID	230	554	.68	.030→.063	CRES 321 INCO 718	2.25	MOCK-UP	.026→.030
7)	Oxidizer Tank Pressurant	FLEX & RIGID DUCTS	4460	990	1.00	.138→.285	INCO 718	3.50	90°	.142→.172
8)	Preburner Oxidizer Supply	RIGID	8309	221	1.982 1.097	.096→.205	INCO 718 INCO 675	4.50	90°	.101→.209

conservative manner to calculate life. Geometrical uncertainties in the duct system include variations in thickness, weld mismatches and spatial geometry variations. A probabilistic structural analysis of duct could account for load variations and methods of load combination, material property and geometry variations.

3.0 CONCEPTS OF PROBABILISTIC STRUCTURAL ANALYSIS

3.1 Introduction

As stated in Section 1, a major goal of the PSAM program is to develop a probabilistic finite element code utilizing the state-of-the-art probabilistic structural analysis methods for select space propulsion system components discussed in Section 2.

The objective of this section is to introduce, in a broad sense, the concept of probabilistic structural analysis. Probability analysis methods that are applicable to the PSAM program are reviewed. Techniques currently being applied to develop the code are discussed in Sections 4 and 5. It is anticipated that more probabilistic methods will be applied in the remaining years of the PSAM program.

Many approaches have been developed during the past 20 years in the formulation of structural reliability, in the art of modeling uncertainty, and in the development of efficient analytical and numerical tools for the determination of structural reliability. It is generally believed that the theory of structural reliability analysis is sufficiently developed. For instance, it has been suggested [3.1] that the only areas that require further fundamental research are the damage accumulation and aging phenomena and certain cases of system reliability and stochastic dependencies of uncertain variables in parametric problems.

However, most of the structural reliability methods were developed for civil structures. Therefore, substantially modified or new methods might be needed for use in the PSAM program. In particular, the stochastic finite element methods [3.2 to 3.6] have not been developed to a state where reasonably accurate (i.e., better than Mean Value First Order Second Moment method as described in Section 4) probability analyses can be done efficiently for complicated, realistic problems involving a large number of random variables or random processes.

The fundamental problem in probabilistic structural analysis may be stated as follows: Given a function $f(\underline{X})$

$$Z = f(X_1, X_2, ..., X_n) \tag{3.1}$$

where X_i are the given stochastic processes or random variables, determine the probability distribution of Z.

Probabilistic structural analysis generally involve time-dependent problems where part or all X_i are correlated stochastic processes and Z is a function of the system responses such that $f(\underline{X})$ can only be computed using complicated finite element methods or other numerical algorithms.

In many cases, the time-dependent problems may be simplified. For example, consider a time-varying load $F(t)$ on a given structure. At any time t there is a distribution associated with $F(t)$, and $F(t)$ must generally be considered as a random process. However, when dealing with time-varying load in connection with barrier-crossing problems, in which interest lies in the probability of the response process staying within specified bounds during the expected life time of the structure, the required information is the distribution of the maximum value of the loading process, which may be closely approximated by the asymptotic extreme value distribution. In such cases $F(t)$ may be treated simply as a random variable.

When there are many time-varying loads, the methods of "load combinations" are available [Ref. 3.7]. In general, however, time-dependent problems for systems or even components are difficult to generalize. Therefore, some approximations regarding time-varying functions may be needed.

There are other important issues in probabilistic structural analysis that need to be addressed. Methodologies must be established to properly model both the statistical uncertainty (due to finite sample size) and modelling uncertainty (due to approximation of mathematical models for the mechanical behavior of structural components). A methodology to compute confidence levels in the calculated probability must also be developed for the PSAM program.

3.2 Basic Definitions

For the purpose of a generalized formulation, define the cdf (cumulative distribution function) of Z at z_0 as

$$F_Z(z_0) = P[Z < z_0] \tag{3.2}$$

and define a "g-function" as

$$g = Z - z_0 \tag{3.3}$$

then,

$$F_Z(z_0) = P[g < 0] \tag{3.4}$$

In structural reliability, g is called the "performance function," or "limit state function." It is defined such that $g = 0$ is the limit state, and $g \leq 0$ is the event of failure. The reliability methods used in NESSUS are based on the g-function formulations (see Section 4).

Consider a component reliability problem with one failure mode. The probability of failure, for a single g-function, is

$$p_f = \int_{g \leq 0} f_{\underline{X}}(\underline{x}) d\underline{x} \tag{3.5}$$

where $f_{\underline{X}}(\underline{x})$ is the joint probability density function of the design variables. The probability of success (or reliability) is its complement, i.e., $1 - p_f$.

3.3 General Formulation of the Reliability Analysis Methods

When the number of random variables is large and the probability of $g \leq 0$ is small it is difficult to compute the multiple integral (Eq. 3.5) accurately and efficiently, noting that the g-function is generally non-linear and the joint distribution function is generally non-normal. To overcome the difficulties, some approximation methods have been developed [3.8 - 3.15]. These methods usually involve some variable transformation schemes.

In the general cases which involve correlated non-normal $\underline{X}$, the Rosenblatt transformation [3.16] can be used to generate uncorrelated normal variables as follows:

$$
\begin{aligned}
u_1 &= \Phi^{-1}[F_1(x_1)] \\
u_2 &= \Phi^{-1}[F_2(x_2 \mid x_1)] \\
&\vdots \\
u_n &= \Phi^{-1}[F_n(x_n \mid x_1, \ldots, x_{n-1})]
\end{aligned}
\tag{3.6}
$$

where u_i are the standard normal variables, Φ^{-1} is the inverse of the standard normal cdf, and $F_i(x_i \mid x_1, x_2, x_{i-1})$ is the conditional cdf of the i-th random variable, given that the previous variables have the values x_1, x_2, x_{i-1}. After the transformation, the probability can be estimated more easily in the "u-space".

In practice, it is difficult to collect sufficient experimental data to establish joint probability distributions. For PSAM applications, it seems more likely that the information about the joint distribution can be characterized by marginal distributions and the associated correlation coefficients.

Assuming that marginal distributions and the correlation coefficients can be defined, a probability analysis procedure suggested by Der Kiuregian and Ke [3.17] can be used which requires a transformation from the non-normal variables to the standard normal variables. In this context, an efficient procedure for determining the transformed normal correlation coefficients using a series expansion has been developed for PSAM (Section 5, Volume III). In Section 4, a special case, which assumes that the transformation to the normals has already been made, is presented to demonstrate the procedure for generating uncorrelated normals.

3.4 First-Order and Second-Order Reliability Analysis Methods

There are many approximation methods available for fast probability computations. In general, these methods approximate the g-function by expanding g at the "design point" where the

probability of occurrence reaches its maximum on $g(\underline{u}) = 0$. It is now common to categorize the methods in accordance with how an exact g-function is being approximated. The First-Order Reliability Method (FORM) assumes linear g-function. The Second-Order Reliability Methods (SORM) are based on the assumption of a quadratic g-function.

The first-order probability estimation is

$$p_f = \Phi(-\beta) \tag{3.7}$$

where Φ is the standard normal cdf and β is the "minimum distance" from the origin to the limit state in the u-space. FORM is "fast" because it requires only the determination of the design point which defines β.

To illustrate, consider a linear performance function defined as

$$g = X_1\,(\text{Strength}) - X_2\,(\text{Stress}) = 0 \tag{3.8}$$

in which X_1 and X_2 are the independent random variables with known distributions. One solution for obtaining the probability of $g \leq 0$, i.e., the probability that the stress exceeds the strength, is to apply Eq. 3.6 , which for independent variables reduces to

$$u_i = \Phi^{-1}[F_i(x_i)]\,;\, i = 1,2 \tag{3.9}$$

Applying the inverse of Eq. 3.9 to Eq. 3.8, a limit state can be established in the u-space and the design point can be obtained.

In Fig. 3.1, X_1 has a Weibull distribution with a mean of 20 and a standard deviation of 1.2 , and X_2 is a normal variable with a mean of 10 and a standard deviation of 3. In the figure, the original linear limit state becomes non-linear in the u-space because of the non-linear transformation of Eq. 3.9. FORM approximates the exact non-linear g by a linear g at the design point Q. Since Q has a maximum joint pdf, and because of the fast decaying rate of the joint pdf in the failure

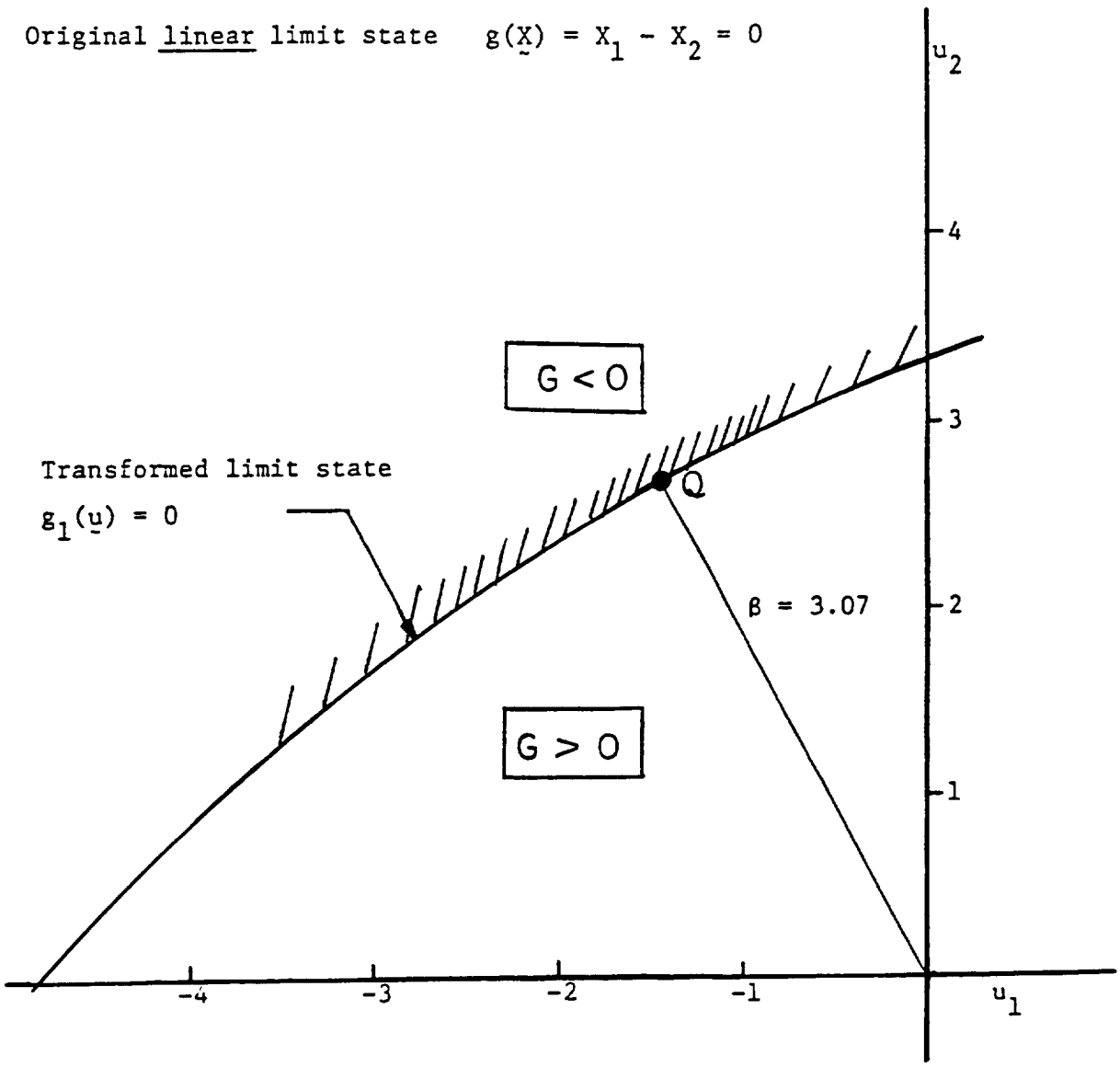

Figure 3.1 Exact Transformation of a Linear Limit State

region, the FORM error is only 17 percent. Considering the fact that the p_f is small (0.00127), this error is acceptable for a preliminary analysis.

The previous example demonstrates the procedure of converting a double-integration problem into a simple geometry problem. The idea can be extended easily to problems with higher dimensions.

The experience gained in the past year has indicated that FORM is very fast and gives reasonable results for typical problems. However, FORM is subject to a large error when the transformed limit state has a large curvature at the design point. This fact motivated the development of SORMs which provide improvement on probability estimates by including second-order effects. These SORMs require more computational effort.

In the NESSUS code, both FORM and SORM are available. FORM is used for a fast but preliminary analysis, and SORM is used for a detailed analysis. The Rackwitz-Fiessler normal tail approximation scheme [3.9] was implemented for searching the design point which is subsequently used for a second-order reliability analysis.

The method used in the FPI code (see Section 4) applies an optimized three-parameter normal concept [3.15]. It is categorized as a SORM because the method considers the quadratic terms. Currently, the mixed terms in the quadratic g-function are not included in the FPI formulation. However, log-transformation of the variables (either in the X-space or in the u-space) is allowed to help linearize the g-function.

In general, the second-order methods may be used as an accuracy indicator. If the difference between the first-order method and the second-order method is not particularly large, the results using SORM tend to be quite accurate. If a highly accurate solution is needed, a Monte Carlo simulation (see Section 4) should be used.

In addition to providing solution efficiency, the design point provides useful information on the probabilistic sensitivities of the random variables. System reliability analysis methods based on the design point concept are available in the literature to treat multiple-failure-mode and multiple-component problems.

3.5 Define Performance Functions

One of the PSAM goals is to evaluate structural response cdf such as "the probability that the maximum displacement exceeds 0.1 inch". In other words, the required performance functions are related to structural responses.

The NESSUS code developed in the first year of the PSAM project was designed to construct the cdf of user-selected response functions such as displacements, stresses, or other structural responses. Once the cdf's of response functions are available, they can be used to compute reliability. To perform probabilistic structural analysis using the first-year NESSUS code, the analyst must define the g-functions. How to construct g-functions is discussed further in Section 4.

3.6 Approximate Performance Functions

The cdf computation can be made efficiently if the g-function is simple. For SSME structural components, the g-functions are implicitly defined in the finite element code. To simplify the analyses, the complicated g-functions can be approximated by the following methods:

(1) Expanding the g-function into a Taylor's series at a deterministic state [3.5, 3.6]. Many stochastic finite element methods require the computations of the partial derivatives of the stiffness and other matrices, such as SwRI's formulation of a Level 2 first-order stochastic finite element method (Section 3, Volume III). Der Kiureghian suggested the construction of the partial derivatives of the assembled stiffness matrix by starting from the formulations at the element level [3.4]. When combined with a design point search algorithm, these methods seem fast. Unfortunately, these methods require major modifications of the original finite element code.

(2) An efficient perturbation method is discussed in Section 5. This method does not require a major modification of the code and has been implemented in the NESSUS code.

3.7 References

3.1 Rackwitz, R., "Implementation of Probabilistic Safety Concepts in Design and Organizational Codes," Structural Safety and Reliability, T. Moan and M. Shinozuka, ed., Elsevier, 1981.

3.2 Handa, K., and Anderson, K., "Application of Finite Element Methods in the Statistical Analysis of Structures," in Proceedings, Third International Conference on Structural Safety and Reliability, pp. 409-417, Trondheim, Norway, June 1981.

3.3 Hisada, T., and Nakagiri, S., "Stochastic Finite Element Method Developed for Structural Safety and Reliability," in Proceedings, Third International Conference on Structural Safety and Reliability, pp. 395-408, Trondheim, Norway, June 1981.

3.4 Der Kiureghian, A., "Finite Element Methods in Structural Safety Studies," in Proceedings, Symposium on Structural Safety Studies, ASCE Convention, Denver, Colorado, April 1985.

3.5 Hisada, T., and Nakagiri S., "Role of the Stochastic Finite Element Method in Structural Safety and Reliability," in Proceedings, Fourth International Conference on Structural Safety and Reliability, Kobe, Japan, May 1985.

3.6 Der Kiureghian, A., and Ke, J.-B., "Finite-Element Reliability Analysis of Frame Structures," in Proceedings, Fourth International Conference on Structural Safety and Reliability, Kobe, Japan, May 1985.

3.7 Turkstra, C.S., "Theory of Structural Design Decision, Solid Mechanics Study No. 2," University of Waterloo, 1970.

3.8 Hasofer, A.M., and Lind, N.C., "Exact and Invariant Second-Moment Code Format," Journal of Engineering Mechanics Division, ASCE, Vol. 100, No. EM1, February 1974.

3.9 Rackwitz, R., and Fiessler, B., "Structural Reliability Under Combined Random Load Sequences," Journal of Computers and Structures, Vol. 9, pp. 489-494, 1978.

3.10 Fiessler, B., Neumann, H.J., and Rackwitz, R., "Quadratic Limit States in Structural Reliability," Journal of the Engineering Mechanics Division, ASCE, Vol. 105, pp. 661-676, August 1979.

3.11 Ditlevsen, O., "Principle of Normal Tail Approximation," Journal of Engineering Mechanics Division, ASCE, Vol. 107, pp. 1191-1208, December 1981.

3.12 Hohenbichler, M., and Rackwitz, R., "Non-normal Dependent Vectors in Structural Safety," Journal of the Engineering Mechanics Division, ASCE, Vol. 100, No. EM6, pp. 1227-1238, December 1981.

3.13 Tvedt, L., "Two Second Order Approximations to the Failure Probability, "Det Norske Veritas (Norway), RDIV/20-004-83, 1983.

3.14 Chen, X., and Lind, N.C., "Fast Probability Integration by Three Parameter Normal Tail Approximation, Structural Safety, Vol. 1, pp. 169-176, 1983.

3.15 Wu, Y.-T., and Wirsching, P.H., "A New Algorithm for Structural Reliability Estimation," Journal of the Engineering Mechanics Division, ASCE, submitted for review, 1985.

3.16 Rosenblatt, M., "Remarks on a Multivariate Transformation," Annals of Mathematical Statistics, Vol. 23, No. 3, pp. 470-472, September 1952.

3.17 Der Kiureghian, A., and Liu. P.-L., "Structural Reliability Under Incomplete Probability Information," Report No. UCB/SESM-85/01, Department of Civil Engineering, Division of Structural Engineering and Structural Mechanics, University of California, Berkeley, California, January 1985.

3.18 Frangopol, D.M., "Structural Optimization Using Reliability Concepts," Journal of the Engineering Mechanics Division, Vol. 111, No. 11, pp. 2228-2301, November 1985.

3.19 Ditlevsen, O., "Narrow Reliability Bounds for Structural Systems," Journal of Structural Mechanics, Vol. 4, No. 9, 1979.

4.0 COMPUTATIONAL STRATEGIES FOR PROBABILISTIC ANALYSIS

4.1 The General Problem of Probabilistic Structural Analysis

The general goal of a structural reliability analysis is to compute a probability of failure, or to construct a distribution function for a critical response, e.g., stress at a notch. Described herein are strategies for efficient solution of these two related problems.

As an example, consider the cantilever beam of Fig. 4.1. Design factors are random variables, and the responses of interest to the designer, maximum stress, tip deflection, fundamental natural frequency, are all random variables. Given the statistical distribution of all of the design factors, it is possible to estimate the distribution of each of the responses.

In general, consider a component failure mode which involves n random design factors,

$$\underline{U} = (U_1, U_2, \ldots U_n) \tag{4.1}$$

It is assumed that the n design factors are mutually independent. Define a performance function such that the event of failure is

$$g(\underline{U}) \leq 0 \tag{4.2}$$

$g(\underline{U})$ is also called a limit state function of failure function. In the example

$$g = R - S = R - \frac{6QL}{bh^2} \tag{4.3}$$

Note that g is a random variable having its own density function $f_g(g)$, mean μ_g and standard deviation σ_g. Define the limit state as

$$g = 0 \tag{4.4}$$

In our example

$$R = \frac{6QL}{bh^2} \tag{4.5}$$

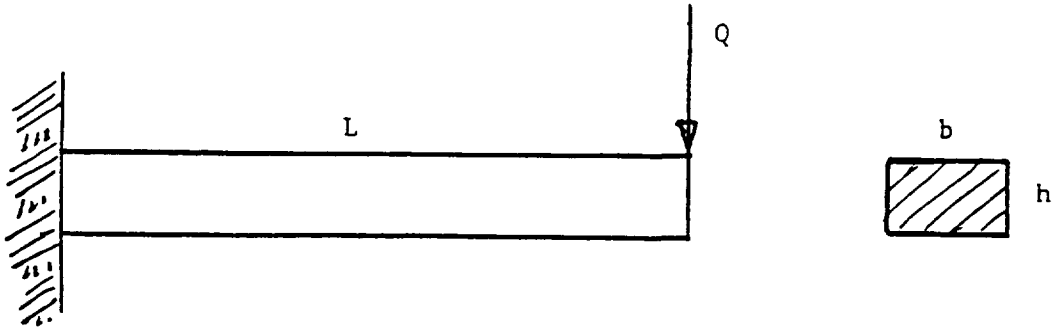

Assume that all of the design factors are random variables because their exact value will not be known.

Q = load
L = length of beam
b, h = cross sectional dimensions
E = modulus of elasticity
ρ = weight density

- Maximum stress at root

$$S = Mc/I = \frac{6QL}{bh^2}$$

Because Q, L, b, and h are random variables, S will be a random variable.

- Maximum tip defection

$$\Delta = \frac{QL^3}{3EI} = \frac{4QL^3}{Ebh^3}$$

Because Q, L, b, h, and E are random variables, Δ will be a random variable.

- Natural frequency

$$f_1 = \frac{3.2h^2}{L^2}\sqrt{\frac{E}{\rho}}$$

Because h, L, E, and ρ are random variables, f_1 will be a random variable.

- The event of failure (yielding)

R = yield strength, a random variable Failure $\rightarrow (S > R)$

Figure 4.1 Elementary Design Considerations of Simple Structural Component

is the limit state. This is the boundary between the safe and failed regions in the space of design parameters.

Define the probability of failure as,

$$p_f = P\{g(\underline{U}) \leq 0\} \tag{4.6}$$

or in our example,

$$p_f = P\left(R \leq \frac{6QL}{bh^2}\right) \tag{4.7}$$

Evaluation of p_f is, in general, a very difficult probability problem. An exact solution is given by,

$$p_f = \int_{\Omega} f_{\underline{U}}(\underline{u}) d\underline{u} \tag{4.8}$$

where Ω is the region of failure. Except in the cases of one or two random design factors, solution of Eq. 4.8 is a practical impossibility.

Construction of a cumulative distribution function (cdf) of $Z = Z(\underline{U})$, denoted as $F_Z(z)$, can be made in a similar fashion. Let,

$$p = F_Z(z) = P\{Z(\underline{U}) \leq z\} \tag{4.9}$$

Define

$$g(\underline{U}) = Z(\underline{U}) - z \tag{4.10}$$

Then p is identical to Eq. 4.6. Thus, in fact, the problem of computing probabilities of failure for design is identical to that of computing a point on the cdf. However, to construct the cdf, it is required to compute several points to define the function.

Summarized in the following sections are strategies for computing point probability estimates and constructing distribution functions. General references for modern reliability analysis are Refs. 4.1 through 4.13. This list is not comprehensive, but the major recent works are included.

4.2 Exact Solutions of Probabilities

Exact solutions of Eq. 4.8 are possible for some special cases.

Only one random variable. If there is only one random variable, U, then Eq. 4.8 reduces to

$$p \equiv P(U \le u_o) = \int_{-\infty}^{u_o} f_U(u)du \tag{4.11}$$

where f_U is the probability density function (pdf) of U.

The basic stress-strength interference problem. Consider the basic variables of stress S and strength R (e.g., as shown in Fig. 4.1). It can be shown that,

$$p_f = \int_0^{\infty} f_S(s)F_R(s)ds \tag{4.12}$$

or, the equivalent statement,

$$p_f = 1 - \int_0^{\infty} f_R(r)F_S(r)dr \tag{4.13}$$

where $f \equiv pdf$, and $F \equiv cdf$, with subscripts denoting the random variables.

Numerical integration is generally required, but it can be done very accurately and quickly.

The normal format. Assume all U_i have normal distributions and that the limit state has the linear form. Let

$$g(\underline{U}) = A + \sum_{i=1}^{k} B_i U_i \tag{4.14}$$

where A and B_i are constants. From elementary probability theory the random variable g will also have a normal distribution. The mean and standard deviation of g are

$$\mu_g = A + \sum_{i=1}^{k} B_i \mu_i \qquad \sigma_g = \sqrt{\sum_{i=1}^{k} B_i^2 \sigma_i^2} \tag{4.15}$$

where μ_i and σ_i are the mean and standard deviation of U_i respectively.

The failure condition is $g \leq 0$. The probability of failure is

$$p_f = P(g \leq 0) \tag{4.16}$$

Using standard methods of calculating probabilities for a normal variate,

$$p_f = P(g \leq 0) = P\left(\frac{g - \mu_g}{\sigma_g} \leq \frac{-\mu_g}{\sigma_g}\right) \tag{4.17}$$

$$p_f = \Phi(-\beta) \tag{4.18}$$

where Φ is the standard normal cdf, and

$$\beta = \mu_g / \sigma_g \tag{4.19}$$

β is called the <u>safety index</u>.

<u>The lognormal format</u>. The lognormal distribution plays an important role in probabilistic design and in particular for problems which involve fatigue.

Consider a restatement of the limit state and a redefinition of g.

Let,

$$g(\underline{U}) = R(\underline{X})/S(\underline{Y}) = 1 \tag{4.20}$$

Now the failure condition is $g \leq 1$. Assume that $g(\underline{U})$ is a multiplicative function of the design factors

$$g(\underline{U}) = B \prod_{i=1}^{n} U_i^{a_i} \tag{4.21}$$

where B and all a_i are constants. Let $Z = ln\ g$.

$$Z = lnB + \sum_{i=1}^{k} a_i ln\, U_i \tag{4.22}$$

Now assume that all U_i have lognormal distributions. Because U_i is lognormal, it follows that all $ln\ U_i$ are normal. Then this format becomes identical to the normal format.

The failure condition is $g \leq 1$, or, as above, $Z \leq 0$. The p_f is given by Eq. 4.18 with $\beta = \mu_Z/\sigma_Z$, and

$$\mu_Z = \tilde{Z} = ln\,\tilde{g} = 1n\left[B\prod_{i=1}^{k}\tilde{U}_i^{a_i}\right] \tag{4.23}$$

$$\sigma_Z^2 = ln\left[\prod_{i=1}^{k}(1+C_i^2)^{a_i^2}\right]$$

where the tilde indicates a median value and C_i is the coefficient of variation (COV) of U_i. For a random variable U, the median and COV in terms of the mean μ_U and standard deviation σ_U are respectively,

$$\tilde{U} = \mu_U\sqrt{1+C_U^2} \qquad C_U = \sigma_U/\mu_U \tag{4.24}$$

4.3 Monte Carlo Methods

In practice, a Monte Carlo solution provides an approximation to point probabilities or to cdf's. As the sample sizes become infinite, the estimates approach the exact value.

Because Monte Carlo is widely used, there is no need to go into much detail here. The following example is presented only as a reminder that Monte Carlo can provide approximate solutions to extremely complicated probability problems.

Consider a design problem having a limit state, such as

$$g(\underline{U}) = (AX^a/Y^b) + CU^c ln\,V + D = 0 \tag{4.25}$$

in which A, C, a, b, c, and D are constants and X, Y, U, and V are random variables having a Weibull, normal, lognormal and gamma distribution respectively. Evaluation of p_f using Eq. 4.8 is a practical impossibility.

But estimating p_f for the above equation using Monte Carlo could proceed as follows:

1. Sample $X_i; i = 1,K$ from the Weibull

   $Y_i; i = 1,K$ from the normal

   $U_i; i = 1,K$ from the lognormal

   $V_i; i = 1,K$ from the gamma

K = sample size, typically 10,000 for many Monte Carlo applications.

2. Obtain, by calculating each g_i, a random sample of $g\,(i = 1, K)$

$$g_i = (AX_i^a / Y_i^b) + CU_i^c \ln V_i + D \tag{4.26}$$

3. Statistically analyze g. Some options . . .

   a) Compute mean, standard deviation and maybe higher order moments.

   b) If $p_f = P(g_i < 0)$, you can count the number N of values of g_i less than zero. Then

$$p_f \cong N/K \tag{4.27}$$

   c) The cdf of g can be estimated by a probability plot. Note that g_i first has to be sorted.

A major shortcoming of Monte Carlo for structural reliability analysis is that very large samples are required to get good resolution at the low probability levels (e.g., 10^{-3} to 10^{-4}).

4.4 Mean Value First Order Second Moment Method (MVFOSM)

Assume that each random design factor is characterized by its mean and standard deviation. The distribution of these factors may or may not be known.

The basic measure of reliability is the safety index $\beta = \mu_g / \sigma_g$. From examination of Fig. 4.2 it is clear that β can be employed for any performance function $g(\underline{U})$ and any distribution of each U_i. In the special case where g is linear and all U_i are normally distributed, the β defined here and the β of the normal format are identical.

Determination of μ_g and σ_g of a complicated g-function, is in general very difficult. However, these terms are relatively easy to evaluate if $g(\underline{U})$ can be linearized by a Taylor's series expansion about the means of all U_i. Excluding higher order terms and assuming that all U_i are independent, it can be shown that

$$\mu_g \cong g(\underline{\mu}) \tag{4.28}$$

Failure $\rightarrow Z = g(\underset{\sim}{U}) \leq 0$

Mean and Standard Deviation of Z;

$\mu_Z = E[g(\underset{\sim}{U})]$ $\qquad$ $\sigma_Z = \sqrt{Var\ [g(\underset{\sim}{U})]}$

Safety Index;

$\beta = \mu_Z/\sigma_Z$

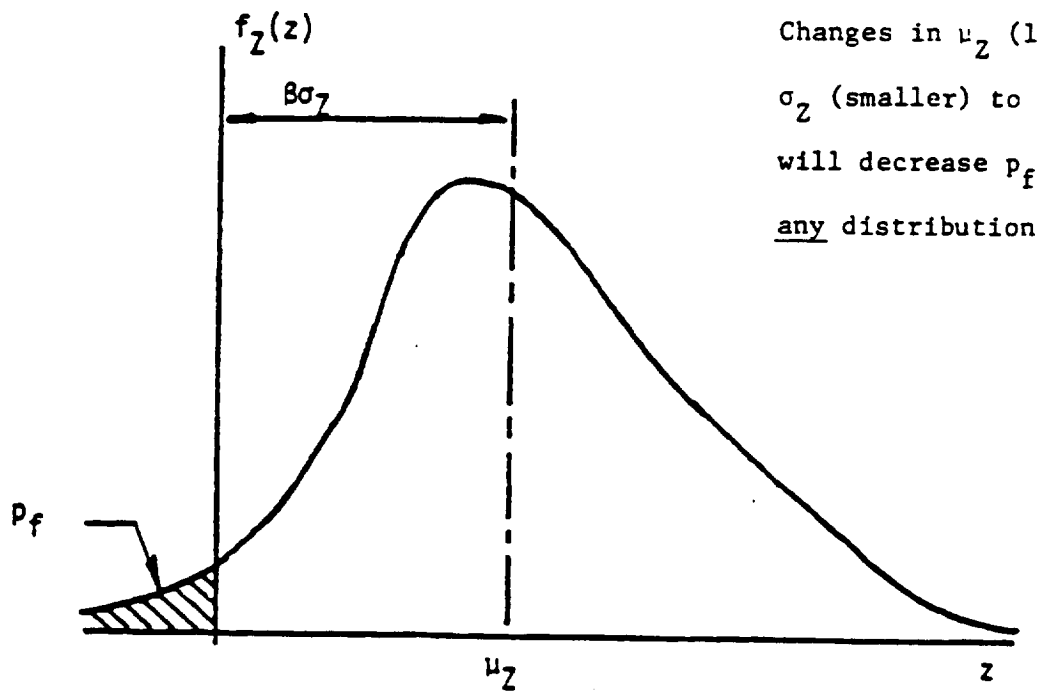

Changes in μ_Z (larger) and σ_Z (smaller) to increase β, will decrease p_f, . . . for <u>any</u> distribution of Z.

Figure 4.2 Relationship of Safety Index to Risk and to μ_Z and σ_Z

$$\sigma_g \cong \left[\sum_{i=1}^{n} \left(\frac{\partial g}{\partial U_i} \right)_{\underline{\mu}}^2 \sigma_i^2 \right]^{1/2} \tag{4.29}$$

where $\underline{\mu}$ is the vector of mean values and σ_i is the standard deviation of U_i. Evaluation of β is relatively easy, even for complicated performance functions. On the other hand there are significant limitations and criticism of the MVFOSM method:

(a) In this approach, the measure of safety is β, which in some cases gives weak information on the probability of failure: $p_f \cong \Phi(-\beta)$.

(b) Information on distributions, if available, cannot be included in a logical way.

(c) The linear approximation of $g(\underline{U})$ at the mean of the various variables appears to be too inaccurate in the face of severe non-linearities of this function in many design situations, i.e., the higher-order terms in the Taylor's series expansion are important.

(d) Eqs. 4.28 and 4.29 for μ_g and σ_g are valid only for relatively small variances (typically for $C_i < 0.15$).

(e) And the most important, the method fails to be invariant in that β depends upon the mechanical formulation of the problem, e.g., $g = RA - Q$ and $g = R - Q/A$ are two equally valid performance functions involving variables R, Q, and A. But the value of β will be different in both cases.

These shortcomings of MVFOSM, and the difficulty of integrating Eq. (4.8), motivated the development of the fast probability integration methods as described below.

4.5 Fast Probability Integration (FPI) Methods

All of the FPI methods can be thought of as extensions to the Hasofer-Lind (H-L) scheme [4.11]. Transform each U_i to a reduced coordinate $u_i = (U_i - \mu_i)/\sigma_i$ where (μ_i, σ_i) is the mean and standard deviation respectively of U_i. Substitute into $g(\underline{U})$ to obtain the performance function in reduced coordinates, $g_1(\underline{u})$. Define the <u>safety index</u> β as

$$\beta = \min \sqrt{\Sigma u_i^2} \tag{4.30}$$

subject to $g_1(\underline{u}) = 0$. Thus, β is the minimum distance from the origin of the reduced coordinates to the limit state in design parameter space. The point on $g_1(\underline{u})$ closest to the origin is called the design point.

In the special case $g(\underline{U})$ is linear in the U_i, and all U_i are normal, then $p_f = \Phi(-\beta)$ is exact, i.e., the safety index is identical to that of the normal format (and MVFOSM). For other cases, p_f computed is only an approximation, with errors which are difficult to quantify.

The Rackwitz-Fiessler (R-F) [4.12], Chen-Lind (C-L) [4.13], and Wu [4.14, 4.15] methods provide mathematical adjustments and extensions to H-L in an attempt to improve the estimate p_f. The Wu method provides by far the most accurate estimates of p_f. Detailed descriptions of these methods are given in the indicated references.

As implied by the name, the FPI methods are "fast." For example, on the CYBER 175, a problem involving 20 variables will take about 2 CPU seconds for R-F and 4 CPU seconds for Wu. The same problem by Monte Carlo may take 10 to 100 times as long depending upon the required resolution in the tails.

As an example, consider a simple brittle fracture problem. Failure in a component occurs when the stress intensity factor $K = S\sqrt{\pi a}$ (S = stress, a = crack length) exceeds fracture toughness K_C. S, K_C, and a are random variables. The data and the results are given in Table 4.1. Based upon analysis of a large number of problems, the error in the Wu method is typically less than 3%.

In summary, the FPI methods provide efficient approximate solutions to very complicated probability problems.

Now consider the problem of reliability analysis when the performance function is not available in closed form. A closed form expression relating the design variables is a necessary

Table 4.1

Example of FPI Performance

- Failure Function; $g = K_C - S\sqrt{\pi a}$

Variable	Distribution	Mean/Median*	COV
K_C	Weibull	150	0.167
S	EVD	80	0.20
a	lognormal	0.10*	1.00

*Median value for the lognormal only

- Comparisons of β and p_f

	β	p_f	%Error**
R-F	2.482	6.534E-3	24.3
Wu	2.380	8.672E-3	0.5
Monte Carlo (K=100,000)		8.630E-3	0

**Monte Carlo solution is considered exact here

requirement to run a FPI program. But often the relationship is implicit, and a computer program is necessary, e.g., to compute stress and deflection using a finite element code, or cycles to failure using a local strain analysis or a fracture mechanics fatigue life prediction program. In such cases,

the computer code can be run repeatedly using various combinations of perturbed values of the random design factors. Several data sets are obtained, from which an empirical approximating polynomial function can be fit. Then FPI can be employed on the polynomial. A summary of the process is given in Fig. 4.3. The general procedure was demonstrated by Wu and Wirsching [4.16].

The major difficulty of such a strategy is that it may be very expensive to run the computer code (e.g., finite element program) several times to construct the data set. However, in any reliability analysis, it is necessary to describe how the distributions of all variables relate to each other. Therefore, repetition of the basic code is unavoidable.

As an example, consider a simple three bar truss carrying a static load Q, as shown in Fig. 4.4. The cross sectional area A of each bar is assumed to be constant. But the moduli of elasticity E_1, E_2 and E_3, and load Q are considered as random variables as presented in Table 4.2. All five random variables are independent.

The goal of the analysis is to derive the distribution of the vertical deflection δ of point B. Execution of an FPI method requires that δ be expressed as a closed form algebraic function of the random variables. In this case, an exact form for δ can be derived. But ordinarily we would not have a closed form expression, e.g., in a finite element code. As described above, a structural analysis program would have to be run several times with various combinations of parameters to obtain several points on the function, . . . and then fit an approximating polynomial.

To demonstrate reliability analysis with implicit functions, pretend that a closed form expression for δ is not available. Assume that δ is related to the random variables through the following empirical form,

$$\delta = a_o E_1^{a_1} E_2^{a_2} E_3^{a_3} Q^{a_4} \tag{4.31}$$

Upon making a log transformation of Eq. (4.31), the general linear model is used to establish empirical values of a_i; $i = 0, 4$ by fitting the function to select points. Because there are four variables, at least five points are required.

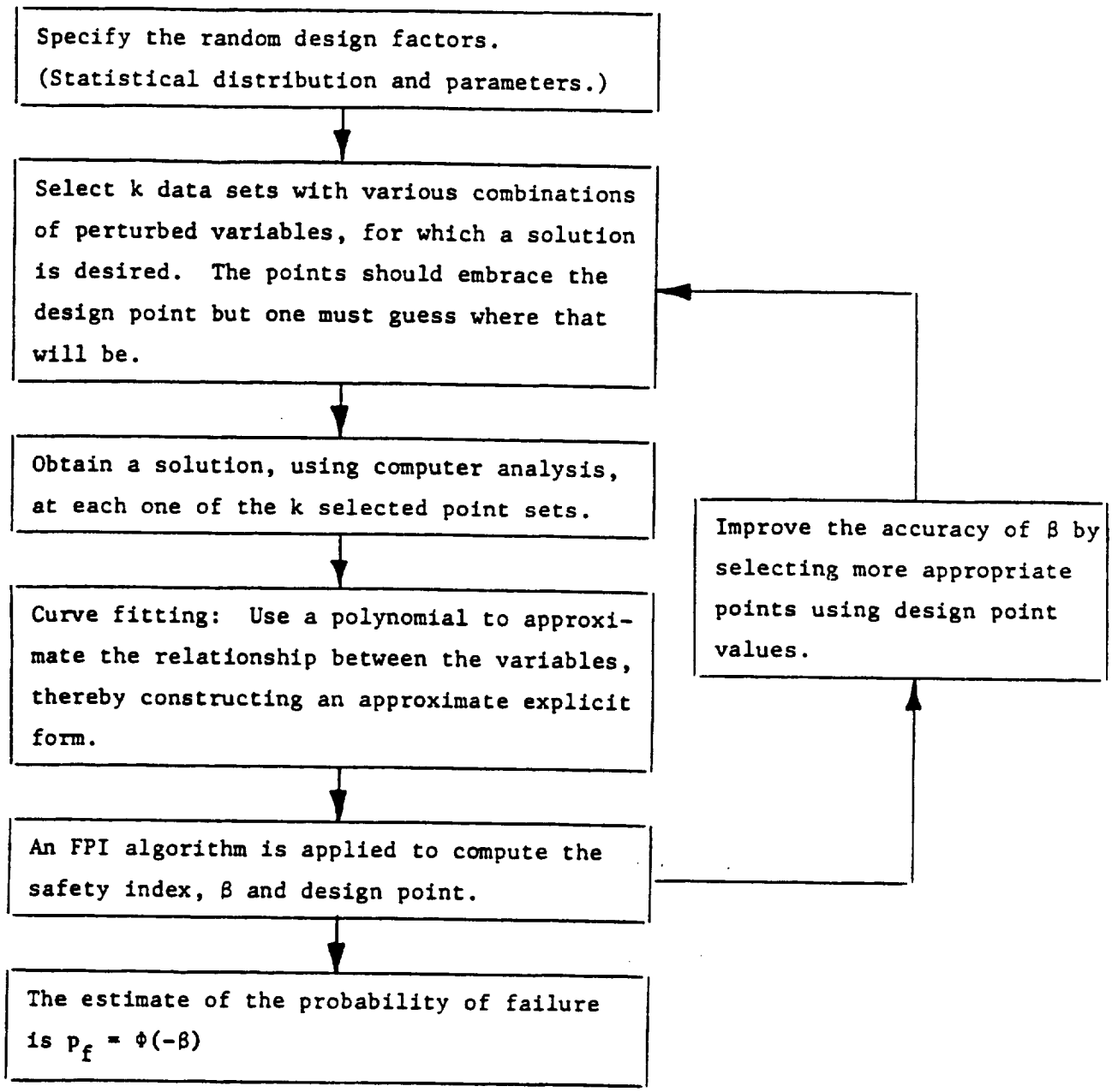

Figure 4.3 Block Diagram for Computation of the Safety Index, β, when the Failure Function is not Available as a Closed Algebraic Form

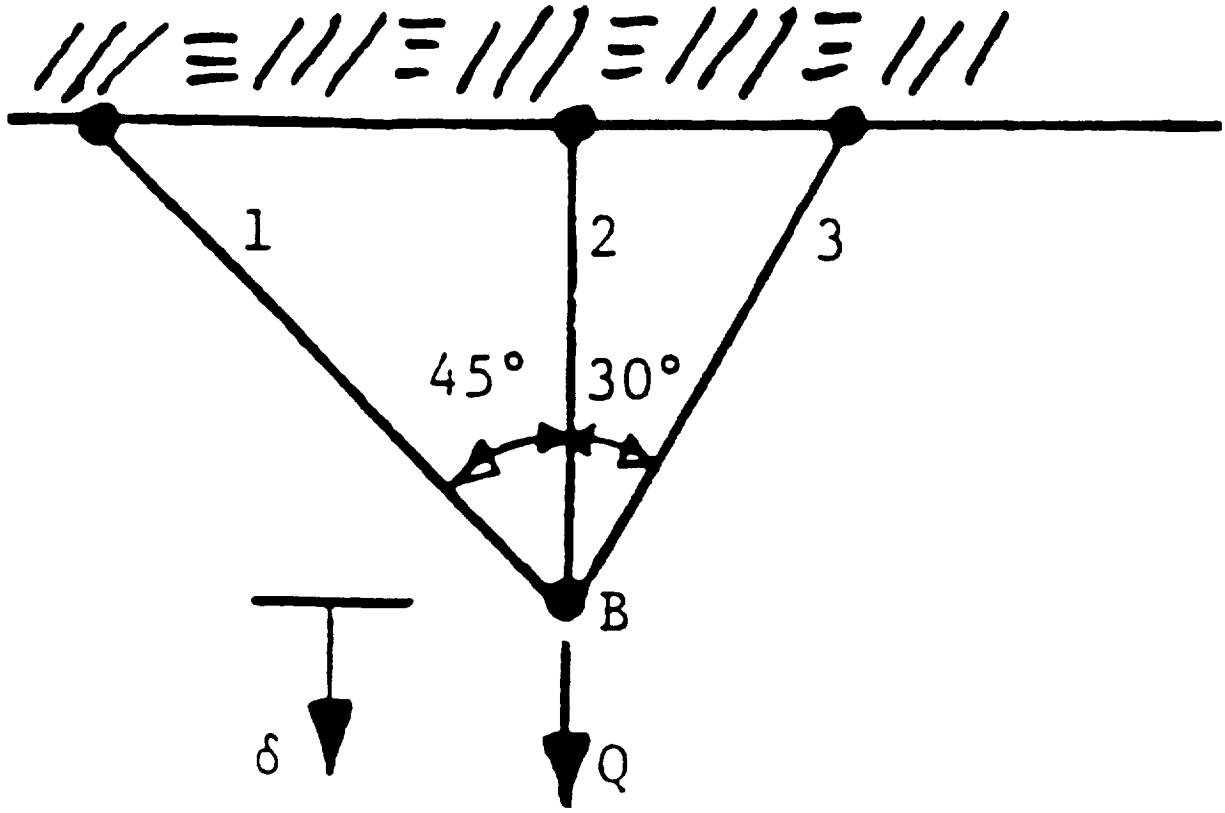

Figure 4.4 Three Bar Truss

In this demonstration case, the reference point, or expanding point, for fitting the polynomial is arbitrarily chosen as $\mu \pm 1.5\sigma$, the (+) used for "stress variables" and (-) for "strength" variables. A total of nine points was selected for solution of δ with perturbed values of each variable. A structural code can be used to calculate δ in each case. The details of this example are given in Ref. 4.17.

Table 4.2

Design Factors for Example

		Distribution	Mean[a]	COV
L	length of bar 2	constant	12 in	0
A	cross sectional area	constant	1.0 in^2	0
E_1	modulus of elasticity, Bar 1	lognormal	10^4 ksi	0.10
E_2	modulus of elasticity, Bar 2	Weibull	10^4 ksi	0.10
E_3	modulus of elasticity, Bar 3	normal	10^4 ksi	0.10
Q	load	EVD	100 ksi	0.15

(a) Median for lognormal variates related to the random variables through the empirical form

The distribution function of δ is constructed in Fig. 4.5 by using Monte Carlo on the exact form and FPI on the empirical form Eq. (4.31). Two FPI methods used to construct the cdf were: a) Rackwitz-Fiessler (R-F) and b) Wu algorithm.

Note that FPI must be run several times (with different z: See Eq. 4.10) to construct the cdf. The points are shown on Fig. 4.5. Because FPI methods are "fast," this is not a serious limitation. Also note that only the right tail of the distribution of δ was plotted. It was assumed that, for design purposes, this was the only region of interest.

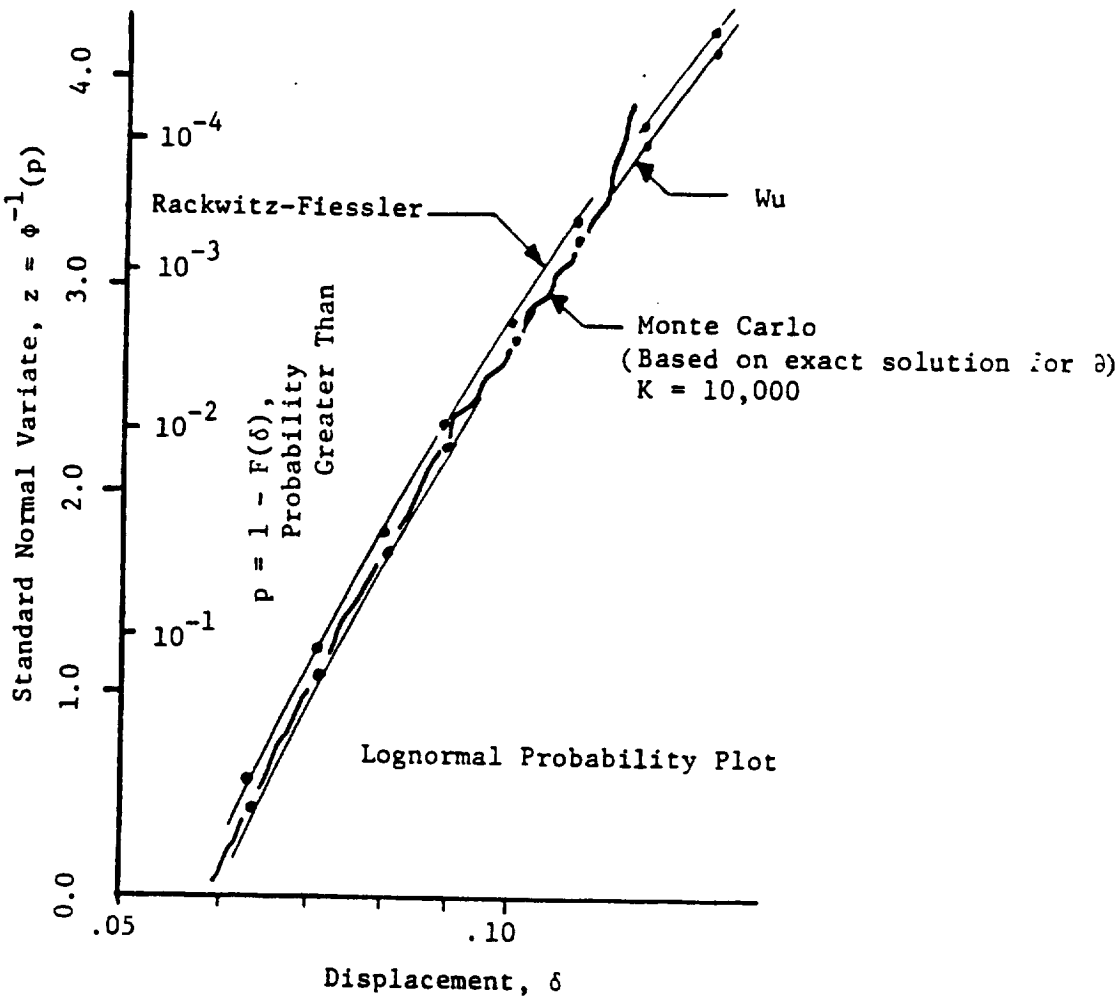

Figure 4.5 Comparison of Monte Carlo ("exact") to Fast Probability Integration (FPI) [Ref. 41.7]

Both FPI methods give close results as Monte Carlo. If the cdf was to be extended to lower right tail probabilities, Monte Carlo costs would become exorbitant. But FPI costs are independent to the probability level.

4.6 Random Fields and Correlated Variables

Examples of random fields in the context of this PSAM project are the distribution of pressure over a plate and the distribution of modulus of elasticity throughout a member. For numerical analysis, the continuous field must be discretized into a set of random variables which will be correlated. However, by a transformation of coordinates, a random field can be represented by a set of independent random variables, thereby facilitating use of FPI for point probability estimates.

The method is summarized as follows (See Ref. 4.ll). Let V_x be the covariance matrix for the n basic variables $\underline{X}$ describing the discretized random field. Let T be the matrix of eigenvectors of V_x. Define new coordinates $\underline{Y}$ by the transformation,

$$\underline{X} = T\underline{Y} \tag{4.32}$$

The transformed coordinates $\underline{Y}$ will be mutually independent. The variance of Y_i is λ_i, the ith eigenvalue. The mean of Y_i is,

$$\mu_{Y_i} = \sum_{j=1}^{n} T_{ji}\mu_{x_j} \tag{4.33}$$

where μ_{x_j} is the mean of x_j and T_{ji} is the jth component of eigenvector i.

As in dynamic analysis, sometimes an adequate description of the random field can be made by consideration of only a few modes. Thus, a small number of Y's may be all that is necessary.

Two problems exist in the implementation of this analysis: (1) it is often difficult to obtain the needed correlation coefficients to construct the covariance matrix, and (2) it may be difficult to establish the distribution of Y_i. If all X_i are normal, then Y_i is exactly normal and FPI should proceed smoothly. If any X_i is not normal, it must be transformed to normal. The correlation coefficients between any two of the transformed normals must be computed (see Section 3).

4.7 Choice of Distribution Functions

To run a probabilistic finite element (PFE) code, it is necessary, in general, to identify all random design factors and assign statistical distributions to each. A computer code is available for determining which of several competing distributional models (e.g., normal, Weibull, etc.) best "fits" a random sample, i.e., the data which the designer has [4.18].

Two statistics, having a similar form, are used in the program. The statistics are shown in Fig. 4.6. $G(x;\underline{\hat{\theta}})$ is the cdf of a statistical model, e.g., Weibull. $\underline{\hat{\theta}}$ is the maximum likelihood estimate of the statistical parameters. $F(x_i)$ is the empirical cdf, an estimate of the actual underlying distribution.

$$F(x) = \frac{i-a}{n+b} \text{ for } x_i \le x < x_{i+1} \tag{4.34}$$

where a and b are constants, and n is the total number of data. The S-statistic is based on a form closely related to the Kolmogorov-Smirnov statistic, the two being computationally equivalent. For the jth statistical model considered,

$$S_j = \frac{1}{n} \sum_{i=1}^{n} \Delta_{ij} \tag{4.35}$$

where

$$\Delta_{ij} = \max\,[|\, G_j(x_i;\underline{\hat{\theta}}) - F_{i-1} \,|, |\, G_j(x_i;\underline{\hat{\theta}}) - F_i \,|] \tag{4.36}$$

Here the constants a and b of Eq. 4.34 are both zero. Thus, S_j is the sum of the deviations, at each x_i, between the empirical and hypothesized distribution functions. The deviation Δ_{ij} is illustrated in Fig. 4.6.

The W-statistic is based upon a form similar to the Cramer-von Mises statistic when used for goodness-of-fit tests

$$W_j^2 = \frac{1}{n} \sum_{i=1}^{n} D_{ij}^2 \tag{4.37}$$

where,

$$D_{ij} = G_j(x_i;\underline{\hat{\theta}}) - F_i \tag{4.38}$$

Here, $a = 1/2$ and $b = 0$ in Eq. 4.34. Deviations D_{ij} associated with the W-statistic are shown in Fig. 4.6.

The rationale for the test is that if $G_i(x;\underline{\hat{\theta}})$ is the real underlying distribution of X, or a good approximation thereof, then F_i will tend to be small. With m competing models for X, one chooses the preferred model as the one with smallest value of S or W, whichever is used.

The two statistics give almost identical results. It would be difficult to prove which one on the average performs better.

For most design variables, one tail of the distribution is of principal interest. It is also possible to bias the data by increasing the emphasis on either the left or right tail (See Ref. 4.18).

Example: The yield strength of a random sample of $n = 92$ specimens of MAR-M-246 was analyzed; the results are presented in Table 4.3. The best fit distribution indicated by both the W and S statistic was the lognormal (by a very slim margin). The lognormal pdf is drawn relative to the histogram for this data in Fig. 4.7.

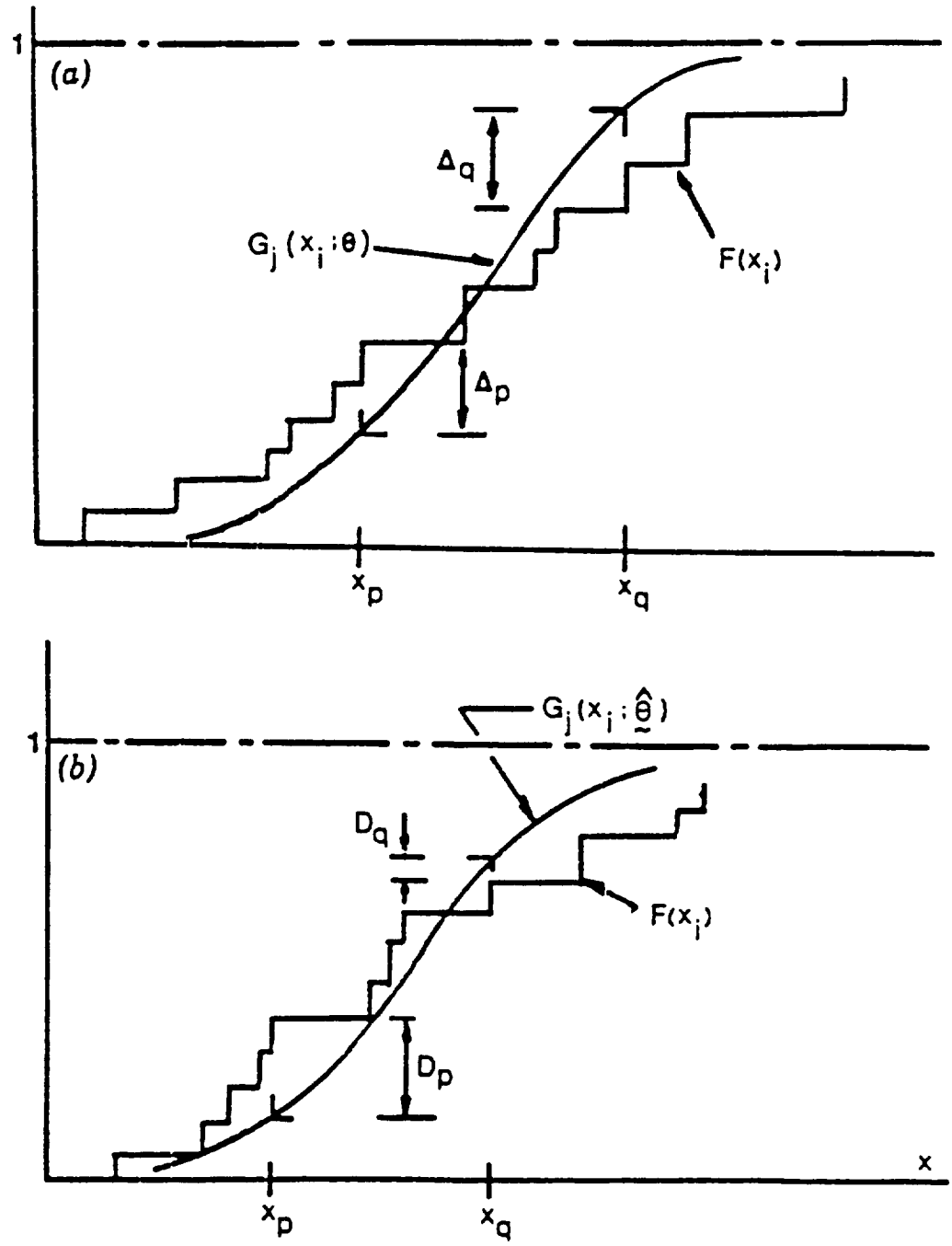

Figure 4.6 Deviations for: (a) S-Statistic; (b) W-Statistic

Table 4.3

Statistical Analysis of Yield Strength Data of MAR-M-246 to Obtain the Best Fit Distribution

Attachment B; Yield Strength; No bias in tails

Sample size, N = 92

DATA

122.00000	121.00000	117.00000	120.00000	117.00000
120.00000	117.00000	122.00000	120.00000	122.00000
121.00000	123.00000	120.00000	122.00000	119.00000
122.00000	121.00000	120.00000	118.00000	117.00000
119.00000	118.00000	119.00000	120.00000	119.00000
118.00000	117.00000	121.00000	120.00000	119.00000
121.00000	118.00000	117.00000	121.00000	119.00000
116.00000	119.00000	115.00000	116.00000	116.00000
118.00000	122.00000	119.00000	118.00000	120.00000
115.00000	122.00000	125.00000	124.00000	120.00000
117.00000	122.00000	120.00000	120.00000	119.00000
121.00000	123.00000	121.00000	118.00000	122.00000
119.00000	116.00000	123.00000	126.00000	124.00000
122.00000	121.00000	118.00000	121.00000	117.00000
119.00000	126.00000	118.00000	114.00000	117.00000
124.00000	125.00000	110.00000	124.00000	117.00000
117.00000	113.00000	19.00000	117.00000	117.00000
116.00000	114.00000	120.00000	116.00000	116.00000
113.00000	116.00000			

SORTED DATA

110.00000	113.00000	113.00000	114.00000	114.00000
115.00000	115.00000	116.00000	116.00000	116.00000
116.00000	116.00000	116.00000	116.00000	116.00000
117.00000	117.00000	117.00000	117.00000	117.00000
117.00000	117.00000	117.00000	117.00000	117.00000
117.00000	117.00000	117.00000	118.00000	118.00000
118.00000	118.00000	118.00000	118.00000	118.00000
118.00000	118.00000	119.00000	119.00000	119.00000
119.00000	119.00000	119.00000	119.00000	119.00000
119.00000	119.00000	119.00000	119.00000	120.00000
120.00000	120.00000	120.00000	120.00000	120.00000
120.00000	120.00000	120.00000	120.00000	120.00000
120.00000	121.00000	121.00000	121.00000	121.00000
121.00000	121.00000	121.00000	121.00000	121.00000
121.00000	122.00000	122.00000	122.00000	122.00000
122.00000	122.00000	122.00000	122.00000	122.00000
122.00000	123.00000	123.00000	123.00000	124.00000
124.00000	124.00000	124.00000	125.00000	125.00000
126.00000	126.00000			

SAMPLE MEAN OF X = 119.23912

SAMPLE STD DEV OF X = 3.00684

COEFF OF VAR (PERCENT) = 2.52169

ESTIMATES OF LOGNORMAL PARAMETERS, BASE E
MU = 4.78082
SIGMA = .02528

WEIBULL PARAMETERS
ALPHA = 41.32573
BETA = 120.68865

EVD PARAMETERS
ALPHA = .31084
BETA = 117. 72941

WEIGHTING FUNCTION
ETA = 1.00 Z = 1.00

CVM STATISTIC, W

NORMAL =	.03209
EXPONENTIAL =	.30932
WEIBULL =	.04946
EVD =	.05583
LOGNORMAL =	.03206

F-S STATISTIC, S

NORMAL =	2.88762
EXPONENTIAL =	24.47048
WEIBULL =	4.21337
EVD =	4.81005
LOGNORMAL =	2.87459

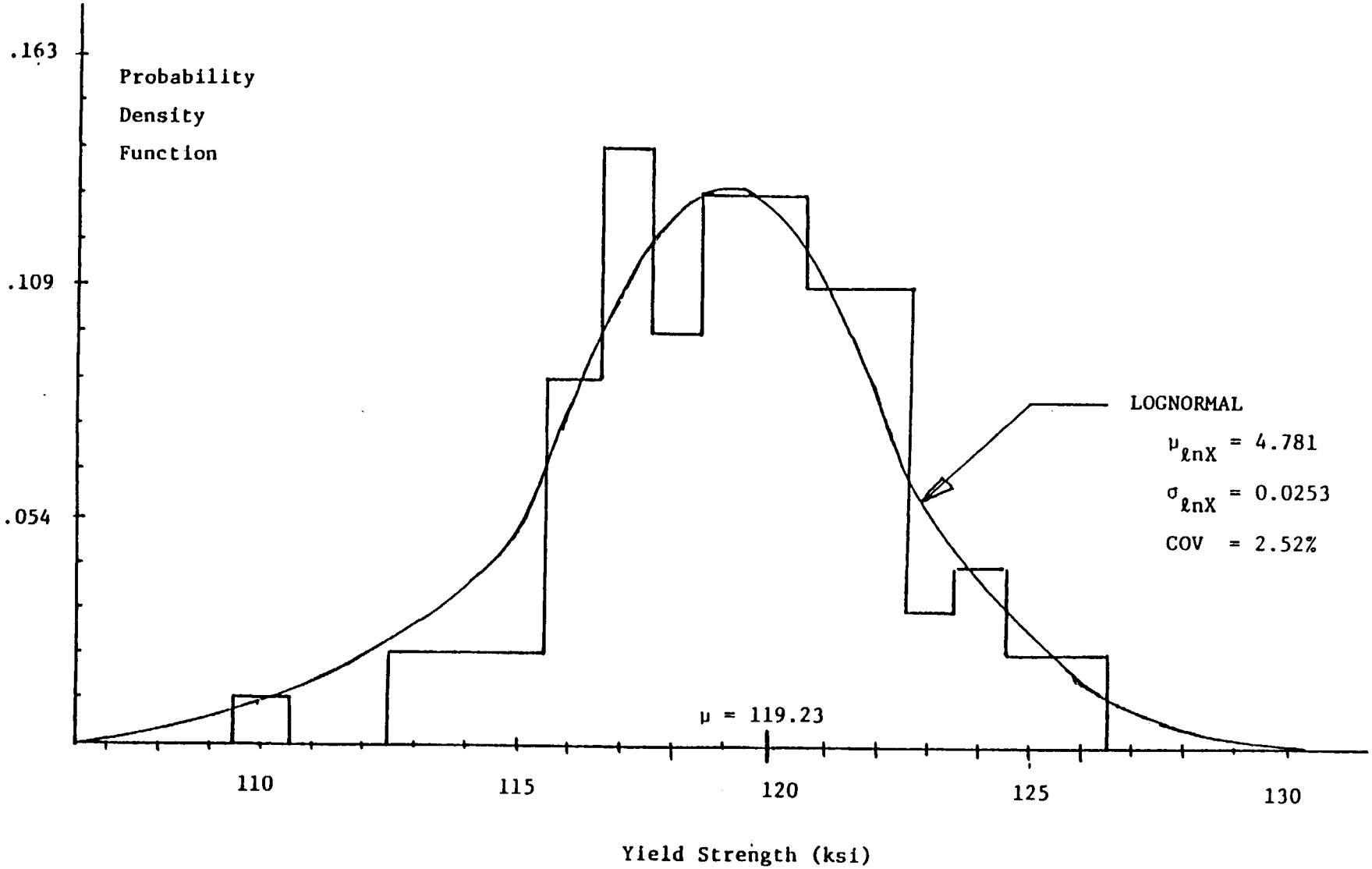

Figure 4.7 **Comparisons of Histogram with Best Fit Distribution (No Tail Bias) for Yield Strength of MAR-M-246; Room Temperature; n = 92**

4.8 The Maximum Entropy Model

For engineering design purposes, commonly used models include normal, lognormal, Weibull, and extreme value distributions, all two parameter models. A designer who seeks a more discriminating model might use the more complicated three parameter Weibull or lognormal. Siddall has presented a multi-parameter model which can provide a more refined fit to a set of data [4.19].

Siddall's maximum entropy model has the form of the pdf,

$$f(x) = \exp\left[\sum_{i=0}^{m} \lambda_i x^i\right] \quad a \le x \le b \tag{4.39}$$

$$0, \quad otherwise$$

The parameters include the bounds of the distribution (a and b) and $\lambda_i; i = 0, m$, where the choice of m is arbitrary. The larger the value of m chosen, the better is the fit of the model to the data. For practical purposes however, one does not want to choose m too large, and for many practical problems, m of four or smaller is adequate.

Unfortunately, the cdf is not available in closed form, so that probability estimates require numerical integration.

$$F_X(x) = \int_a^x f_X(s)ds \tag{4.40}$$

Given a random sample, $\underline{x} = (x_1, x_2, \ldots x_n)$, estimation of the parameters requires a numerical solution as follows:

1. Select the upper and lower bound on the sample space Λ, i.e., the values a and b. Here some engineering judgement is required.

2. The first M moments are estimated from the data, $\underline{x}$.

$$M_i = \frac{1}{n}\sum_{j=1}^{n} x_j^i \tag{4.41}$$

3. Numerical solution of the λ's proceeds as follows. The λ's are chosen so that

$$R = \sum_{i=1}^{m} R_i^2 \quad \text{is a minimum} \tag{4.42}$$

where

$$R_i = \frac{\int_\Lambda x^i \exp\left[\sum_{i=1}^{m} \lambda_i x^i\right] dx}{M_i \int_\Lambda \exp\left[\sum_{i=1}^{m} \lambda_i x^i\right] dx} \tag{4.43}$$

where Λ is the sample space. The solution is obtained for λ_1 through λ_m using non-linear programming. Then

$$\lambda_0 = -ln\left[\int_\Lambda \exp\left[\sum_{i=1}^{m} \lambda_i x^i\right] dx\right] \tag{4.44}$$

Example: Consider the data a sample of size $n = 92$ of given in Table 4.3, yield strength of MAR-M-246. The maximum entropy model is fit to the data

1. The bounds are chosen (arbitrary and out of the range of the data)
   $a = 104$ $\quad b = 135$

2. The number of parameters is chosen as five (m = 4). Computed values of λ are

   λ_0 = 0.67438E4
   λ_1 = -0.23113E3
   λ_2 = 0.29107E1
   λ_3 = -0.15969E-1
   λ_4 = 0.32167E-4

The cdf for this distribution is plotted in Fig. 4.8 on a lognormal probability paper. The plot shows that the maximum entropy model closely follows the lognormal in the center of the distribution, but provides a better fit to the data in the tails.

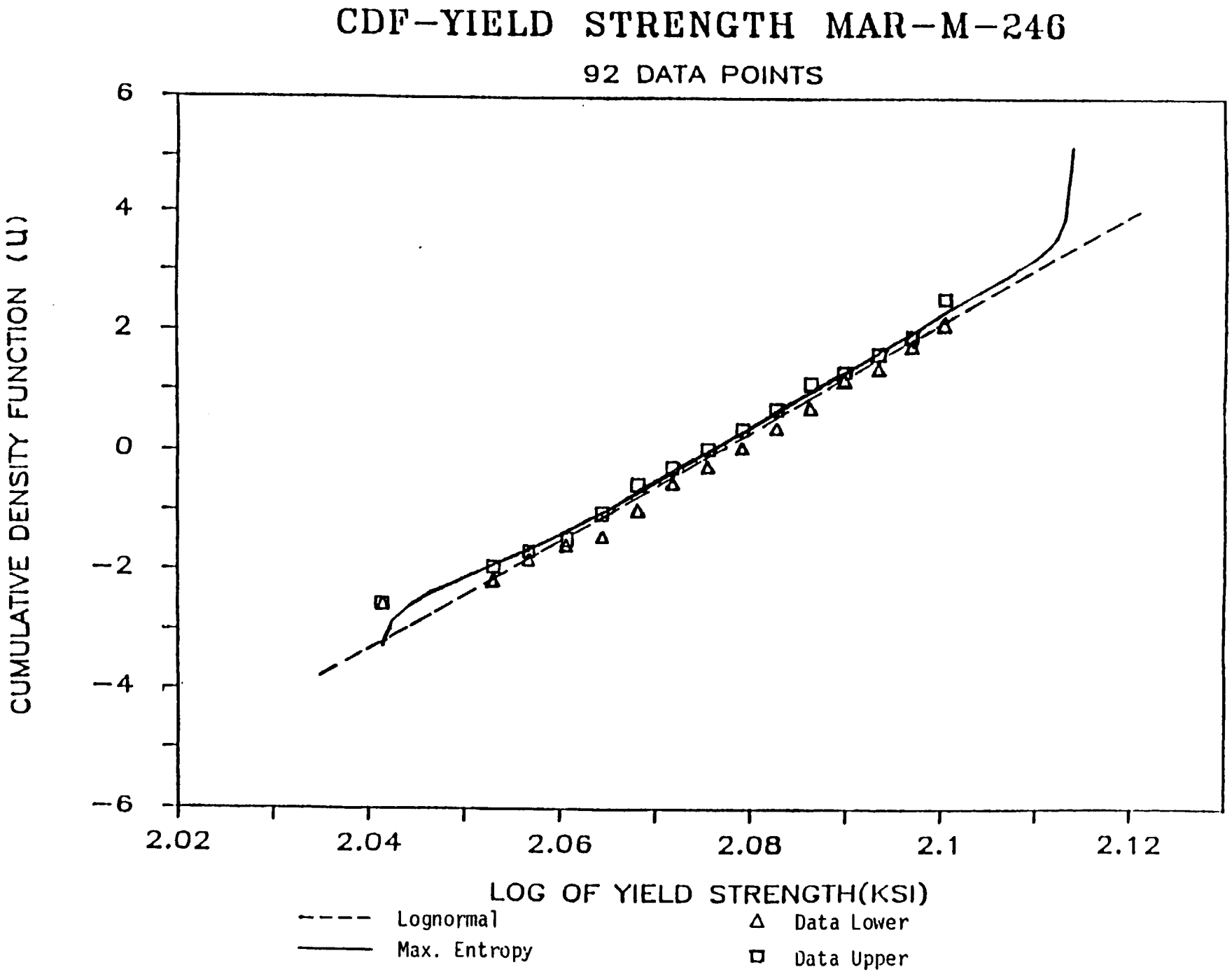

Figure 4.8 Lognormal Probability Plot of Yield Strength of MAR-M-246 (n = 92)

4.9 References

4.1 Thoft-Christensen, P., and Baker, M.J., Structural Reliability Theory and Its Applications, Springer-Verlag, 1982.

4.2 Ang, A. H.-S., and Tang, W., Probability Concepts in Engineering Planning and Design, Wiley, 1984.

4.3 Mann, N.R., et al., Methods of Statistical Analysis of Reliability and Life Data, Wiley, 1974.

4.4 Shinozuka, M., "Basic Analysis of Structural Safety," Journal of Structural Engineering, ASCE, Vol. 109, No. 3, March 1983.

4.5 Lind, N.C., Krenk, S., and Madsen, H. O., Safety of Structures, Prentice-Hall, 1985.

4.6 Hines, W.W., and Montgomery, D.C., Probability and Statistics in Engineering and Management Science, John Wiley, 1980.

4.7 Rationalization of Safety and Serviceability Factors in Structural Codes, Report 63, CIRIA, Construction Industry Research and Information Association, 6 Storey's Gate, London SWIP 3AU. Excellent treatment of safety in structural systems.

4.8 First Order Reliability Concepts for Design Codes, Bulletin d'Information 112, Comite Europeen du Beton. Excellent summary of probabilistic design concepts, but not readily available.

4.9 Galambos, T.V., Ravindra, M.K., (and others), . . . a series of eight papers on Load and Resistance Factor Design (LRFD) in the Journal of the Structural Division, Vol. 104, No. ST9, Sept. 1978. A proposal for an alternative to the AISC codes.

4.10 Ellingwood, B., Galambos, T.V., MacGregor, J.G., and Cornell, A.C., "Development of a Probability Based Load Criterion for American National Standard A58," NBS SP-577, 1980.

4.11 Hasofer, A.M and Lind, N.C., "Exact and Invariant Second-Moment Code Format," Journal of the Engineering Mechanics Division, ASCE, Vol. 100, No. EMI, pp. 111-221, February 1974.

4.12 Rackwitz, R., and Fiessler, B., "Structural Reliability Under Combines Random Load Sequences," Journal of Computers and Structures, Vol. 9, pp. 489-494, 1978.

4.13 Chen, X., and Lind, N.C., "Fast Probability Integration by Three Parameter Normal Tail Approximation," Structural Safety, Vol. 1, pp. 169-176, 1983.

4.14 Wu, Y.-T., and Wirsching, P.H., "A New Algorithm for Structural Reliability Estimation," Submitted for review to Journal of Engineering Mechanics, ASCE, 1985.

4.15 Wu, Y.-T., "Demonstration of a New Fast Probability Integration Method for Reliability Analysis," Proceedings of Symposium on Probabilistic Structural Design and Analysis, ASME, 1985.

4.16 Wu, Y.-T., and Wirsching, P.H., "Advanced Reliability Method for Fatigue Analysis," Journal of Engineering Mechanics, ASCE, Vol. 110, No. 4, April 1984.

4.17 Wirsching, P.H., and Wu, Y.-T., "Advanced Reliability Methods for Structural Evaluation," Proceedings of Symposium on Probabilistic Structural Design and Analysis, ASME, Miami, FL, 1985.

4.18 Wirsching, P.H., and Carlson, J.R., "Model Identification for Engineering Variables," Journal of the Engineering Mechanics Division, ASCE, Vol. 103, No. EMI, July 1975.

4.19 Siddall, J.N., Probabilistic Engineering Design, Dekker, 1983.

5.0 NESSUS PROBABILISTIC STRUCTURAL ANALYSIS CODE

5.1 Overview

The probabilistic finite element computer code NESSUS (Numerical Evaluation of Stochastic Structures Under Stress) is being developed by MARC Analysis Research Corporation for the analysis of critical structural components for reusable space propulsion systems. This program has evolved from the HOST code, developed by MARC for Pratt & Whitney Aircraft Company under NASA contract NAS3-23697, and which is now in use for the analysis of hot-section air-breathing turbine components at both Pratt & Whitney and the NASA Lewis Research Center.

The development of the NESSUS code is scheduled to take three years. First year efforts involved the formulation of the probabilistic analysis strategy and the development of a probabilistic linear analysis code. The ultimate goal of the three-year program is the development of a finite element code capable of performing nonlinear static and dynamic analysis of structures having stochastic material properties, geometry and boundary conditions, and that are subjected to a random loading environment.

The NESSUS code is written primarily in FORTRAN ANSI-66 to guarantee portability of the program to a wide range of computer and operating systems. Exceptions are made for the I/O routines (in FORTRAN ANSI-77) and machine-dependent routines to determine the time and date. All floating-point calculations are carried out using double-precision arithmetic (64 bit/word) on the 32 bit/word systems, or in single precision (60 or 64 bit/word) on high accuracy super-computers. The database of the NESSUS program is designed to store dynamically the problem-dependent data to an upper limit of 600,000 words. This upper limit can be tailored to the user's need by changing the dimension statement and creating a new executable copy of the code.

5.2 General Capabilities

The NESSUS code is built around a set of seven driver modules, which reflect the major analysis options available in the code. These are:

i) A static analysis module, using a band-storage type equation solver, and providing in-core solution for linear elastic and elastoplastic problems, either in a purely iterative manner or in an incremental-iterative fashion.

ii) An alternate static analysis module, offering essentially the same features as the preceding module, but using a frontal equation solver with out-of-core solution capability.

iii) A bifurcation buckling module, used for stability analysis.

iv) A modal extraction module, used in the determination of undamped natural frequencies and mode shapes for linear dynamics problems.

v) A mode superposition module, used in the analysis of steady-state and/or transient linear vibration problems in the time domain.

vi) A random vibration module, used in the analysis of problems involving stationary random excitation, via the frequency domain.

vii) A direct time integration module, using the Newmark-β scheme, for the solution of both linear and material-nonlinear transient dynamics problems.

A common element library is shared by all the driver modules. Likewise, the constitutive model library is available to all the driver modules, before eigenvalue extraction. The eigenvalue extraction subsystem uses subspace iteration, with multiple power shift capability, and is shared by all the linear dynamics modules, together with the bifurcation buckling module.

User-defined subroutines that are linked with the program at load time, add to the flexibility of the NESSUS program by providing the analyst with the capability to re-program specific areas of the code. The program provides the analyst with a set of controls to activate or deactivate each user routine at run-time, without having to reload the code each time.

5.2.1 Static Analysis

Both linear elastic and elastoplastic analyses are available using either one of the two static analysis modules. A time scale may be defined, allowing incremental-iterative solution of quasi-static problems involving time-dependent phenomena, such as creep-plasticity.

The main difference between the two static solution modules involves the way in which the global stiffness array is formed and factorized. By default, the in-core equation solver is used, with the global stiffness array stored in band form. For larger problems, the frontal solution module may

be invoked. This module offers out-of-core solution capability, although the fullfront width must still fit in-core. Both bandwidth and frontwidth optimizers are available, to minimize the storage of data.

Several iteration pre-conditioners are available for nonlinear quasi-static problems. The default algorithm is of the Tangent Newton type (full Newton-Raphson), requiring global stiffness assembly and factorization at each iteration. Greater computational efficiency may be achieved by invoking the modified Newton-Raphson algorithm, thus avoiding the update of the tangent stiffness array at each iteration. Efficient updates of the iteration pre-conditioner may be obtained by the use of the BFGS update or Secant Newton method. Additional control over the iteration process is available with the use of the line search option.

The constitutive model library implemented in NESSUS includes:

- Linear Elasticity
- Secant Elasticity, a simplified plasticity model
- von Mises Plasticity, using a radial return algorithm with associative flow
- Integrated Creep-Plasticity model (Walker's model)

Anisotropic elasticity, yield surface and thermal strains may be modeled with the use of user subroutines. Temperature-dependent material properties, work hardening curves, deviatoric and dilatational creep laws, and the material parameters for the Walker creep-plasticity model may also be specified via user subroutines.

Temperatures, concentrated loads and prescribed displacements are applied at the nodes. Body force loads, such as those resulting from gravity or centrifugal acceleration, as well as surface pressures and/or edge tractions on individual elements are also available. In a quasi-static analysis, any of the loads and/or boundary conditions may be modified between increments. Proportional incrementation of all but the thermal loads and body force by a prescribed factor is also permitted. An adaptive load increment procedure, based on the arc-length method, is available for the automatic adjustment of the load increment size at each iteration step. A pulse load time history, with starting

times specified on a nodal basis, may also be specified in a quasi-static analysis with a prescribed time scale.

5.2.2 Dynamic Analysis

5.2.2.1 Linear Dynamics Using Normal Modes

Two main driver routines are available in NESSUS for the solution of linear dynamics problems via normal modes. One driver performs the analysis in the time domain and provides the solution to transient dynamic loading problems using the analytical solution to the uncoupled oscillator equation for an assumed linear load variation within each time increment. No restrictions are imposed on the duration of the time increment, which may vary throughout the time history. All the mechanical loads available for quasi-static analysis (but none of the displacement constraints) may be used in this type of analysis. Initial displacements and/or velocities may also be prescribed. Two types of steady state solution may also be obtained with this module. The first one corresponds to harmonic nodal loads at a given frequency, but with phase and amplitude specifiable separately at each node. The second type of steady-state solution corresponds to harmonic base excitation at some fixed frequency, and again allowing for individual phase and amplitude specification at each base point.

The second driver routine performs random vibration analysis in the frequency domain. Acceptable mechanical loads include nodal point loads, as well as element pressures and/or edge tractions on shell and beam elements. Other random load types may be implemented as the need becomes apparent. The loading is assumed to be stationary in time, and may be treated as fully correlated or completely uncorrelated in space. Partial correlation may be defined in a user subroutine, which is invoked on a node pair basis. In the case of distributed load fields, such as element pressures and/or edge tractions, the element shape functions are used to interpolate both the loading and the correlation function. The power spectral density function is also interpolated

linearly between the entries in a table of user-defined data points. The integral of the spectral density function for modal response is computed in the frequency domain using five point Gauss quadrature over each one of a number of frequency subranges separated by user defined breakpoints.

Most linear dynamics analyses may be performed with either (a) Rayleigh proportional damping, (b) viscous modal damping, or (c) structural modal damping. The one exception is the transient dynamic analysis, which is presently limited to viscous modal damping.

5.2.2.2 Direct Integration Transient Dynamics

A single-step direct time integration scheme based on the Newmark-β family of algorithms is available as the main driver routine in NESSUS for both linear elastic and elastoplastic problems involving transient dynamics. Several members of this family of algorithms may be obtained by selecting the control parameters for the time integration scheme as follows:

γ	β	INTEGRATION SCHEME
1/2	0	Central Explicit
3/2	1	Backward Difference
1/2	1/10	Linear Acceleration
3/2	4/5	Galerkin
1/2	1/12	Fox-Goodwin
1/2	1/4	Average Acceleration

The "average acceleration" scheme is the system default, with the stress and strain recovery at the mid-point of each time step. Only Rayleigh-type damping may be used in this type of analysis. In addition to all the mechanical loadings available for quasi-static analyses, a general periodic loading or displacement constraint can be used, with period and amplitude both specified on a nodal basis. Nodal displacements, velocity or acceleration may also be specified as part of the initial condition for the dynamic analysis.

5.2.3 Finite Element Library

All the elements currently available in the NESSUS code use linear isoparametric shape functions and are integrated numerically. Stresses and strains are evaluated and stored on a nodal basis. Geometric quantities such as beam cross sections and shell thickness are defined at the nodes and interpolated with shape functions. Only in the plane stress element is the thickness constant over the element. The overall characteristics of each element are summarized in Table 5.1.

5.3 Strategy for Probabilistic Structural Analysis

A promising alternative to the use of perturbation expansion series in a probabilistic finite element context is provided by the family of Fast Probability Integration (FPI) algorithms. These algorithms offer the means for bypassing the computational and data management bottleneck inherent to the perturbation expansion approaches, since the computation and manipulation of explicit partial derivatives with respect to each random variable present in the analysis is no longer required as a fundamental ingredient of the method. The philosophy and the origins of the FPI methods are described elsewhere in the report.

To use the FPI algorithm efficiently in a finite element environment, two major issues need special consideration. One issue arises from the fact that the FPI problem must be formulated in terms of a set of uncorrelated random variables. This will in general present a problem, since many of the field variables used to describe the FE problem are often correlated to some degree. Assuming that a satisfactory model can be achieved (i.e., a model involving only uncorrelated random variables), a method must then be developed for efficiently obtaining the response of the deterministic system to a number of prescribed perturbations of the random variables. These perturbed solutions constitute the raw data on which the FPI algorithm will base the reliability analysis of the structural model.

5.3.1 Representation of Correlated Fields

There are several ways to represent a field of correlated variables. The most familiar way is,

Table 5.1

Summary of the NESSUS Element Library

	P.STRS	P.STRN	AXSYM	BRICK	SHELL	T. BEAM
ITYPE	3	11	10	7	75	98
NELCRD	2	2	2	3	3	6
NELNFR	2	2	2	3	6	6
NELNOD	4	4	4	8	4	2
NELSTR	3	4	4	6	8	6
NELCHR	5	5	5	5	5	5
NELINT	4	4	4	8	4	1
NELLV	3	3	3	3	4	3
NELLAY	1	1	1	1	5	1
NDI	2	3	3	3	2	3
NSHEAR	1	1	1	3	1	3
JLAW	2	3	4	5	6	7

ITYPE Element type number.
NELCRD Number of coordinate data per node.
NELNFR Number of degrees-of-freedom per node.
NELNOD Number of nodes per element.
NELSTR Number of stress and strain components per node.
NELCHR Number of material property data for the element.
NELINT Number of "full" integration points per element.
NELLV Number of distributed load types per element.
NELLAY Number of layers of integration through the thickness of the shell element.
NDI Number of direct stress components
NSHEAR Number of shear stress components.
JLAW Type of the constitutive equation.

perhaps, that of a correlation function, expressing the way in which the strength of correlation decays with distance or time. One alternative calls for the definition of a scale of fluctuation, which is a measure of the distance required for a given decay of the correlation function. Given the nature of Finite Element interpolation, the correlation data need only be defined at a finite set of discrete Points, which typically will correspond to the mesh nodes or the integration points. This suggests that the correlation data may be represented as a variance-covariance matrix of the form:

$$C_{X_iX_j} = \rho_{ij} S_{X_i} S_{X_j} \tag{5.1}$$

where $C_{X_iX_j}$ is the covariance between the values of $\tilde{X}$ at points i and j, $S_{X_i}^2$ is the variance of $\tilde{X}$ at i, and ρ_{ij} is the coefficient of correlation between $\tilde{X}_i$ and $\tilde{X}_j$. The variance-covariance matrix is symmetric, positive semi-definite. It may be singular, as evidenced by the special case where all $C_{X_iX_j}$ are identical.

By the Spectral Decomposition Theorem this matrix can be represented as a summation of the form

$$[C_{X_iX_j}] = \sum_{i=1}^{N} \{\phi_i\} \lambda_i \{\phi_i\}^T \tag{5.2}$$

where the λ_i are the eigenvalues of the variance-covariance matrix, and the $\{\theta_i\}$ are the corresponding eigenvectors, normalized such that

$$\{\phi_i\}^T \{\phi_j\} = 1, \quad i = j \tag{5.3}$$

In addition, from the symmetry of $[C_{X_iX_j}]$, it follows that

$$\{\phi_i\}^T \{\phi_j\} = 0, i \neq j \tag{5.4}$$

i.e., the eigenvectors are mutually orthogonal. This orthogonality property of the eigenvectors suggests a strategy for representing the correlated field in terms of a set of uncorrelated random variables.

To obtain the uncorrelated variables, the random vector $\{\tilde{X}\}$ defining the random field at a finite set of discrete points, is transformed into a new vector of random variables $\{\tilde{x}\}$ defined by

$$\{\tilde{x}\} = [\phi]^T \{\tilde{X}\} \tag{5.5}$$

where

$$[\phi] = [\{\phi_1\}\{\phi_2\}...\{\phi_N\}] \tag{5.6}$$

What are the properties of the transformed variables? The means of the transformed variables are simply the transformed means of the original variables, i.e.,

$$\{\mu_x\} = E(\{\tilde{x}\}) = E([\phi]^T\{\tilde{X}\}) = [\phi]^T E(\{\tilde{X}\}) = [\phi]^T\{\mu_X\} \tag{5.7}$$

The variance-covariance matrix for the transformed variables may be obtained in a similar fashion.

$$\begin{aligned}
[C_{x_i x_j}] &= E((\{\tilde{x}\} - \{\mu_x\})(\{\tilde{x}\} - \{\mu_x\})^T) \\
&= E\Big(([\phi]^T\{\tilde{X}\} - [\phi]^T\{\mu_X\})([\phi]^T\{\tilde{X}\} - [\phi]^T\{\mu_X\})^T\Big) \\
&= [\phi]^T E((\{\tilde{X}\} - \{\mu_X\})(\{\tilde{X}\} - \{\mu_X\})^T)[\phi] \\
&= [\phi]^T [C_{X_i X_j}][\phi] = [\Lambda]
\end{aligned} \tag{5.8}$$

Thus, the advantages of representing the correlated field in terms of the transformed variables become apparent. The orthogonality property of the eigenvectors [cf. Eq. (5.4)] implies that the correlation matrix $[\Lambda]$ is diagonal, which is to say, that the transformed variables $\{\tilde{x}\}$ are uncorrelated. Furthermore, the uniqueness of the spectral representation (5.2) may be invoked to identify the ith entry in the diagonal of $[\Lambda]$ as the eigenvalue λ_i associated with the eigenvector $\{\phi_i\}$. Therefore, the variances of the transformed variables are simply the eigenvalues of the variance-covariance matrix for the original variables.

5.3.2 Perturbation of Correlated Fields

By representing a correlated random field in terms of its spectral decomposition, a set of transformed variables is obtained, which are uncorrelated and, therefore, provide an appropriate basis for the FPI formulation. In addition, the FPI algorithm will require the computation of the

response of the deterministic model for selected perturbations of these transformed variables. Typically, each perturbation is parameterized by some factor κ_i of the standard deviation (the positive square root of the variance) of the transformed variables. Both the number and the form of the individual perturbations will depend on the scheme used within the FPI algorithm. A typical first-order perturbation of the ith transformed variable will correspond to the following perturbation in the original variables.

$$\{X\} = \{\mu_X\} + \kappa_i \lambda_i^{\frac{1}{2}} \{\phi_i\} \tag{5.9}$$

Assuming that the strength of correlation is such that the use of a truncated set of transformed variables is justified, as will be the case in many practical applications, the number of perturbations required in the analysis may be reduced dramatically. This is of particular interest, since much of the computational effort in the analysis is spent in the evaluation of the perturbed solutions. It should be emphasized that the use of Eq. (5.9) will not introduce any truncation error on the means, since Eq. (5.7) already expresses $\{\mu_X\}$ as a summation over the full eigenvector space. The only truncation error results from neglecting the perturbations to the least significant eigenvectors.

5.3.3 Efficient Computation of the Perturbed Solutions

Once the nature of the required perturbations has been established, the response of the perturbed model must be obtained with an algorithm that must combine versatility and computational efficiency. If the effects of the perturbation are confined to the forcing vector, the solution of the linear static problem reduces to a simple back substitution of the perturbed load vector, using the stiffness factorization available from the deterministic analysis. However, many of the variables of interest will affect the stiffness terms. Although approximate factorizations of the modified stiffness matrix may be constructed in terms of perturbation expansions, the computational and data management bottlenecks inherent to these approaches make them less than attractive for implementation in a Finite Element code.

The simplicity of the problem for perturbations confined to the load vector suggests an alternative scheme, in which the unbalanced load corresponding to the difference between the internal forces of the original and perturbed systems is iteratively applied as a load correction term to the unperturbed system. This is no more than a different application of the familiar modified Newton iteration method, which is used in many finite element codes with nonlinear capabilities. The basic algorithm is outlined in Box 5.1. A graphical interpretation of the one-dimensional version of the algorithm is provided in Figure 5.1. The stability characteristics of this algorithm are good and well understood. Loss of stability is only possible in the case of stiffening, and even then the symptoms of the problem can be readily detected by the control logic in the code. The algorithm has good convergence properties for small perturbations about the deterministic state, but its performance can deteriorate greatly if large changes in stiffness are imposed.

5.4 Integration of the Finite Element and Probabilistic Codes

The theory outlined in the preceeding section provides the basis for a very clean integration of the finite element and probabilistic analysis modules in the NESSUS code. The basic flow diagram to be implemented for probabilistic linear static analysis is shown in Figure 5.2. This approach has so far been applied in an ad-hoc fashion to linear elastostatics only, but it appears to be readily extendable to the nonlinear regime. With the proposed scheme, the probabilistic analysis will be carried out in five distinct phases:

PHASE I: Analysis of the Deterministic Model

This phase involved the determination of a deterministic state, and the solution of the problem using conventional finite element methods. Updated deterministic state is obtained after the reliability analysis.

PHASE II: Preparation of the Statistical Model

This phase involves the preparation of a statistical model from the variance and correlation data available, and includes any pre-processing that may be required to arrive at a problem definition in terms of uncorrelated random variables. Although this phase need not necessarily follow Phase I, the results at the deterministic state may often provide useful insight into the identification of the significant random variables. This stage should result in a simplified statistical model in which only bona fide random variables are present.

Box 5.1 Solution of the Perturbed Elastostatic Problem

A. Solution of the Deterministic Problem

1. Assemble $[K]$ and $\{F\}$

2. Factorize the $[K]$ matrix

3. Solve for the deterministic displacements
$\{u\} = [K]^{-1}\{P\}$

   and stresses
$\{\sigma\} = [D][B]\{u\}$

B. Perturbation Loop: For each perturbed variable, do

1. Use the deterministic displacement as a first approximation
$\{\hat{u}^{(0)}\} = \{u\}$

2. Compute an approximation to the perturbed stresses
$\{\hat{\sigma}^{(0)}\} = [\hat{D}][\hat{B}]\{\hat{u}^{(0)}\}$

   and use these to form a residual force vector
$\{R^{(0)}\} = \{P\} - \int_v [\hat{B}]^T \{\hat{\sigma}^{(0)}\} dv$

3. Iteration Loop: While $\| \{R^{(i)}\} \| > \varepsilon$, do

   (i) solve for the displacement correction
   $\{d\hat{u}^{(i+1)}\} = [K]^{-1}\{R^{(i)}\}$

   (ii) Compute the improved approximation
   $\{\hat{u}^{(i+1)}\} = \{\hat{u}^{(i)}\} + \{d\hat{u}^{(i+1)}\}$

   (iii) Compute the new approximation of the stresses
   $\{\hat{\sigma}^{(i+1)}\} = [\hat{D}][\hat{B}]\{\hat{u}^{(i+1)}\}$

   and use these to form a residual force vector
   $\{R^{(i+1)}\} = \{P\} - \int_v [\hat{B}]^T \{\hat{\sigma}^{(i+1)}\} dv$

   (iv) Increment the iteration counter, i = i + 1

4. Save/print-out the results for the converged perturbation problem.

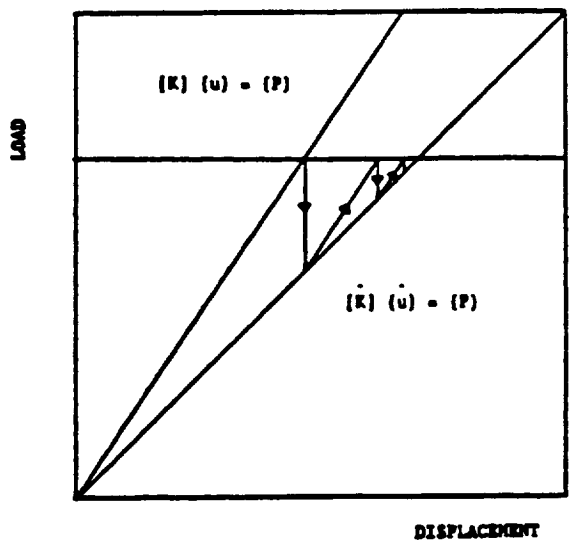

b) Softening

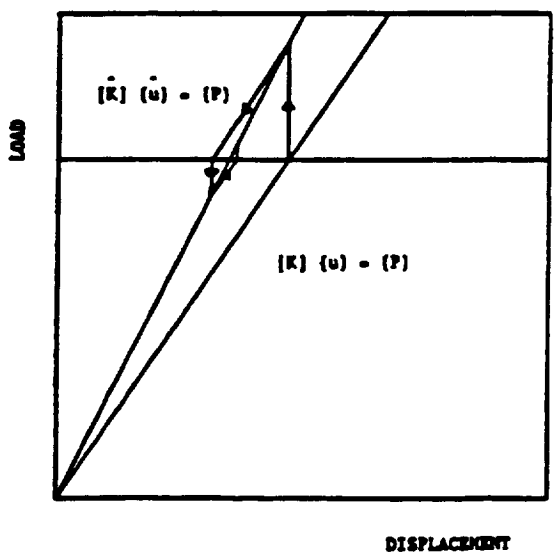

a) Stiffening

Figure 5.1 1-D Interpretation of the Algorithm in Box 5.1

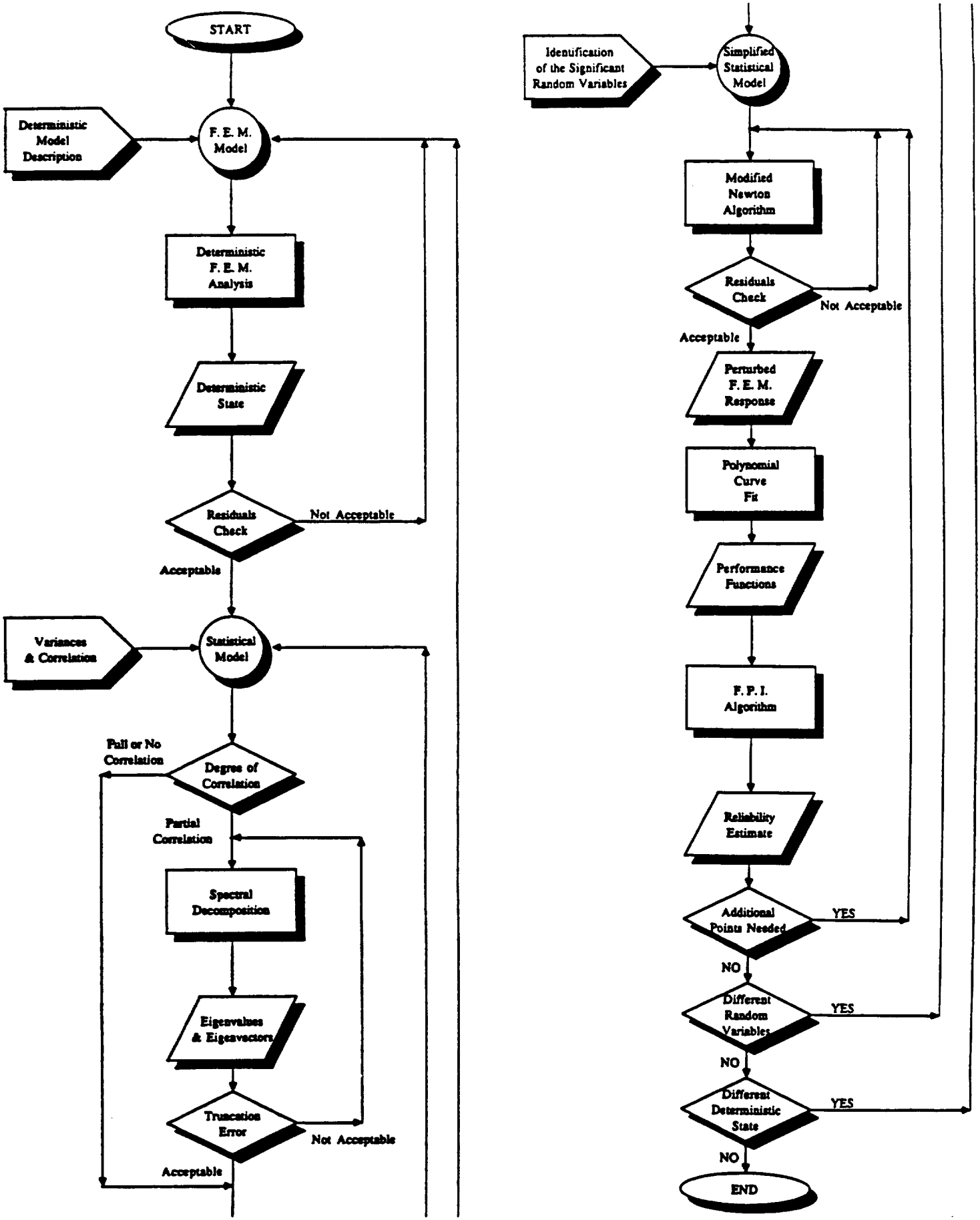

Figure 5.2 Flow Diagrams for the Integration of the FE and FPI Modules of the NESSUS Code

PHASE III: Generation of Perturbed Solutions

This phase involves the generation of perturbed solutions about the deterministic state, corresponding to selected variations in the stochastic variables present in the statistical model. The outcome of this phase consists of a database of perturbed results, which will be used to compute a measure of the reliability of the structural system.

PHASE IV: Probability or Reliability Analysis

This phase involves the computation of a measure of probability via FPI or some equivalent methods. With the present approach, a polynomial representation of the structural response in the neighborhood of the deterministic state is obtained and used in the FPI algorithm to obtain a safety index for a given performance function. Probability distribution function for any response variable are obtained by repeated computation of the safety index.

PHASE V: Evaluation of Results

This phase involves the evaluation of the modeling assumptions in the light of the results from the reliability analysis. These results might indicate a need for a more complete set of Perturbations or a higher order approximation. The adequacy of the assumed set of random variables may be re-investigated, and the use of the updated deterministic state using the design point information (see Section 3) may be necessary. Such considerations underscore the need for an implementation which allows for a certain degree of interaction between the software and the analyst, and which is reflected in the modular design of the probabilistic analysis code.

6.0 WORK IN PROGRESS

6.1 NESSUS Code Validation and Verification

To ensure that all theoretical formulations and solution algorithms are correctly implemented in NESSUS, SwRI has proposed a set of nine preliminary validation cases (see Section 4, Volume III). These validation problems addresses rather simple beam and shell finite element models under static and dynamic loadings. Effects important to SSME components such as correlation between the random variables, centrifugal forces, and stress stiffening effects are included. Validation cases will be selected and exercised in the NESSUS Code throughout the duration of Task 1, namely the Probabilistic Finite Element Methods for Plates and Shells.

To ensure that the NESSUS Code gives reasonable results for actual problems in the domain of the code, verification will be done by comparing deterministic solutions from other Rocketdyne deterministic FEM analysis on SSME components. Three Rocketdyne finite element models for turbine blades are in the process of being converted to the NESSUS Code format. These are:

SSME High Pressure Fuel Turbopump Second Stage Blade
SSME High Pressure Oxidizer Turbopump First Stage Blade
SSME High Pressure Oxidizer Turbopump First Rotor-blade Beam

Fig. 6.1 and Fig. 6.2 show the Rocketdyne finite element model of the SSME second stage blade. The model has:

302	Quadrilateral Flat Plate Shell Elements
8	Triangular Flat Plate Shell Elements
43	Three-Dimensional Beam Elements
374	Nodes
2154	Total Degrees of Freedom

The Rocketdyne model is in a STARDYNE format. As part of the NESSUS code verification, NESSUS and STARDYNE will be compared for static blade pressure and centrifugal loading cases.

6.2 Statistical Analysis of Physical Stochastic Variables

The first year of PSAM program has produced methods for analyzing data and has resulted

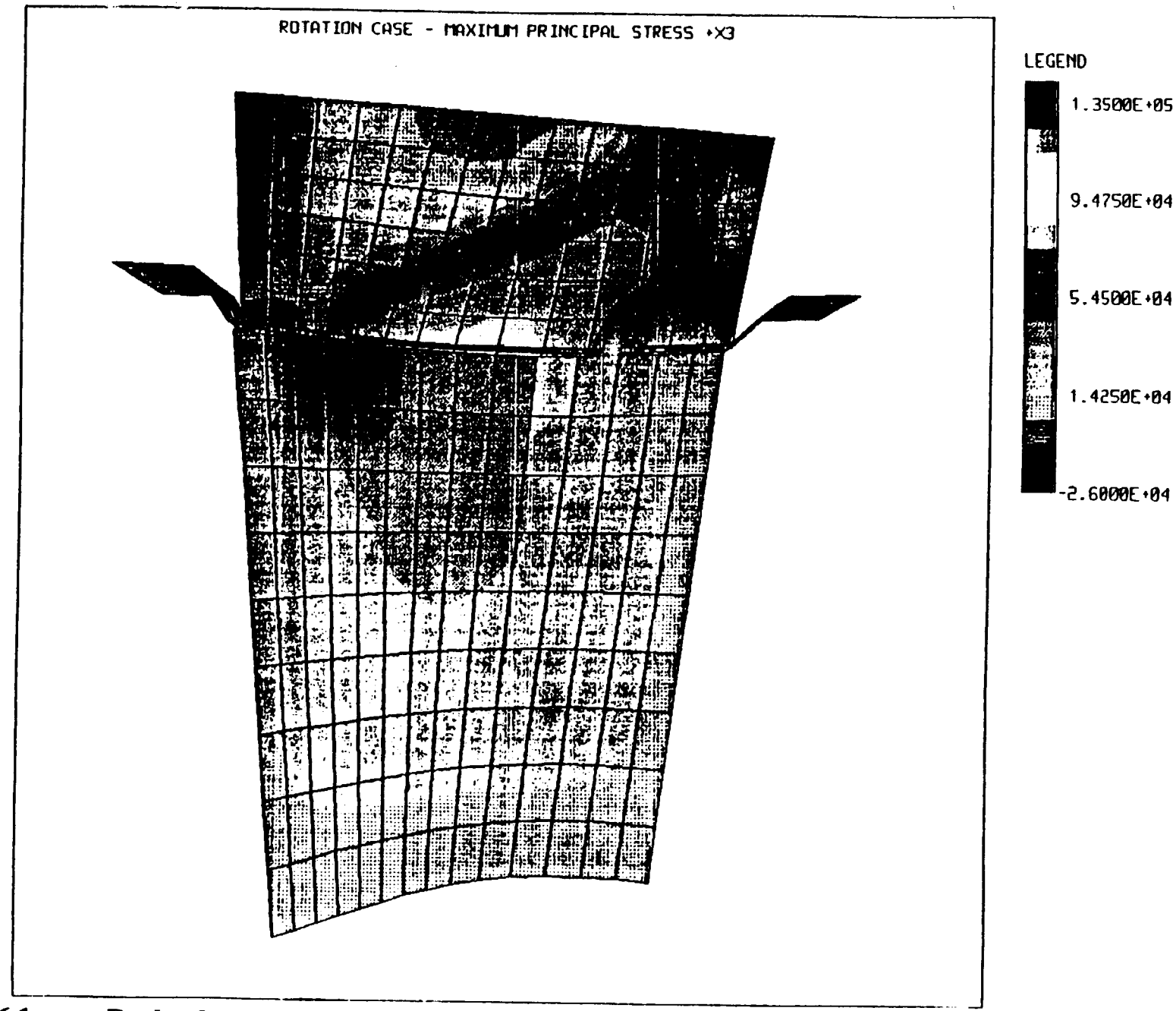

Figure 6.1 **Rocketdyne Finite Element Plate Model of the SSME High Pressure Fuel Turbopump Second Stage Blade (a)**

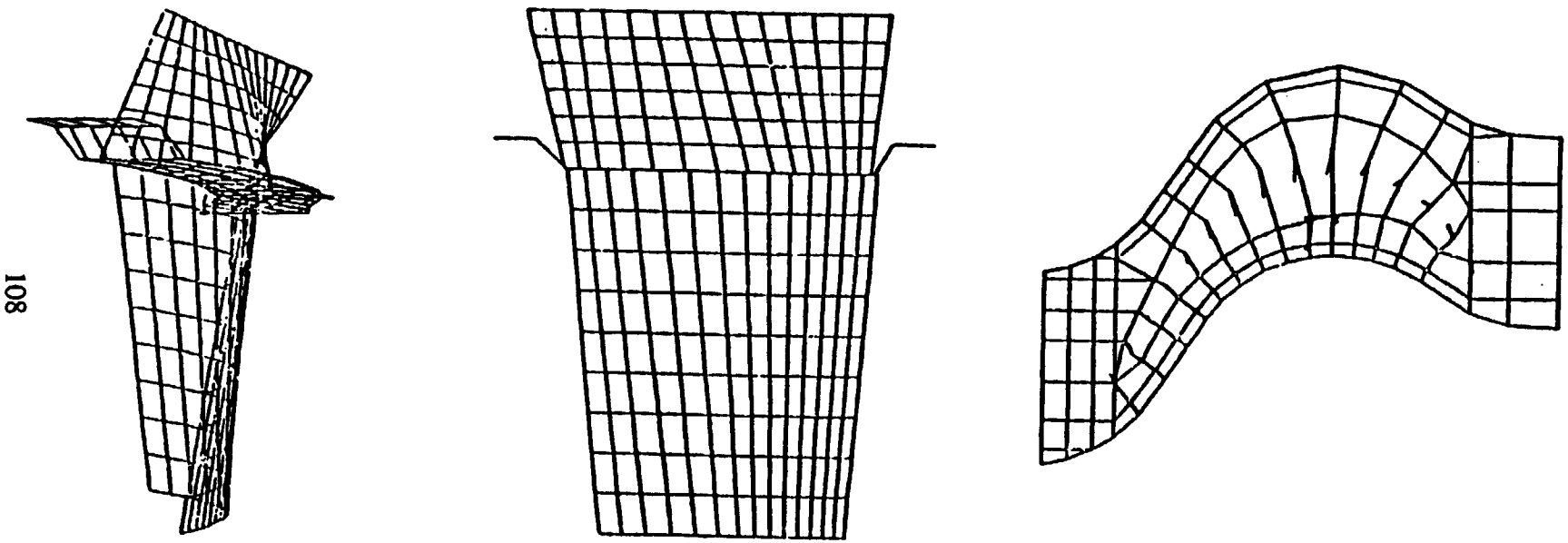

Figure 6.2 **Rocketdyne Finite Element Plate Model of the SSME High Pressure Fuel Turbopump Second Stage Blade (b)**

in distributional models and their parameters for several SSME materials and geometries (see Section 1). The analysis of available Rocketdyne data will continue. The University of Arizona is examining geometric uncertainties of the SSME high pressure Oxidizer turbopump First Stage Blade. Distributional models and spatial correlations will be considered. SwRI and the University of Arizona are in the process of establishing a catalog of recommended distributional models for the stochastic variables of interests to be used as default values for the analysis when data are not available.

REPORT DOCUMENTATION PAGE

Form Approved
OMB No. 0704-0188

Public reporting burden for this collection of information is estimated to average 1 hour per response, including the time for reviewing instructions, searching existing data sources, gathering and maintaining the data needed, and completing and reviewing the collection of information. Send comments regarding this burden estimate or any other aspect of this collection of information, including suggestions for reducing this burden, to Washington Headquarters Services, Directorate for information Operations and Reports, 1215 Jefferson Davis Highway, Suite 1204, Arlington, VA 22202-4302, and to the Office of Management and Budget, Paperwork Reduction Project (0704-0188), Washington, DC 20503.

1. AGENCY USE ONLY (*Leave blank*)

2. REPORT DATE
April 1992

3. REPORT TYPE AND DATES COVERED
Annual Contractor Report

4. TITLE AND SUBTITLE
Probabilistic Structural Analysis Methods for Select Space Propulsion System Components (PSAM)
Volume I

5. FUNDING NUMBERS
WU–590–21–11

6. AUTHOR(S)

7. PERFORMING ORGANIZATION NAME(S) AND ADDRESS(ES)
Southwest Research Institute
6220 Culebra Road
San Antonio, Texas 78228

8. PERFORMING ORGANIZATION REPORT NUMBER
None

9. SPONSORING/MONITORING AGENCY NAMES(S) AND ADDRESS(ES)
National Aeronautics and Space Administration
Lewis Research Center
Cleveland, Ohio 44135–3191

10. SPONSORING/MONITORING AGENCY REPORT NUMBER
NASA CR–189157

11. SUPPLEMENTARY NOTES
Project Manager, C.C. Chamis, Structures Division, NASA Lewis Research Center, (216) 433–3252.

12a. DISTRIBUTION/AVAILABILITY STATEMENT
Unclassified - Unlimited
Subject Category 39

12b. DISTRIBUTION CODE

13. ABSTRACT (*Maximum 200 words*)

This annual report summarizes the technical effort and computer code developed during the first year. Several formulations for Probabilistic Finite Element Analysis (PFEA) are described with emphasis on the selected formulation. The strategies being implemented in the first-version computer code to perform linear, elastic PFEA is described. The results of a series of select Space Shuttle Main Engine (SSME) component surveys are presented. These results identify the critical components and provide the information necessary for probabilistic structural analysis. The report is issued in three volumes: Volume I - summarizes theory and strategies; Volume II - summarizes surveys of critical space shuttle main engine components; and Volume III - summarizes literature surveys and technical reports available at that time.

14. SUBJECT TERMS
Finite elements; Strategy; Computer code; Space shuttle main engine; Select components; Literature; Survey

15. NUMBER OF PAGES
116

16. PRICE CODE
A06

17. SECURITY CLASSIFICATION OF REPORT	18. SECURITY CLASSIFICATION OF THIS PAGE	19. SECURITY CLASSIFICATION OF ABSTRACT	20. LIMITATION OF ABSTRACT
Unclassified	Unclassified	Unclassified	